INL/MIS-21-65409-Revision-0

ECAR-5633 AGR-5/6/7 Daily As-Run Thermal Analyses

January 2022

Changing the World's Energy Future

Grant L Hawkes

Idaho National Laboratory

INL/MIS-21-65409-Revision-0

ECAR-5633 AGR-5/6/7 Daily As-Run Thermal Analyses

Grant L Hawkes

January 2022

Idaho National Laboratory
Idaho Falls, Idaho 83415

http://www.inl.gov

Prepared for the
U.S. Department of Energy
Under DOE Idaho Operations Office
Contract DE-AC07-05ID14517

1. Effective Date	01/10/2022	Professional Engineer's Stamp N/A See LWP-10010 for requirements
2. Does this ECAR involve a Safety SSC?	No	
3. Safety SSC Determination Document ID	N/A	
4. SSC ID	N/A	
5. Project No.	23841	
6. Engineering Job (EJ) No.	N/A	
7. Building	N/A	
8. Site Area	N/A	

9. Objective / Purpose

The purpose of this engineering and calculations report is to document the results of the thermal analyses performed to calculate the Advanced Gas-Cooled Reactor (AGR)-5/6/7 as-run daily temperatures of the fuel compacts. Temperature data provided by this report will be used to evaluate fuel performance. The AGR-5/6 portion of the experiment was for fuel qualification at prototypic temperatures, while the AGR-7 portion of the experiment was a margin test at very high temperatures.

10. If revision, please state the reason and list sections and/or page being affected.
N/A

11. Conclusion / Recommendations

This report documents the results of thermal analyses to predict the daily as-run temperatures for the AGR-5/6/7 experiment. A finite element model was created for the entire test train with all five capsules. The fuel compacts, graphite holders, stainless-steel capsule walls and all other major components were individually modeled along with each thermocouple. Gas gaps were modeled to change with fast neutron fluence and thermal expansion. Daily heat rates for each compact and component in the model were input from daily as-run physics analyses. Daily gas compositions for each capsule were input. The thermal conductivity of the compacts and graphite holders varied with fast neutron fluence.

Gas mixture thermal conductivity was implemented using experimentally attained values from literature. Fluence and temperature-dependent thermal conductivity was used for the graphite components and the fuel compacts. Radiation heat transfer was implemented. The model was tuned to try and match the thermocouple readings during the first cycle by adjusting the Neolube (graphite lubricant used to increase emissivity on stainless steel capsule) thickness. The gas mixture for capsule 1 during the final cycle was undetermined. A run was made for a lower limit and upper limit for the neon gas fraction for this cycle.

Capsule 5 thermal model predictions agreed the best with measured thermocouples at about -30 °C for the entire irradiation based on inspection from figures. Capsule 1 and capsule 3 had the largest variation in difference between measured and calculated thermocouple temperatures. This difference was about ±120 °C for capsule 1 for the first cycle and about ±75 °C for capsule 3 for the first cycle. Capsule 2 averaged a temperature difference (measured minus calculated) of about ±50 °C while capsule 4 averaged about -40 °C.

Thermocouple failure is lightly discussed in this report. The thermocouples failed the earliest and most often in capsule 1 (most failures) while capsule 5 had the fewest failures.

Time-average, volume-average (TAVA) temperature values were calculated and discussed. These TAVA temperatures showed that the fuel temperatures were controlled very evenly throughout irradiation. Target temperature bins for AGR-5/6 were mostly met except for the highest temperature. Target temperature bins for AGR-7 (1500 ±50 °C) were not quite achieved.

Waterfall plots showing the fraction of fuel below a specified temperature band for each day were displayed and discussed. Calculations were performed for offsetting the holder in various directions by 0.001 in. for the first cycle when compared with the measured thermocouple values. Future uncertainty and sensitivity reports will investigate this further.

Contents

1.0 PROJECT ROLES AND RESPONSIBILITIES 4

2.0 SCOPE AND BRIEF DESCRIPTION 5

3.0 DESIGN OR TECHNICAL PARAMETER INPUT AND SOURCES 5

4.0 EXPERIMENT DESCRIPTION AND OTHER BACKGROUND DATA 5

5.0 ASSUMPTIONS 8

6.0 COMPUTER CODE VALIDATION 9

7.0 MODEL DESCRIPTION 10

8.0 ANALYSIS RESULTS 32

9.0 DATA FILES 55

10.0 DRAWINGS 59

11.0 CONCLUSIONS 60

12.0 REFERENCES 61

APPENDIXES

- Appendix A – ABAQUS 6.14-2 Validation
- Appendix B – Compact Time-averaged Temperature, Burnup, and Fast neutron Fluence at the End of Irradiation (168A)

1.0 PROJECT ROLES AND RESPONSIBILITIES

Project Role	Name	Organization	Pages Covered (if applicable)
Performer	Grant L. Hawkes	C140	-----
Checker[a]	Jason W. Barney	C140	-----
Independent Reviewer[b]	N/A	N/A	-----
CUI Reviewer[c]	Michael E. Davenport	C640	-----
Manager[d]	Richard H. Howard	C140	-----
Requestor[ef]	Paul A. Demkowicz	C600	-----
ESA Author[f]	N/A	N/A	-----
Document Owner[f]	Michael E. Davenport	C640	-----
Reviewer[f]	N/A	N/A	N/A

Responsibilities:

a. Confirmation of completeness, mathematical accuracy, and correctness of data and appropriateness of assumptions.

b. Concurrence of method or approach. See definition, LWP-10106.

c. Concurrence with the document’s markings in accordance with LWP-11202.

d. Concurrence of procedure compliance. Concurrence with method/approach and conclusion.

e. Authorizes the commencement of work of the engineering deliverable.

f. Concurrence with the document’s assumptions and input information. See definition of Acceptance, LWP-10200.

NOTE: *Delete or mark “N/A” for project roles not engaged. Include ALL personnel and their roles listed above in the eCR system. The list of the roles above is not all inclusive. If needed, the list can be extended or reduced.*

2.0 SCOPE AND BRIEF DESCRIPTION

This ECAR documents the daily as-run thermal analyses for the Advanced Gas Reactor (AGR)-5/6/7 experiment. The AGR-5/6/7 experiment is comprised of 5 individual capsules stacked on top of each other to form the test train. Each capsule contains tristructural isotropic (TRISO) -particle compacts that have approximate dimensions of 0.5 in. diameter and 1.0 in. height. The compacts are composed of TRISO fuel particles bound together by a carbon matrix. Each capsule is supplied with a flowing helium/neon gas mixture to control the test temperature and sweep any fission gases that are released to the fission product monitoring system. Temperature control is accomplished by adjusting the gas mixture ratio of the two gases (i.e., helium and neon) with differing thermal conductivities in the gas gaps. The Advanced Test Reactor (ATR) northeast lobe power is also used to adjust the temperatures of the capsules.

3.0 DESIGN OR TECHNICAL PARAMETER INPUT AND SOURCES

The as-run AGR-5/6/7 thermal calculation used daily (24-hour) time steps, i.e. the same high resolution daily time steps used in the as run analyses for AGR-1, AGR-2, and AGR-3/4. The high-resolution daily time steps calculation was necessary to provide daily compact and component temperatures. Daily helium-neon gas compositions were also part of the thermal model input data. The gas compositions in each capsule were used to control the capsule temperature and were regulated daily. To match the daily gas composition changes, daily heat rates were input from a neutronics/physics calculation to the thermal model. The daily heat rates accounted for the daily core and lobe power fluctuations, outer shim control cylinder (OSCC) movements, and neck shim withdrawals. The thermal model and analysis were expected to be more accurate using daily calculated heat rate and fluence inputs.

The AGR-5/6/7 fuel compacts were irradiated for a total of 360.9 effective full power days (EFPD). This was accomplished over nine ATR cycles. The total number of time steps analyzed in the thermal model was 408, which included 10 days in which the ATR was at zero power due to reactor scrams during a cycle. The zero-power scram durations were often longer than 24 hours.

4.0 EXPERIMENT DESCRIPTION AND OTHER BACKGROUND DATA

A thermal finite element model has been created for the five capsules comprising the AGR-5/6/7 experiment. Previous thermal models [1], [2], [3] of the AGR-1, AGR-2, and AGR-3/4 experiments have been successful in the past. The AGR-5/6/7 Irradiation Test Final As-Run Report [4] discusses the overall experiment in detail. The AGR-5/6/7 experiment was composed of five separate stainless-steel capsules all welded together. There were a total of 194 fuel compacts with 170 in the AGR-5/6 portion and 24 in the AGR-7 portion. Heat rates and fast neutron fluence were input from a detailed physics analysis using the Monte Carlo N-Particle (MCNP) code [5]. Individual heat rates for each non-fuel component were input as well. ATR outer shim control cylinders and neck shim rods along with ATR driver fuel power and fuel depletion were incorporated into the physics heat rate calculations. Surface-to-surface radiation heat transfer along with conduction heat transfer through the gas mixture of helium-neon (used for temperature control) was used in the thermal calculations. Each capsule had its own helium-neon mixture. Graphite shrinkage due to the fast neutron fluence and graphite thermal expansion was incorporated into the model. Gas gaps changed as a function of fast neutron fluence and thermal expansion. This is a large model with more than 1 million finite element brick elements.

More than 150 parts were modeled in the finite element model and communicate with each other from a heat transfer sense. More than 50 thermocouples (TCs) were used in the experiment and calculation results are compared to actual measurements.

The AGR-5/6/7 experiment was placed in the northeast flux trap of the ATR as shown in Figure 1. The experiment is comprised of five individual capsules all welded together in a vertical orientation as shown in Figure 2 (top at left, water flowing down). The outside diameter of the stainless-steel capsules is 2.765 in., with a total experiment length of approximately 48 in. Each capsule contains TRISO compacts that are nominally 0.5 in. diameter with a length of 1.0 in. Capsules 1 and 5 have a TRISO fuel particle packing fraction of 40%, while capsules 2-4 have a packing fraction of 25%. The particles are bound together by a carbon matrix material.

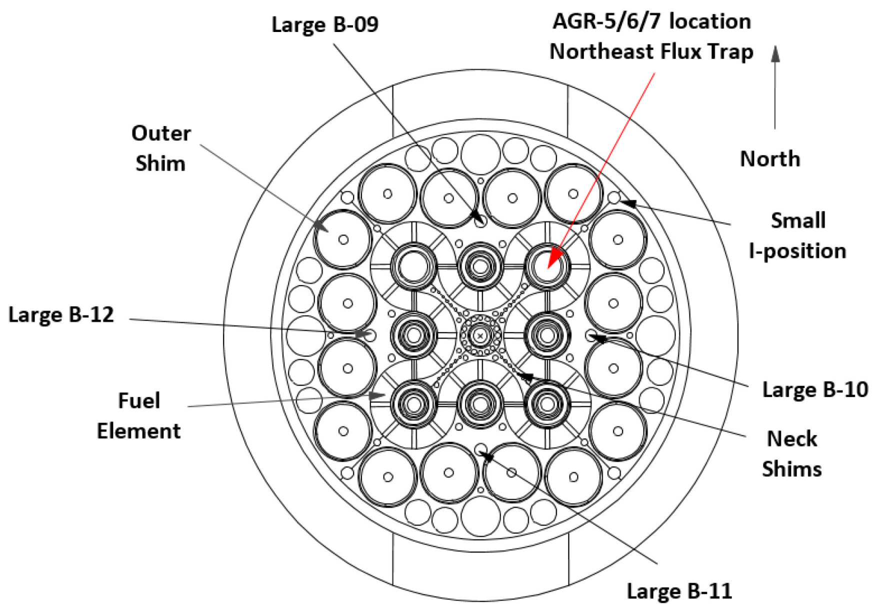

Figure 1. ATR core cross section showing the northeast flux trap position containing the AGR-5/6/7 experiment.

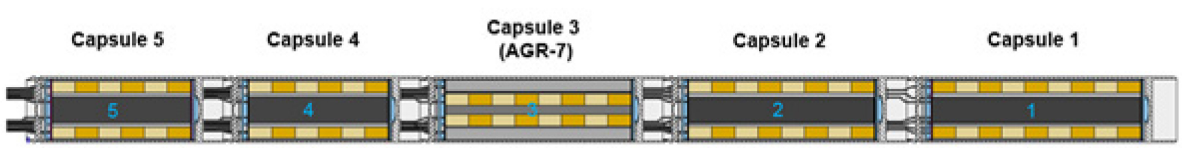

Figure 2. Capsule layout diagram (capsule 5 on top, vertical experiment).

Coolant water flows downward on the outside of the capsules at approximately 40 ft/s and enters the experiment at 125°F. Capsule cross section views are displayed in Figure 3. Capsule 1 has 10 stacks, while capsules 2, 4, and 5 have four stacks, and capsule 3 has three stacks arranged in an inner graphite holder to raise the temperature. Thru tubes are in capsules 2-5 to hold the thermocouple wires and gas lines.

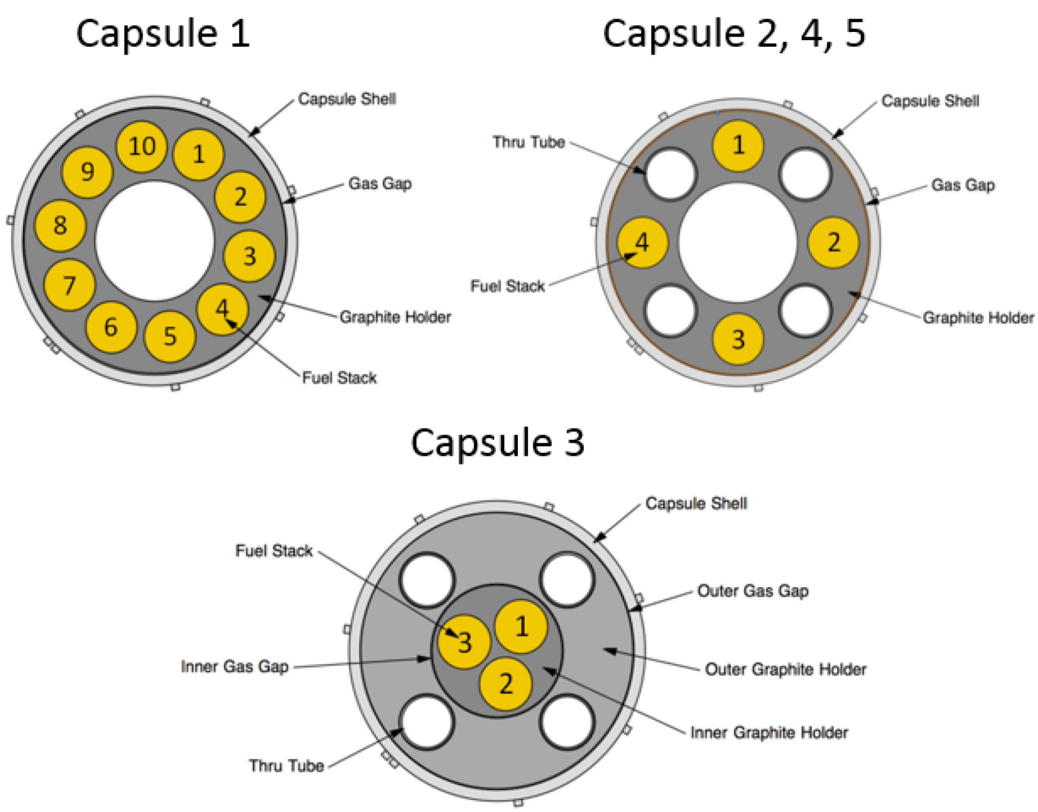

Figure 3. Capsule cross-sectional view for the five capsules.

A summary of the capsule particles, fuel target temperatures, and gas gap between the graphite holder and stainless-steel capsule wall are discussed in the AGR-5/6/7 thermal safety ECAR [6]. Approximately 54% of the particles are in capsule 1. Hot gas gaps are listed in the last column. These hot gas gaps (between the graphite holder and the inside diameter of the capsule) were designed to shape the temperature profile of the compacts. Three different methods were available to control the temperature in each capsule: (1) adjust the helium/neon gas mix, (2) adjust the northeast lobe power, and (3) change the neutron filter on the outside of the experiment. The neutron filter could only be changed during the shutdown time between cycles.

Table 1. Capsule summary for length, compacts, particles, target temperature range, and hot gas gaps.

Capsule Summary					
	Fueled Region Length (in)	Number of Compacts	Number of Particles	Target Temperature Range (°C)	Hot gas gap top half / Hot gas gap bottom half (in)
Capsule 5	6.0	24	82,608	<900	0.013 / 0.008
Capsule 4	6.0	24	54,600	900 – 1050	0.010 / 0.008
Capsule 3	8.0	24	54,600	1350 – 1500	0.008 / 0.006 / 0.008
Capsule 2	8.0	32	72,800	900 – 1050	0.007 / 0.008
Capsule 1	9.0	90	309,780	900 - 1350	0.006 / 0.008

Totals	37.0	194	574,388	

5.0 ASSUMPTIONS

1. All dimensions are based on nominal drawing values.
2. A shrinkage of 0.035 in. was used for all capsule welds.
3. Thermal properties for water were multiplied by 1000 in the X and Y directions to simulate mixing per guidance in GDE-588.
4. The average compact diameter for each fuel stack and the appropriate graphite holder hole were used to calculate the compact-holder gas gap.
5. Thermal expansion of the graphite holder varying with fast neutron fluence and temperature was implemented
6. Mass flow rates and heat transfer coefficients come from ECAR-2966 [6] page A30. (Flow between filter and flux trap was input incorrectly, but had very negligible fuel temperature difference when corrected)
7. Compact and various component heat rates were taken from [7].
8. Graphite and compact thermal conductivity vary with fluence and temperature.
9. The gas mixture ((i.e., helium and, neon) thermal conductivity is correlated from a report from Brown University [8].
10. Heat transfer through gas is done by conduction and radiation only and not advection.
11. Radiation heat transfer occurs across all gas gaps. An emissivity of 0.3 was assumed for the stainless steel, an emissivity of 0.90 for the graphite and grafoil, and an emissivity of 0.52 for the zirconium and zirconia components.
12. The contents of the through tubes are not specifically modeled. A heat flux representing the heat generated from these TCs and gas lines is implemented for each through tube for each capsule. More details in the Excel spreadsheet.
13. Graphite holder annulus mean radial temperature located at each 1.0 in. of elevation located on southeast side of annulus was used for thermal expansion calculations.
14. An effective thermal conductivity for the spring located in capsule 1 was calculated. Results are in the Excel spreadsheet for AGR-5/6/7 calculations and noted in the files section of this ECAR.
15. Perfect thermal contact between compacts is assumed.
16. A thickness for the Neolube was assumed for each capsule and discussed in the model description. This decreased the gap between the graphite holder and capsule wall for each capsule.

6.0 COMPUTER CODE VALIDATION

ABAQUS Version 6.14-2 [9] was used to do the mesh creation, boundary conditions, solving, and post processing. The High-Performance Computing computer named Falcon was used to run ABAQUS. Appendix A is the validation report of ABAQUS Version 6.14-2 run on Falcon. The report is comprised of 12 thermal models validating different aspects of ABAQUS' heat transfer abilities. The maximum difference between the ABAQUS-calculated values and exact theoretical values is just under 2.25%. Many of the test problems have 0% error. For the steady state MP-2 calculations, each run (consisting of 1 timestep with 7 iterations) was done with eight CPUs running in parallel. The average run took approximately 18 minutes of wall clock.

Falcon Specifications

Overview

- 34992-core SGI ICE X distributed memory cluster
- 36 cores per node
- 121.5 TB total memory
- FDR InfiniBand Network (56 Gbit/s), Single-Plane Enhanced Hypercube Topology
- SUSE Linux Enterprise Server 12 Service Pack 4 operating system
- LINPACK: 1087.58 TFlops
- ECCN: 4A003.c

2 Login Nodes

falcon1, falcon2

- 2 Intel Xeon E5-2695 v4 CPUs
    - Broadwell chipset
    - 18 cores per CPU
    - 2.10 GHz
- 128GB of RAM
- FDR InfiniBand Interconnect

972 Compute Nodes with:

- 2 Intel Xeon E5-2695 v4 CPUs
    - Broadwell chipset
    - 18 cores per CPU
    - 2.10 GHz
- 128GB of RAM
- FDR InfiniBand Interconnect

7.0 MODEL DESCRIPTION

A finite element heat transfer model with heat generation and water flow was created in ABAQUS to model the AGR-5/6/7 experiment. Figure 4 shows a cut-away view of the finite element mesh of the entire capsule train with capsule 5 on the left. There are approximately 1,200,000 hexahedral finite element bricks in the model. Figure 5 shows the finite element mesh of capsule 1. The figure shows the TCs and gas lines protruding out of the top. There are no thru tubes in this capsule. There are 10 stacks of fuel. These capsules are designed to transfer heat in the radial direction as zirconia insulators and gaps are placed on top and bottom of the capsule to insulate it in the axial direction. The top of capsule 1 is an exception as a ring spring on the bottom pushes up on the graphite holder and fuel and making good contact with the top. This was done since there is a lot of heat generation at the top of the fuel, and it can conduct out through the top stainless steel cap and into the coolant water. The top and bottom caps of all the capsules are tapered to remove material and hence gamma heat. There are very small gas gaps between the TC and its sheath and between the sheath and the graphite holder. Figure 6 shows the finite element mesh of capsule 2 and represents capsules 4 and 5 also since they are similar. The thru tubes (made of stainless steel) and thru tube protective sleeves (molybdenum) along with TCs and gas lines are protruding out the top of the top cap. Gamma heat produced from the gas lines and TCs that go through the thru tubes is modeled as a surface heat flux on the inside of the thru tubes as discussed in the assumptions.

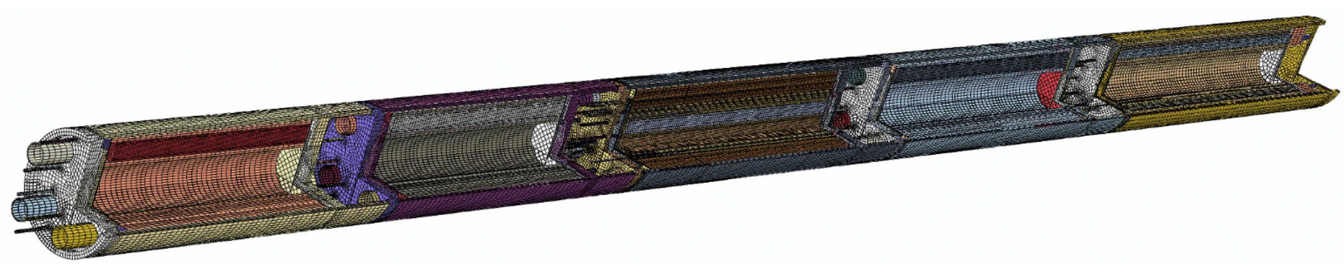

Figure 4. Cut-away view of finite element mesh of entire capsule train. Capsule 5 (top) on left.

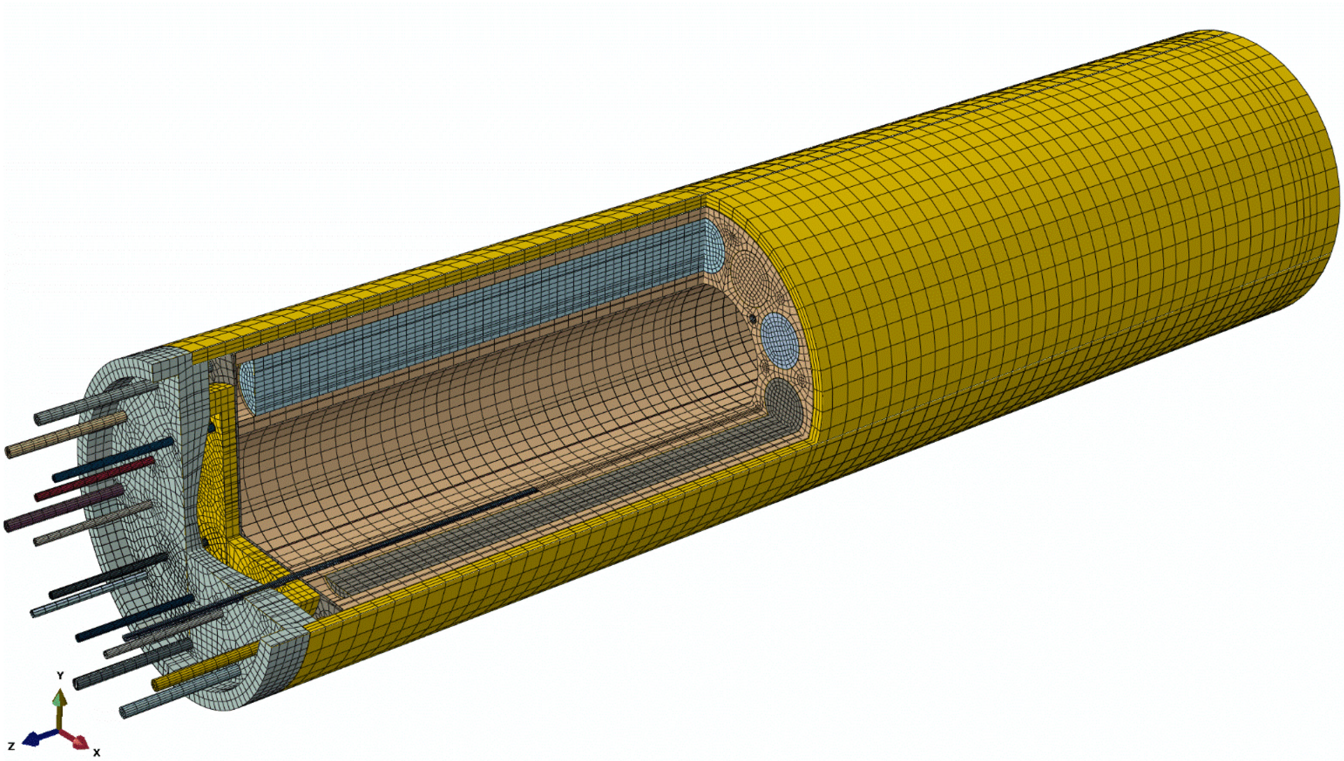

Figure 5. Cut-away view of finite element mesh of capsule 1 (top on left).

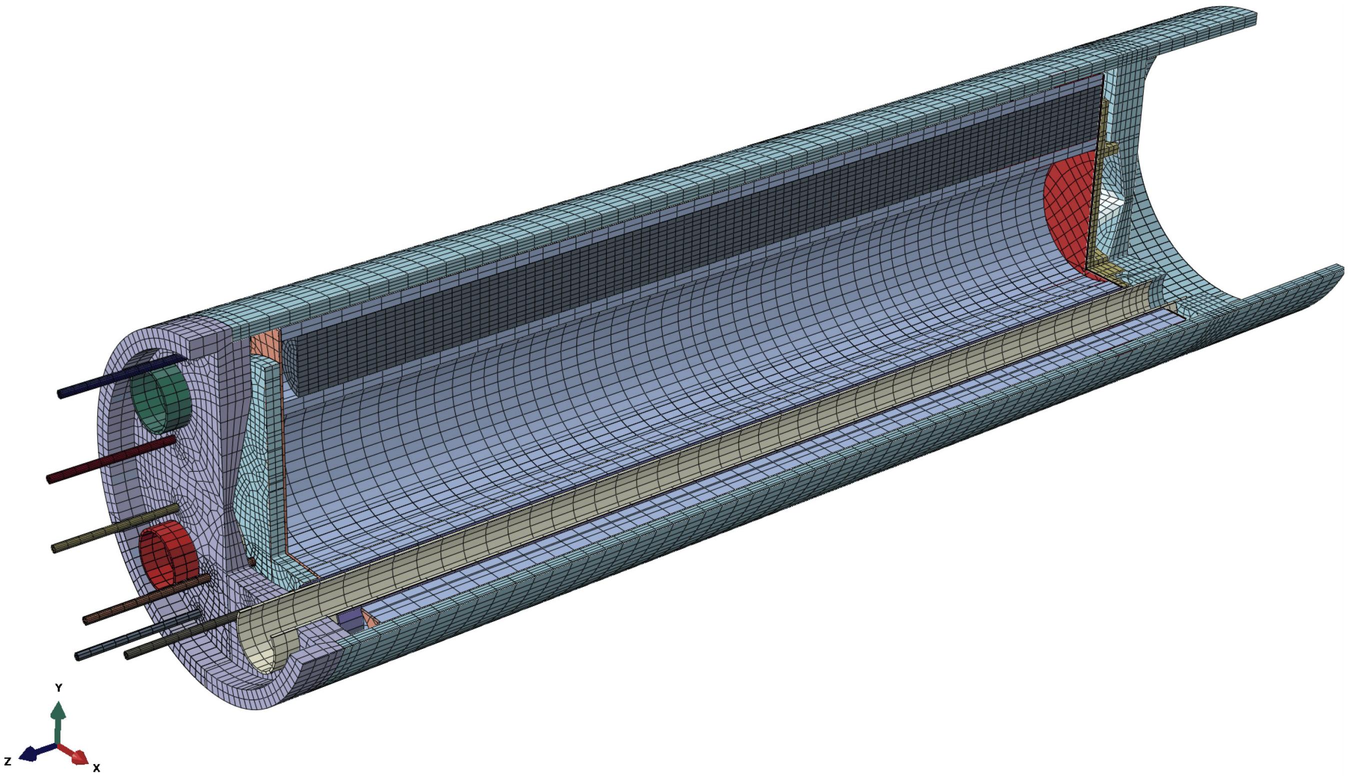

Figure 6. Cut-away view of finite element mesh of capsule 2.

Shown in Figure 7 is a cut-away view of the inside and outside graphite holders and fuel stacks of capsule 3. As noted in Table 1, there are three different outside diameters of the outside holder in order to obtain the temperature distribution necessary. The fuel stacks are all inside the inside graphite holder and run at very high temperatures as noted in Table 1. The actual measured fuel stack height was implemented in the model. Note that the fuel stacks do not go all the way to the top of the graphite holder. Holes bored in the graphite holders for the TCs can be seen. Figure 8 shows a cut-away view of the finite element mesh of capsule 3 with the thru tubes, thru tube liners, and TCs protruding out of the top. A plenum area between the capsules allows for the bending of the TCs and gas lines from the thru tubes above and into their individual holes for the capsule below. This plenum is very cool since there is only a small amount of gamma heat being produced and coolant water running along the outside of the capsule wall. The TCs and thru tubes were modeled as protruding upwards 1.0 in. and radiate and conduct to the cooler plenum walls. Perfect contact is assumed between the TCs and capsule top cap as they were brazed in place. The same is also true for the thru tube protective sleeves and top cap.

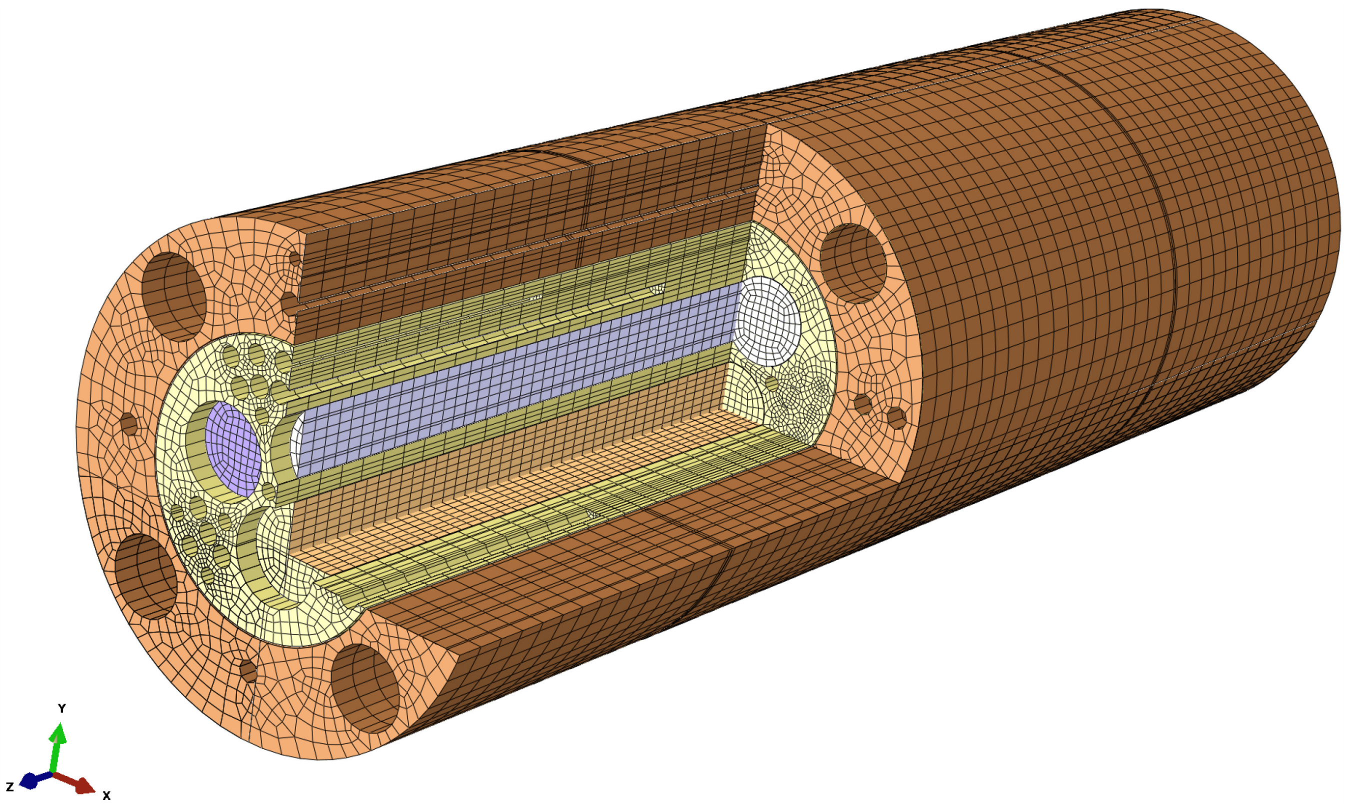

Figure 7. Cut-away view of finite element mesh of inner and outer graphite holder for capsule 3.

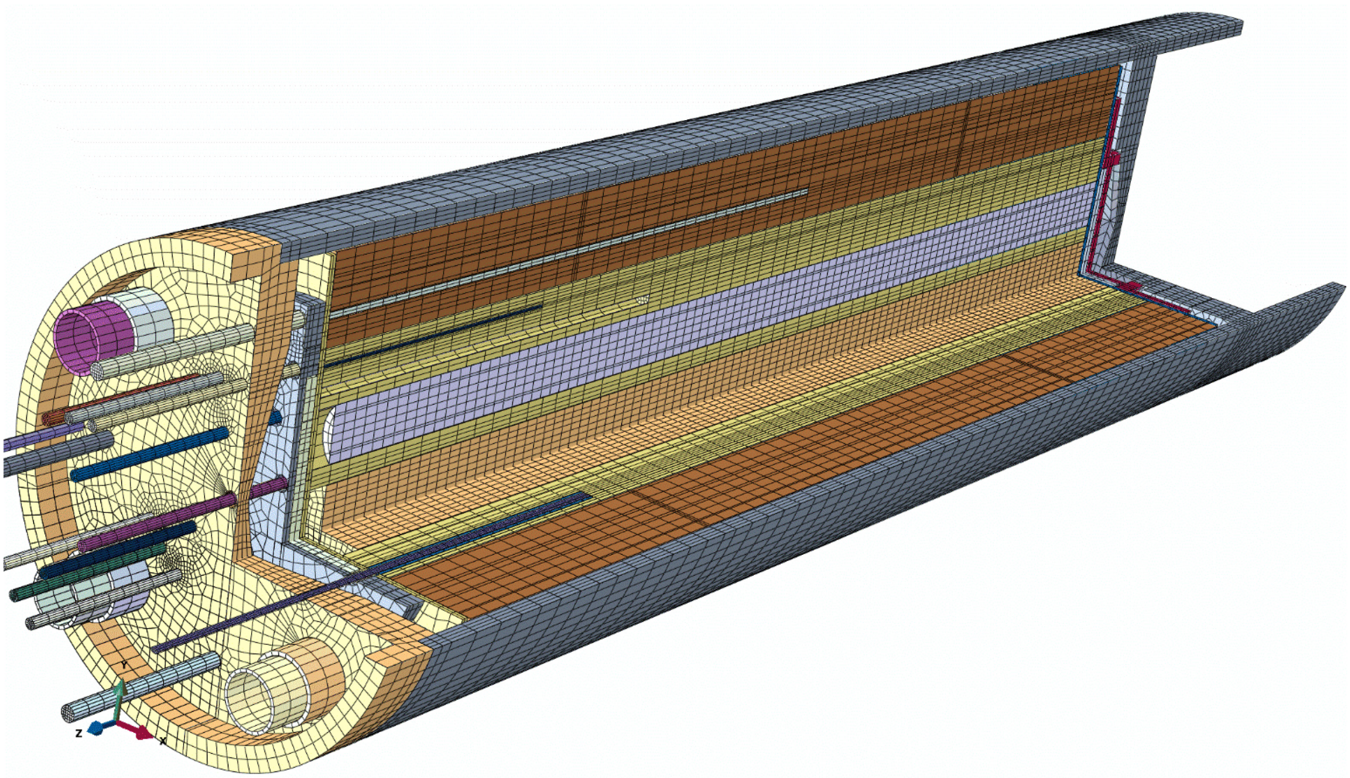

Figure 8. Cut-away view of finite element mesh of capsule 3.

Fuel Compacts

The fuel compact thermal conductivity was taken from correlations presented by Gontard and Nabielek [10] which gives correlations for conductivity, taking into account temperature, temperature of heat treatment, neutron fluence, and TRISO-coated particle packing fraction (where packing fraction is defined as the total volume of particles divided by the total volume of the compact). The packing fraction for compacts in capsules 1 and 5 was modeled at 0.393, while capsules 2,3,4 was modeled at 0.261.

In this work, the convention used to quantify neutron damage to a material is neutron fast fluence, (n/m^2, E_n >0.18 MeV) where E_n is the neutron energy with units of MeV, yet in the work by Gontard, the unit used was the dido nickel equivalent (DNE). In order to convert from the DNE convention to the fast fluence > 0.18 MeV, the following conversion [11] was used:

$$\Gamma_{>0.18MeV} = 1.52\Gamma_{DNE} \quad (1)$$

where Γ is neutron fluence in either the > 0.18 MeV unit or DNE. The correlations in the report by Gontard account for the compact matrix thermal conductivity varying with temperature and fast neutron fluence. This matrix conductivity correlation was further adjusted to account for differences in fuel compact density. The correlations were developed for a fuel compact matrix density of 1750 kg/m^3, whereas the compact matrix used in AGR-5/6/7 had a density of 1728 kg/m^3 for capsules 1 and 5, and a density of 1757 kg/m^3 for capsules 2,3, and 4. The thermal conductivities were scaled according to the ratio of densities (0.987 for capsules 1 and 5) (1.004 for capsules 2,3,4) to correct for this difference.

The actual fuel compact thermal conductivity took the above described matrix conductivity varying with temperature, fast neutron fluence, and density ratio and was further enhanced by the Chiew & Gland correlation [12] which accounts for particles in a matrix. Figure 9 shows a three-dimensional plot of the fuel compact thermal conductivity for capsules 1 and 5 varying with fast neutron fluence and temperature using the Chiew & Gland correlation for particles in a matrix described as:

$$\frac{k_e}{k_m} = \frac{1+2\beta\varphi+\left(2\beta^3-0.1\beta\right)\varphi^2+0.05\varphi^3 e^{4.5\beta}}{1-\beta\varphi} \qquad (2)$$

$$where\ \beta = \frac{\kappa - 1}{\kappa + 2} \quad and\ \kappa = \frac{k_p}{k_m}$$

where k_e is the effective thermal conductivity, k_m is the matrix thermal conductivity (23.6 W/m-K), k_p is the particle thermal conductivity (4.13 W/m-K), and ϕ is the particle packing fraction. Capsules 2,3, and 4 have a slightly higher thermal conductivity due to the correction factor in Eq 2.

For fluences greater than 1.0×10^{25} neutrons/m^2 (E_n > 0.18 MeV), the conductivity increases with temperature because of the annealing of radiation-induced defects in the material is accelerated at higher temperatures.

The compacts are assumed to have perfect contact with the bottom graphitic material (grafoil). The gaps between the compacts and holder are calculated from as-built dimensions [13] and [14]. Each compact was measured and compared to each hole in each graphite holder. The exact as-built dimensions were implemented for every stack top half and bottom half. Heat is transferred via gap conductance and gap radiation. Gap radiation between the compacts and graphite holder was implemented with both surfaces having an emissivity of 0.9.

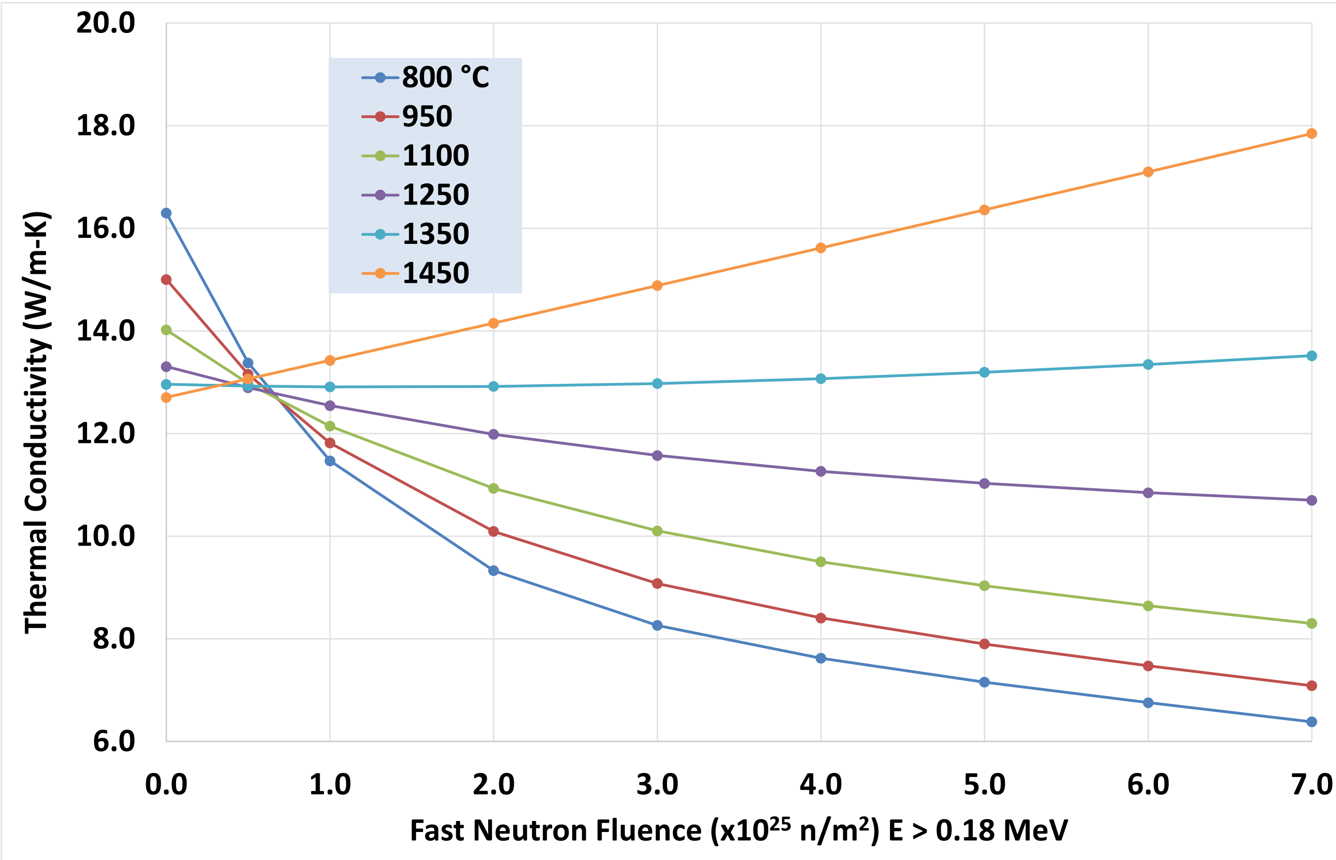

Figure 9. Thermal conductivity (W/m-K) varying with fast neutron fluence and temperature for capsules 1 and 5.

Graphite Holders

The graphite holders are made from IG-430 nuclear grade graphite. Experiments conducted on graphite specimens at the INL [15] were used to obtain material properties such as unirradiated and irradiated thermal diffusivity, and graphite shrinkage due to fast neutron fluence. Specific heat values were taken from [16] and implemented in the following equation with temperature in Kelvin.

$$c_p = \frac{1}{11.07 \cdot T^{-1.644} + 0.0003688 \cdot T^{0.02191}} \left(\frac{J}{kg \cdot K}\right) \tag{3}$$

Density was calculated from the following set of equations considering the expansion of graphite with temperature:

$$\Delta L = \alpha L(T - T_0), \quad \rho(T) = \rho_0 \frac{V_0}{V(T)}, \quad V_0 = L_0^3, \quad V(T) = (L_0 + \Delta L)^3$$

$$\rho(T) = \frac{\rho_0}{[1 + \alpha(T - T_0)]^3} \tag{4}$$

Where T_0 was taken as 20°C. Values of ρ_0 (1.815 g/cm^3) and α_0 (5.5e-6 1/°C) were taken from [17] and [18] respectively. To account for change of conductivity due to neutron damage, a conductivity multiplier [19] taken from JAEA was implemented comparing irradiated graphite to unirradiated graphite at each temperature. To convert the Japanese multiplier data [20] from dpa to fast neutron fluence a conversion multiplier of 0.763*fluence=dpa (fluence units scaled by 1x10^{25}) was implemented and is specific to the northeast flux trap of ATR. The fluence energy band is E>0.18MeV and units of 1x10^{25} n/m^2. To convert from the Japanese data of E>0.10MeV, a multiplier of 0.9 * E>0.10MeV = E>0.18MeV was used. The multiplier and dpa to fluence conversion come from [20]. Unirradiated thermal diffusivity data for IG-430 taken from [15] is shown in Figure 10. Values above 1000°C and up to 1450°C were extrapolated. Unirradiated thermal conductivity varying with temperature was obtained by multiplying the diffusivity by the specific heat from Eq 3, and the density from Eq 4.

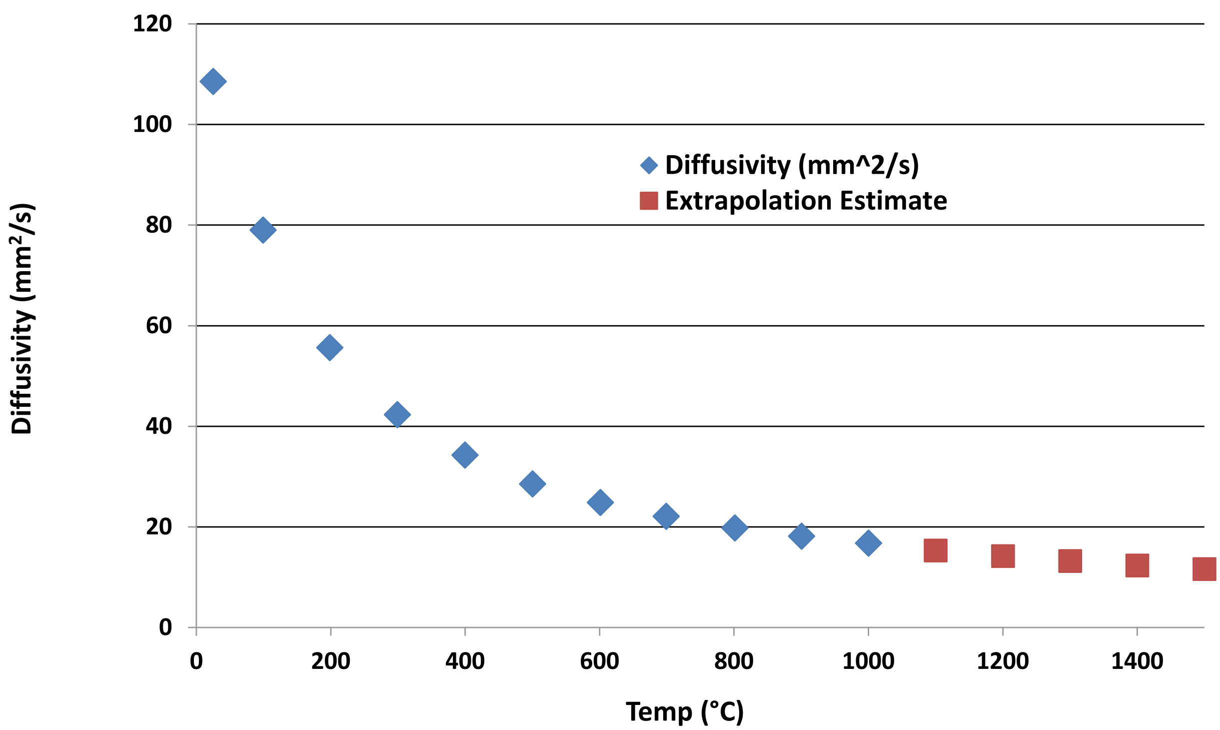

Figure 10. Unirradiated thermal diffusivity of IG-430 nuclear grade graphite.

Figure 11 shows a graph of the thermal conductivity multiplier [19] varying with temperature and fast neutron fluence. The author developed a curve fit for this data and is shown in Eq (5).

$$\frac{k_{irr}}{k_0} = (p_1 + p_2 \cdot T) + [1 - (p_1 + p_2 \cdot T)] \cdot exp\left(\frac{-F \cdot T}{p_3 + p_4 \cdot T + p_5 \cdot T^2}\right) \tag{5}$$

p_1 = 3.100e-02, p_2 = 5.613e-04, p_3 = 1.29077e+02, p_4 = -9.310e-01, p_5 = 1.826e-03

where T is temperature in °C and F is fast neutron fluence (x10^{25} n/m^2, E>0.18 MeV). Parameters $p1$ through $p5$ are listed in the equation.

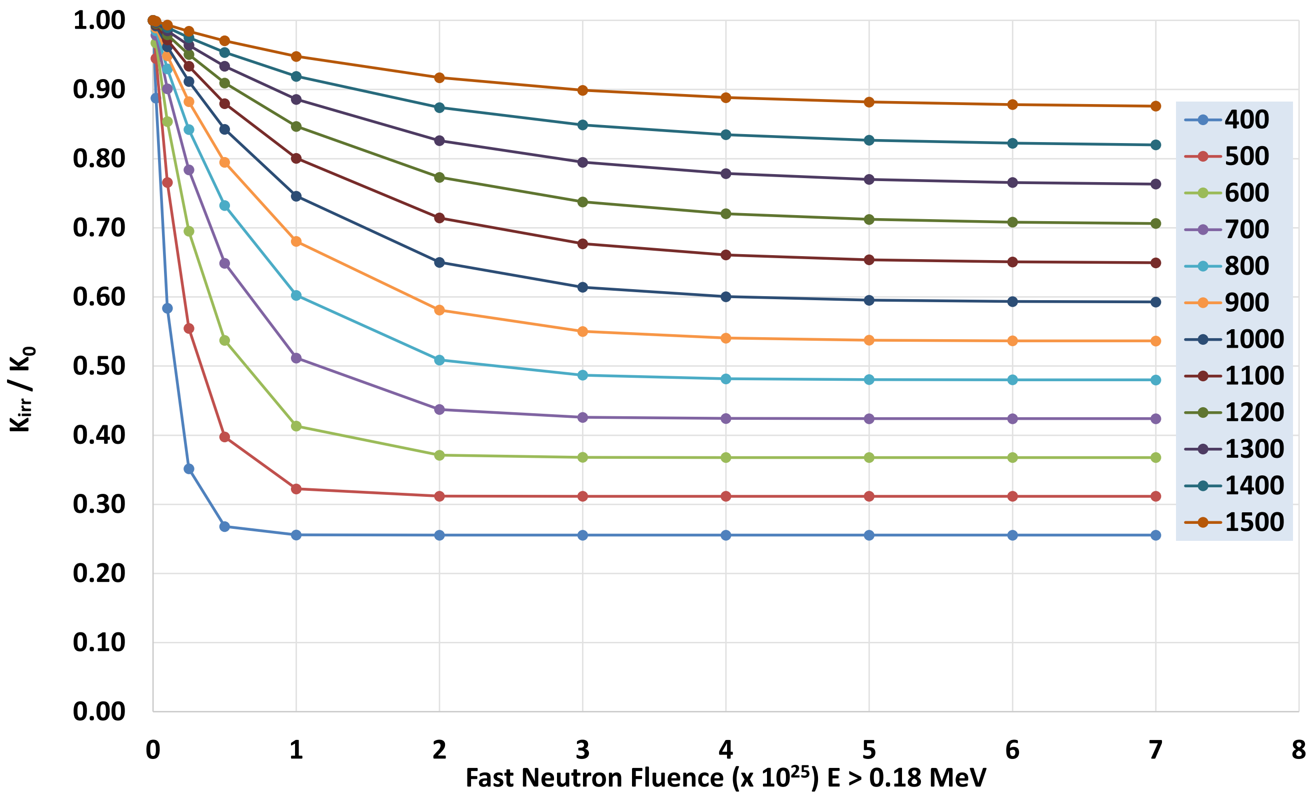

Figure 11. Conductivity multiplier (k_{irr}/k_0) varying with temperature (°C) and fast neutron fluence [19].

Figure 12 shows the thermal conductivity of IG-430 varying with temperature and fast neutron fluence incorporating the multiplier discussed above. Note a very fast drop off in conductivity for low temperature with a small amount of fast neutron fluence. There is almost no change in thermal conductivity above a fluence value of 3.

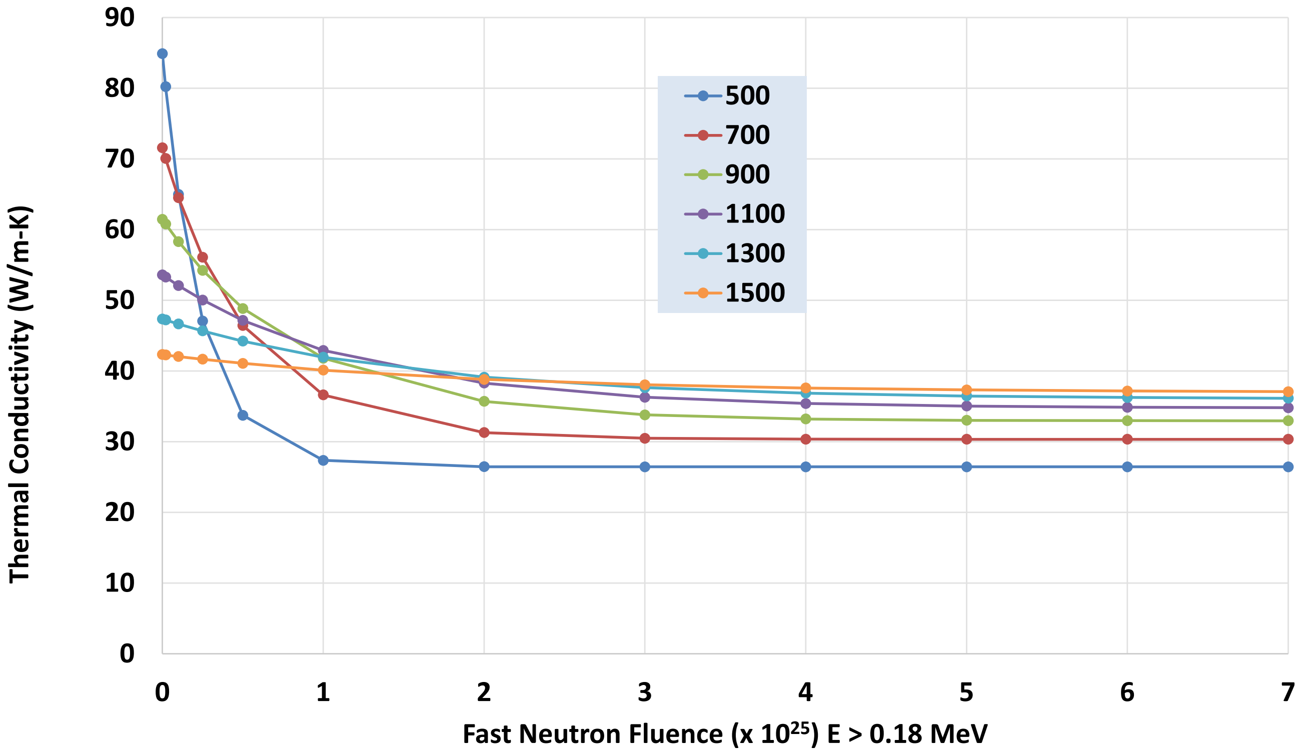

Figure 12. Thermal conductivity of IG-430 varying with temperature (°C) and fast neutron fluence.

Figure 13 shows a graph of the coefficient of thermal expansion multiplier [19] varying with temperature and fast neutron fluence. The author developed a curve fit for this data and is shown in Eq (6).

$$\frac{\alpha_{irr}}{\alpha_0} = 1 + (p_1 + p_2 \cdot T) \cdot F + p_3 \cdot T \cdot F^2 + (p_4 + p_5 \cdot T) \cdot F^3 \tag{6}$$

p_1 = 1.050e-01, p_2 = -2.974e-05, p_3 = -2.298e-05, p_4 = -3.007e-04, p_5 = 1.350e-06

where T is temperature in °C and F is fast neutron fluence (x10^{25} n/m^2, E>0.18 MeV). Parameters $p1$ through $p5$ are listed in the equation.

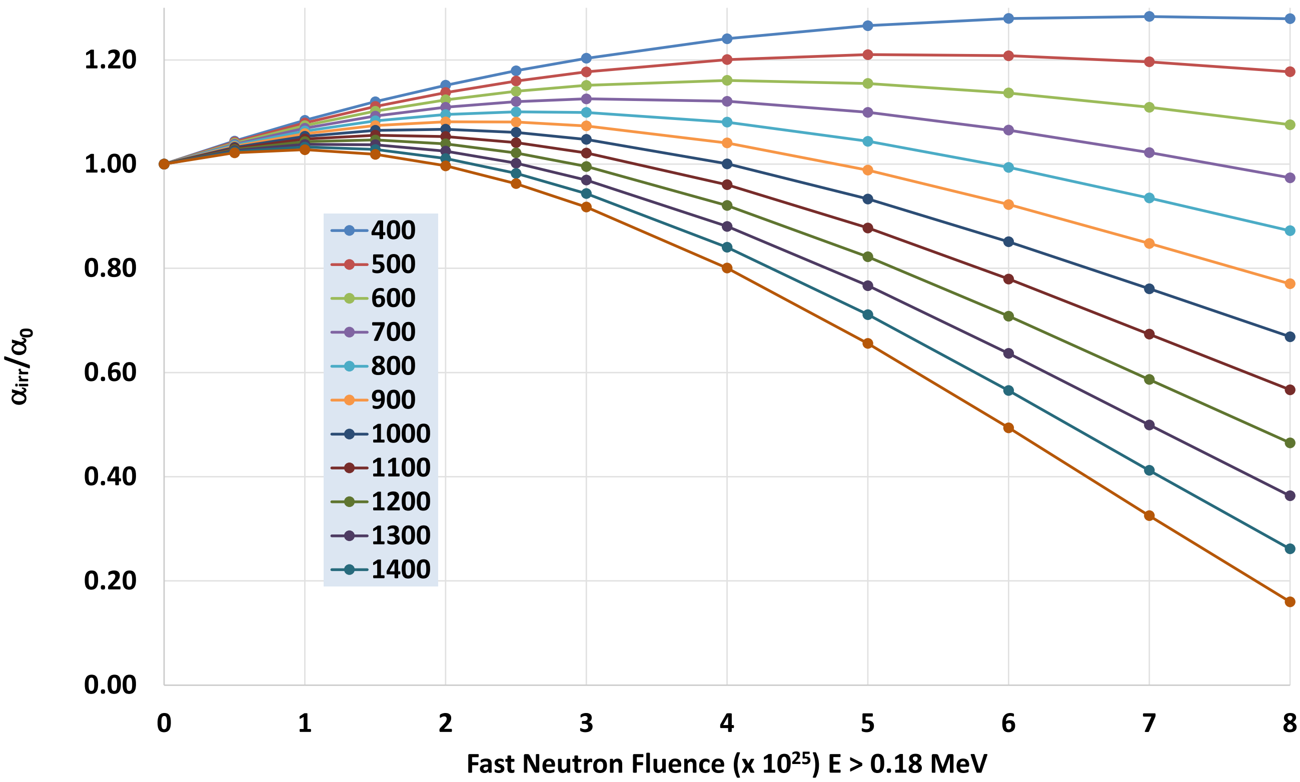

Figure 13. Coefficient of thermal expansion multiplier (α_{irr}/α_0) varying with temperature (°C) and fast neutron fluence [19].

Outer Gas Gaps

The graphite holders undergo neutron damage as irradiation progresses. The graphite also shrinks until a turnaround point and then starts to swell. For this AGR-5/6/7 experiment, this turnaround point is not reached. The diameter change of specimens from fast neutron fluence for IG-430 was taken from [21] and shown in Figure 14. This graphic shows that the outer diameter shrinks (orange), while the inner diameter grows (blue). Since no data was available concerning the inside diameter change of an annular shaped piece of graphite, the author and AGR irradiation team members decided to just invert the slope from the outside diameter. The slope is shown from linear curve fit to be -0.00146 $\Delta D/D$ per unit of fluence.

The helium-neon gas mixture thermal conductivity is shown in Figure 15 varying with neon fraction (NeF) and temperature. As mentioned earlier, these values come from [8].

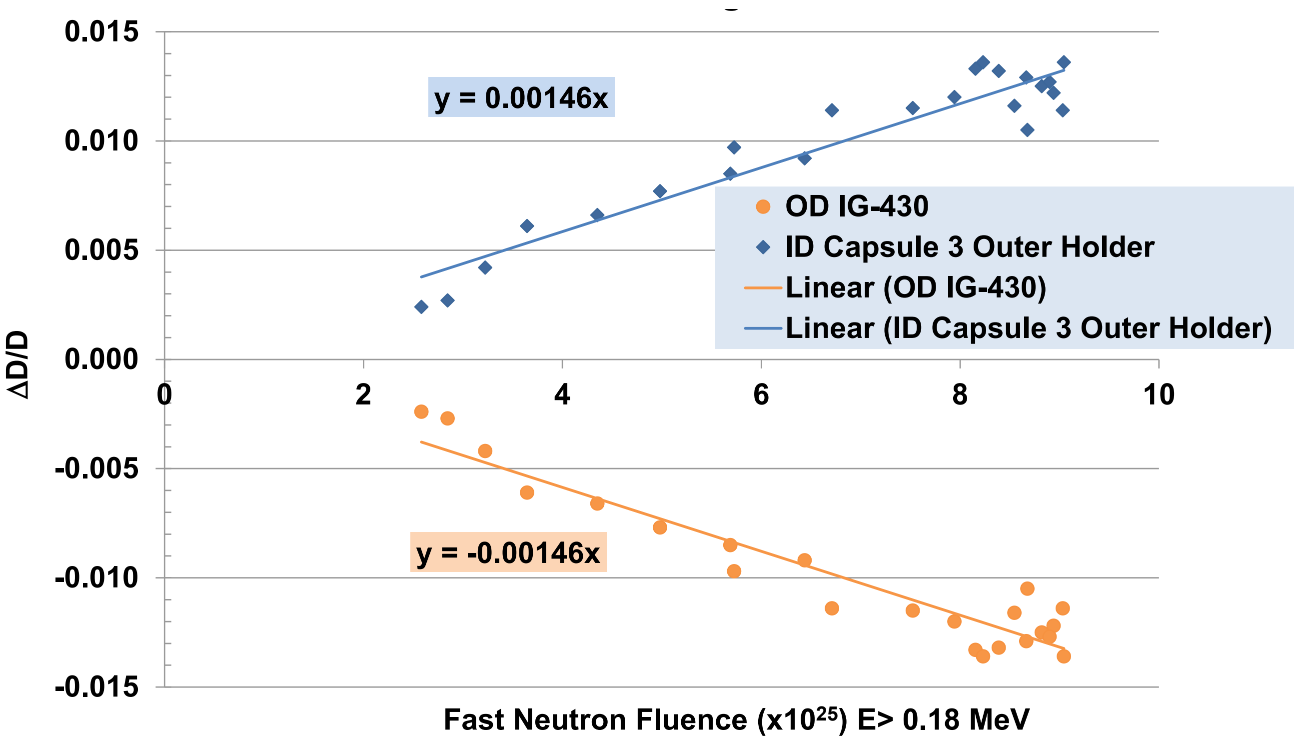

Figure 14. Diametral change of IG-430 varying with fast neutron fluence [21].

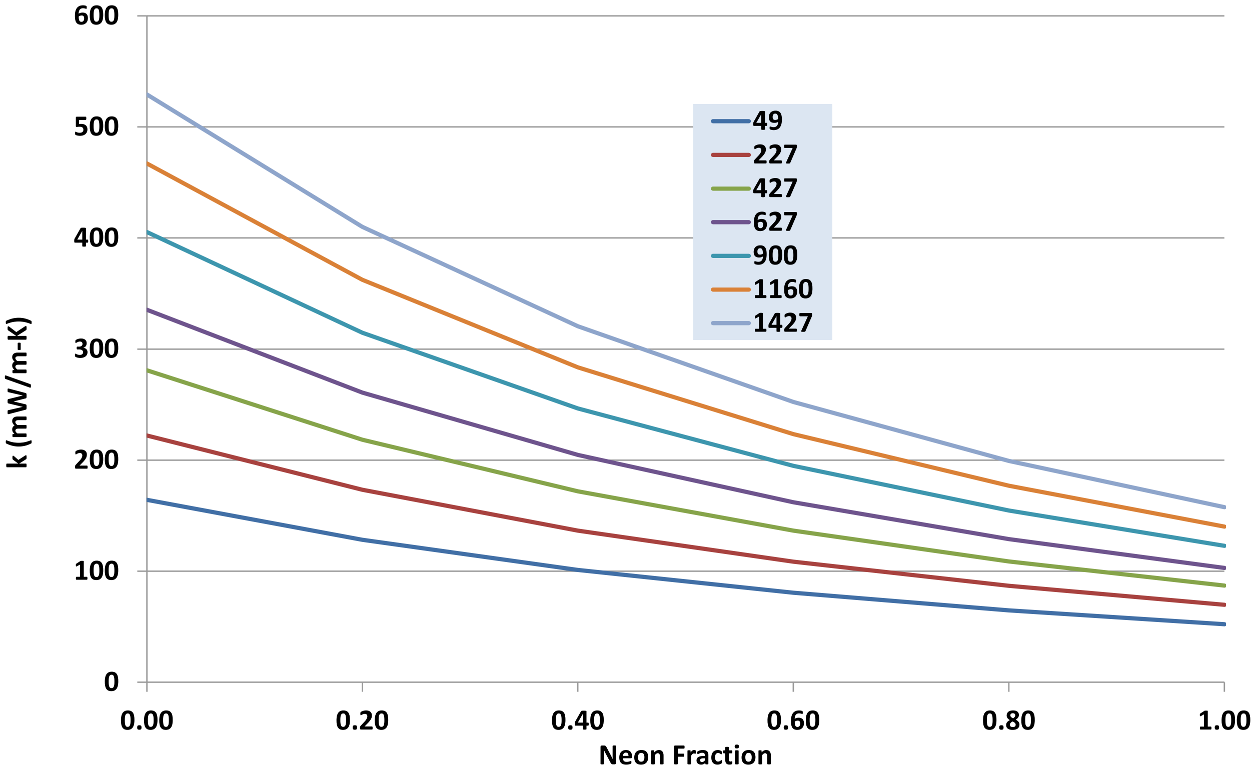

Figure 15. Helium-Neon gas mixture thermal conductivity (mW/m-K) varying with neon fraction and temperature (°C) [8].

The gap conductance user subroutine was used to calculate the heat transfer across the gap between the outside of the graphite holders and the stainless steel capsule wall. The surface temperature of the holder and capsule are made available to the subroutine. Eq. (7) shows the details of the gap conductance across this gap.

$$gap = \left[r_0[\alpha(T_i - T_0) + 1]\right]_{,ss} - \left[r_0\left[1 + \frac{\Delta r \cdot F}{r} + \alpha(F,T)(T_i - T_0)\right]\right]_{,holder}$$

$$gap\ conductance = \frac{kgas(T)}{gap} \quad where\ T = \frac{Ti,ss + Ti,holder}{2}$$

$$where\ T_{i,holder} = \frac{T_{inside,holder} + T_{outside,holder}}{2}$$

$$where\ \ i = instantaneous,\ \ 0 = original\ at\ room\ temperature$$

(7)

where $\Delta r/r$ is the slope from Figure 14. $kgas(T)$ is the gas mixture thermal conductivity and $\alpha(F,T)$ is described above. The average temperature between the inner and outer surface of the graphite holder is used. Since the inside surface temperature is not available in the subroutine, a vector of the inside surface temperature was obtained from the volumetric heat subroutine and passed into the gap conductance subroutine. Eq 8 shows the gap conductance between the inner and outer graphite holders for capsule 3.

$$gap\ inner3 = \left[r_0\left[1+\frac{\Delta r}{r}+\alpha(F,T)(T_i-T_0)\right]\right]_{,outer} - \left[r_0\left[1+\frac{\Delta r\cdot F}{r}+\alpha(F,T)(T_i-T_0)\right]\right]_{,inner}$$

$$gap\ conductance = \frac{kgas(T)}{gap\ inner3}\quad where\ T=\frac{Ti,inner+Ti,outer}{2} \tag{8}$$

Offset Holder Calculations

The graphite holders are held off the capsule wall by small nubs of graphite every 90°. The possibility exists for these nubs to wear down with the vibration in the reactor. There is also a slight bit of clearance between the outside of the nubs and the capsule wall. These nubs are left on the holder while still machining the outside diameter to the dimension needed for the gas gap. An offset calculation where the gas gap varies azimuthally is described below. While it is possible to move the holder and contents inside the capsule with the ABAQUS CAE model, this was not performed as part of the current analysis since the magnitude and direction the holder offset are unknown. During future analyses, several runs will be made to see which direction and how much offset needs to be performed for each capsule to minimize the temperature residual between the measured and calculated temperature values. This offset model is included in the gap conductance subroutine and is taken as the r_0 value of the holder. An offset in +/- x and +/-y is available for each capsule individually. These offset values are in the range of 0.001 in. Figure 16 shows a diagram of the outside (capsule) offset h units in the x direction and k units in the y direction from the graphite holder. Eq. (9) shows the calculations to obtain the x_o, and y_o values since x_i and y_i are given in the subroutine. Even though the finite element mesh model shows the capsule perfectly centered, this new gap will be used for the gap conduction equations in future analyses, but not this one.

Eq. 10 shows the root mean square for temperature difference. This was used for each day during the first cycle (162B) to show a measurement of how good the model is to the TCs when offsetting the holder in various directions.

$$a = \left(\frac{y_i}{x_i}\right)^2 + 1,\quad b = -2\cdot\left(\frac{y_i}{x_i}\right)\cdot k - 2\cdot h,\quad c = k^2 + h^2 - r_o^2$$

$$x_o = \frac{-b \pm \sqrt{b^2-4ac}}{2a},\qquad y_o = \pm\sqrt{r_o^2 - (x-h)^2} + k$$

$$gap = \sqrt{(x_0-x_i)^2 + (y_0-y_i)^2} \tag{9}$$

$$TRMS = \sqrt{\frac{\sum_{i=1}^{n}(Tmeasured - Tcalculated)^2}{n}} \tag{10}$$

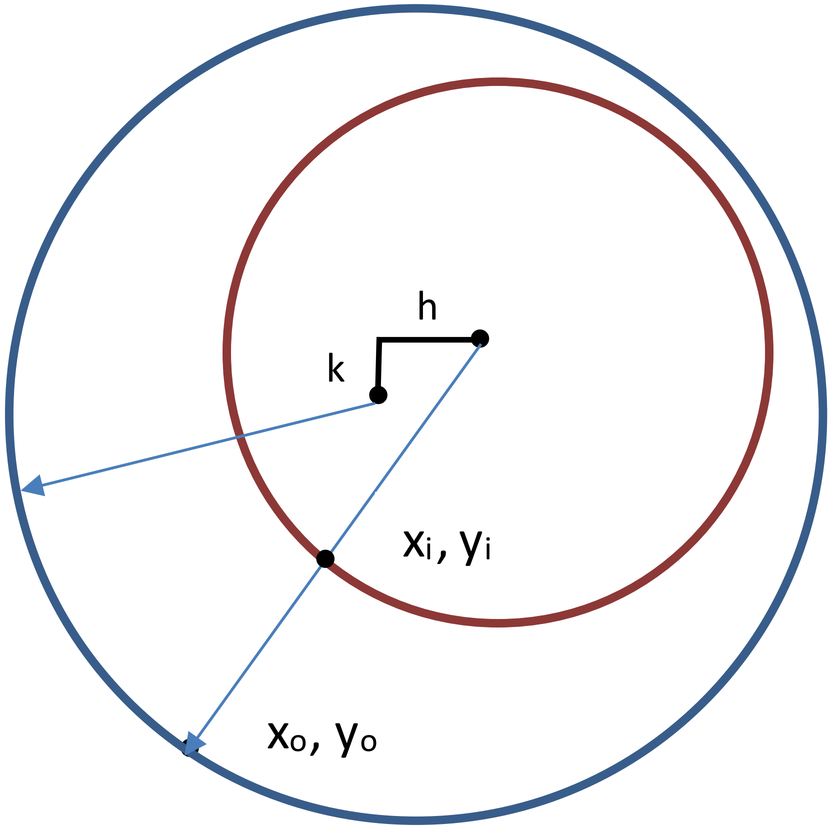

Figure 16. Diagram to calculate gap with capsule wall offset h units x direction and k units y direction.

Heat Rates

Heat rates are taken from results generated from the MCNP code [5] specific to the AGR-5/6/7 experiment and given in [7]. Heat rates were imported into the ABAQUS input file for each ¼ (or ¼ inch) of each compact (fission) and each 1.0 in. of the height of the graphite holders (gamma) for every day during irradiation. Gamma heat rates are also imported for the water, stainless steel capsules, thru tubes, TCs, and all the various components on the top and bottom of each capsule. Figure 17 shows volumetric heat generation rates (HGRs) of all the compacts imported from the physics calculations (top at left) during the first ATR cycle (162B) on the 20th day of irradiation (near the beginning of irradiation). Highest heat rates (166 W/cm^3) are at the top of capsule 1, while the lowest heat rates (61 W/cm^3) are at the bottom of capsule 1. The gamma heat rates for the graphite holders are in a typical chopped cosine profile and displayed for the same day in Figure 18 with the peak being 7.02 W/cm^3 and the minimum being 2.29 W/cm^3. Component heat rates for everything else in the model are shown in Figure 19. The contour color scale was adjusted in this figure to have a more even spread in colors since the zirconia heaters in capsule 3 generate considerable heat compared to the rest of the components.

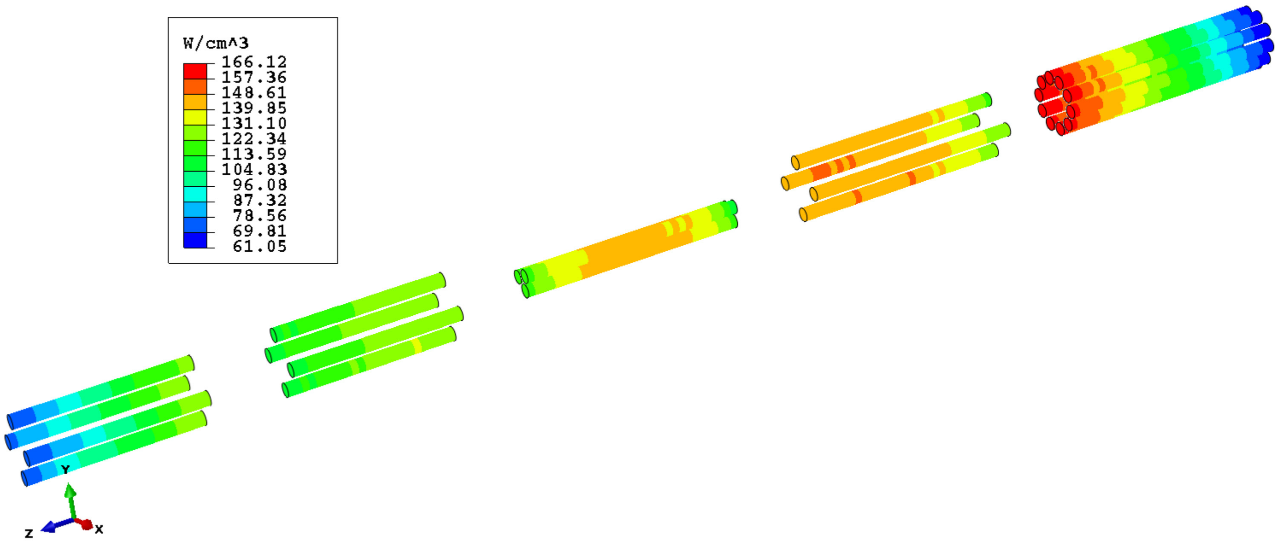

Figure 17. Compact heat rates (W/cm^3) for cycle 162B day 20.

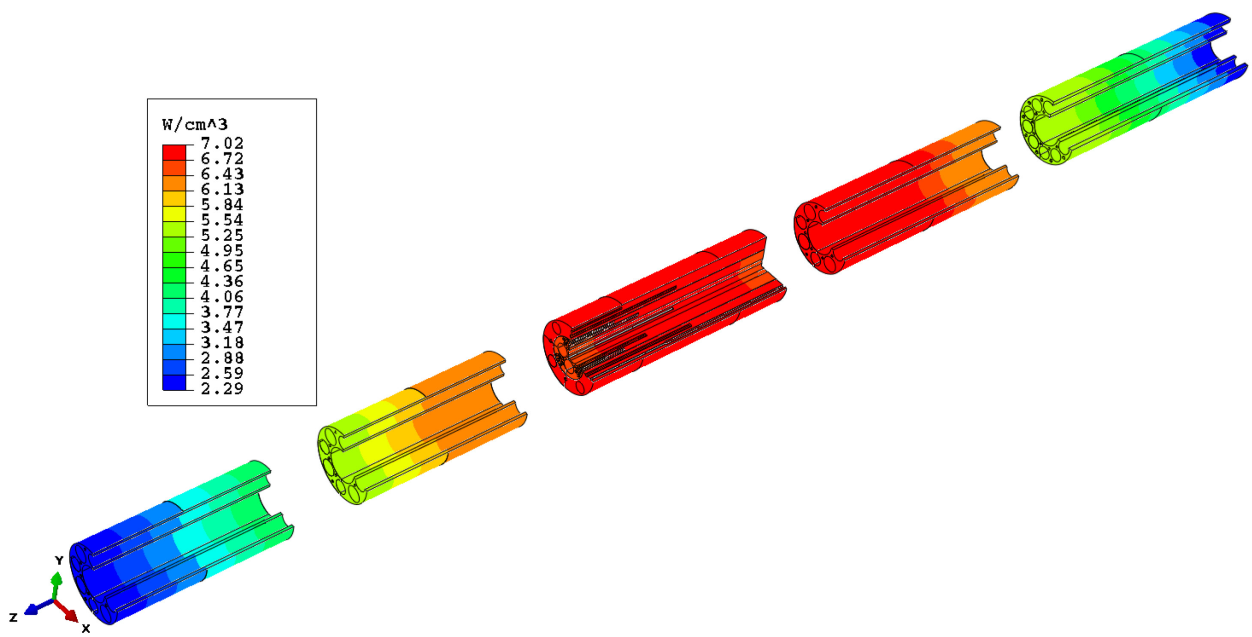

Figure 18. Graphite holders heat rates (W/cm^3) for cycle 162B day 20.

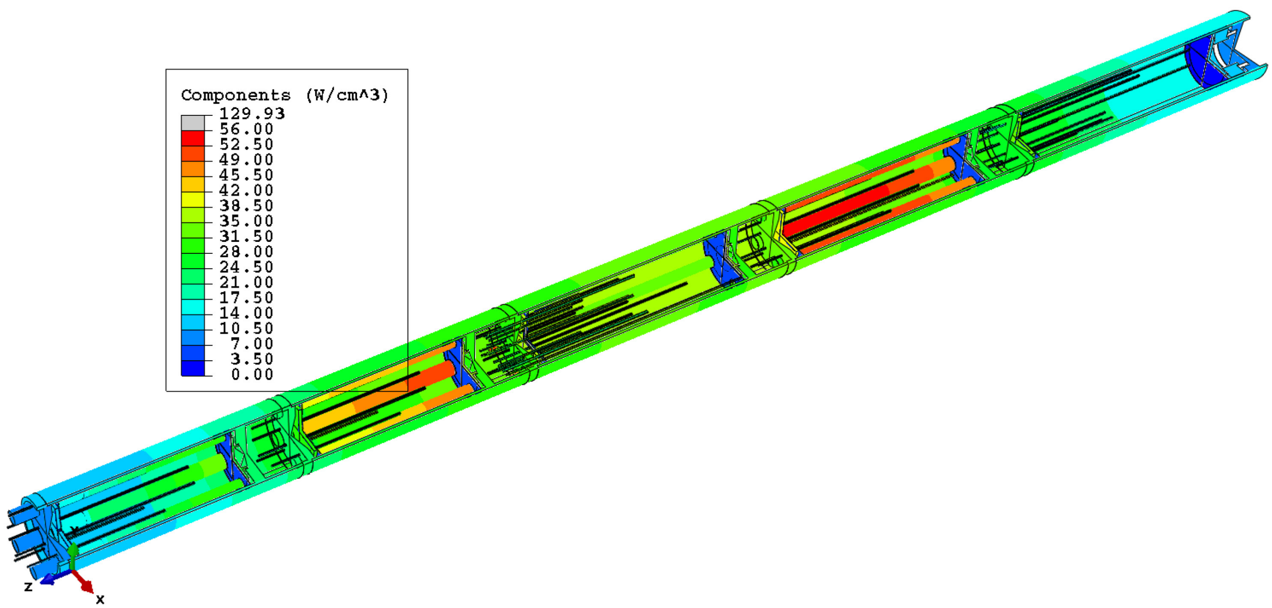

Figure 19. Component heat rates (W/cm^3) for cycle 162B day 20.

Fast Neutron Fluence

Fast neutron fluence (E>0.18 MeV) was imported from the physics calculations for each ¼ of a compact and each 1.0 in. for the graphite holders for each day of irradiation. The compact and graphite thermal conductivity depend on fast neutron fluence. The coefficient of thermal expansion multiplier for the graphite holders also depends on fast neutron fluence. In the ABAQUS model, the fast neutron fluence is taken as field variable # 2.

Conduction and Radiation Heat Transfer

The governing equation for steady-state heat transfer for the solids in the model is:

$$0 = \frac{\partial}{\partial x}\left(k(F,T)\frac{\partial T}{\partial x}\right) + \frac{\partial}{\partial y}\left(k(F,T)\frac{\partial T}{\partial y}\right) + \frac{\partial}{\partial z}\left(k(F,T)\frac{\partial T}{\partial z}\right) + \dot{q} \qquad (10)$$

where *T* is temperature, *x, y*, and *z* are Cartesian coordinate directions; *k(F,T)* is thermal conductivity that varies with fast neutron fluence and temperature, and *q* is the heat source. The equation solved for advection in the water is similar, but the left hand side takes into account the water temperature gradient, velocity, density, and specific heat.

The governing equation for radiation heat transfer across a two-surface enclosure is:

$$q_{net} = \frac{\sigma\left(T_1^4 - T_2^4\right)}{\dfrac{(1-\varepsilon_1)}{\varepsilon_1 A_1} + \dfrac{1}{A_1 F_{12}} + \dfrac{(1-\varepsilon_2)}{\varepsilon_2 A_2}} \qquad (11)$$

where q_{net} is the net heat flux, σ is the Stephan Boltzmann constant, T_1 and T_2 are the surface temperatures, ε_1 and ε_2 are the emissivities of surfaces 1 and 2 (post irradiation viewing (AGR-3/4) of fuel compacts, graphite surfaces, and stainless steel suggest that emissivity does not change with fluence), A_1 and A_2 are the areas of surfaces 1 and 2, and F_{12} is the view factor from surface 1 to 2. Radiation view factors for parallel disk to disk, ring to ring, and inside to outside of annuli were calculated using standard radiation view factor textbooks and implemented across each radial and axial gap.

Daily Gas Mixtures

The neon gas fraction for each day was calculated for each capsule using average daily flow rates for helium and neon through each capsule. These daily values are stored in the Nuclear Data Management and Analysis System (NDMAS) database for the AGR-5/6/7 experiment [22]. As discussed in [4], the gas mixture for Capsule 1 for cycle 168A could not be controlled as intended, so two extremes were considered: a neon fraction of zero and a neon fraction matching the leadout gas mixture.

Thermocouples and Thermocouple Sheaths

Each TC and TC sheath were individually modeled and placed in the correct location according to the capsule drawings. Perfect contact was assumed where the TCs are brazed to the top cap. An appropriate gap conductance was applied between each TC and its sheath and each sheath to the graphite holder. The TC temperature was taken as the average of the finite element temperatures at the tip of each TC. An adiabatic boundary condition was assumed between the tip of the TC and the graphite holder. This was done since the TCs were held off the graphite by the installers. All heat transfer was assumed to be radial. An individual heat generation rate for each day for each 1.0 in. of each TC and TC sheath was implemented from the neutronics calculations. Figure 20, Figure 21, and Figure 22 show the finite element mesh of TC-1-8 and sheath with color contours of HGR for the same day.

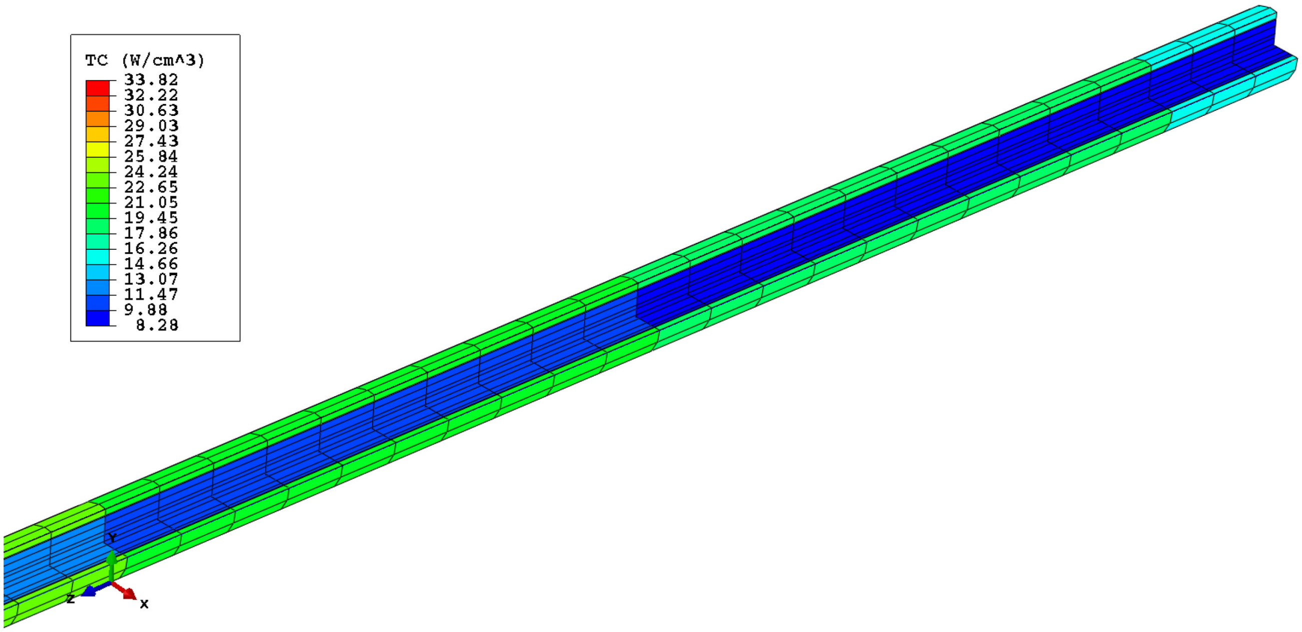

Figure 20. Finite element mesh cut-away view of HGR (W/cm^3) for TC-1-8 cycle 162B day 20.

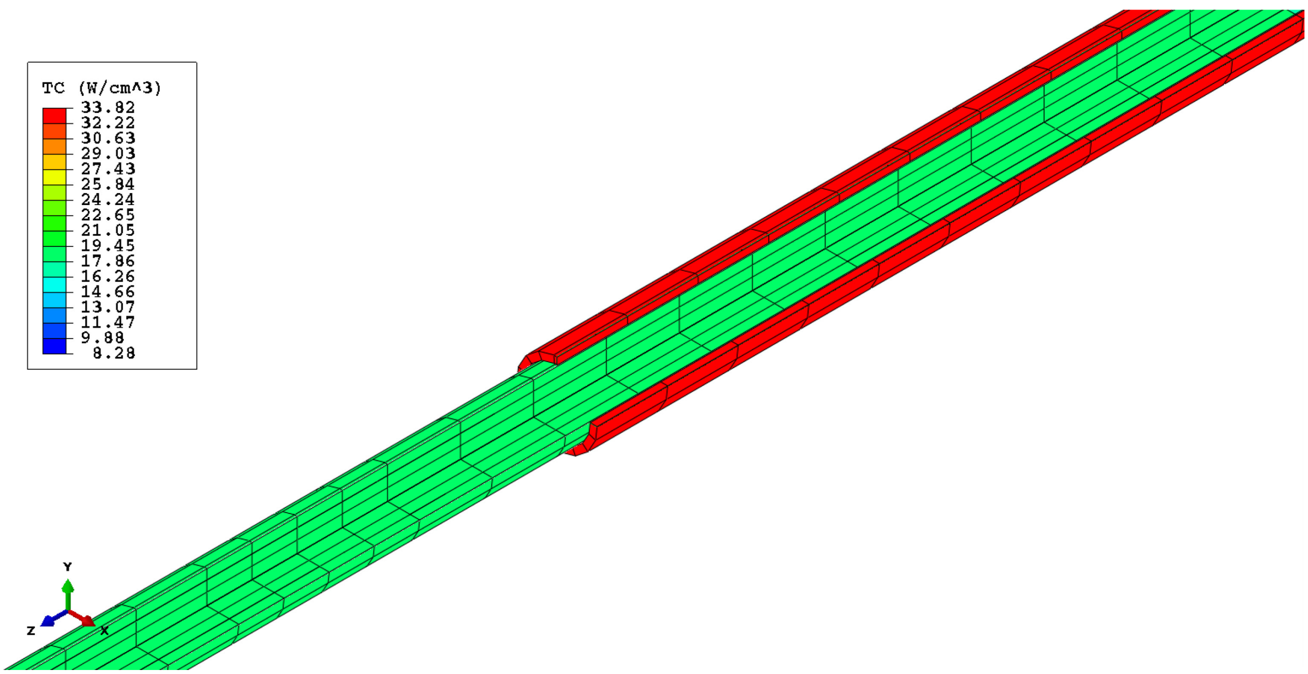

Figure 21. TC-1-8 cut-away view of top of sheath with HGR (W/cm^3) contours for cycle 162B day 20.

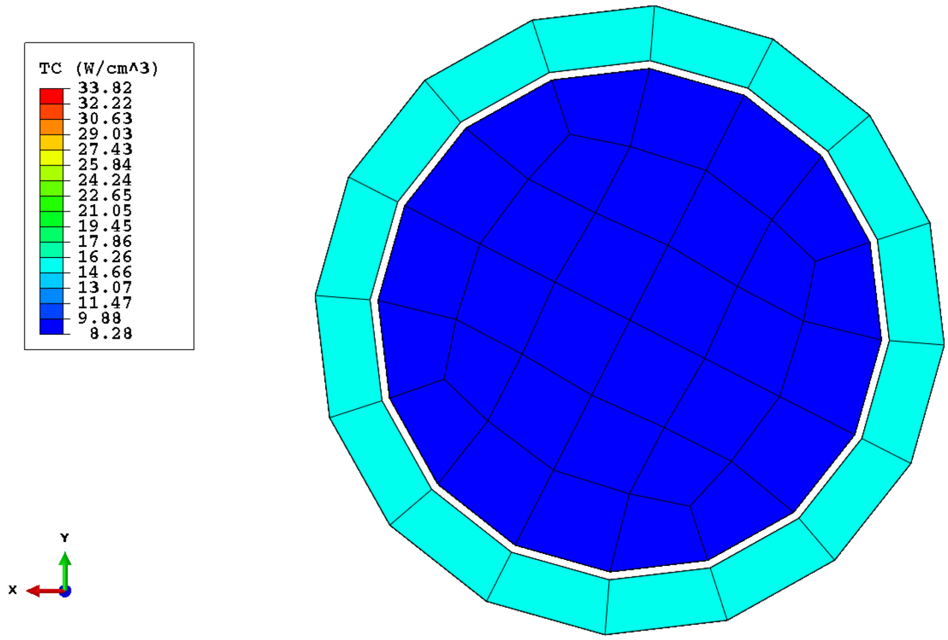

Figure 22. TC-1-8 and sheath bottom end view HGR (W/cm^3) contours for cycle 162B day 20.

Capsule 1 Spring Thermal Conductivity

An effective thermal conductivity of the spring located at the bottom of capsule 1 was calculated considering gas composition, and radiation heat transfer. A finite element model of the spring by itself was created. This effective thermal conductivity method was used so that a simple mesh could be placed where the spring exists without the complications of the spring itself in the big model. A temperature boundary condition was placed on the bottom, while a heat flux was placed on the top. A series of runs was performed with various temperature boundary conditions for various gas mixtures. Figure 23 shows a computer aided drawing (CAD) model of the spring made from a material named X-750. Figure 24 shows the finite element mesh and temperature contour plot of the spring for a boundary condition of 800 °F and a NeF of 0.75. The average temperature between the minimum and maximum was used as the data point for this configuration. Figure 25 shows the effective thermal conductivity plot varying with NeF and temperature for the spring. The X750 material is plotted on the graph also.

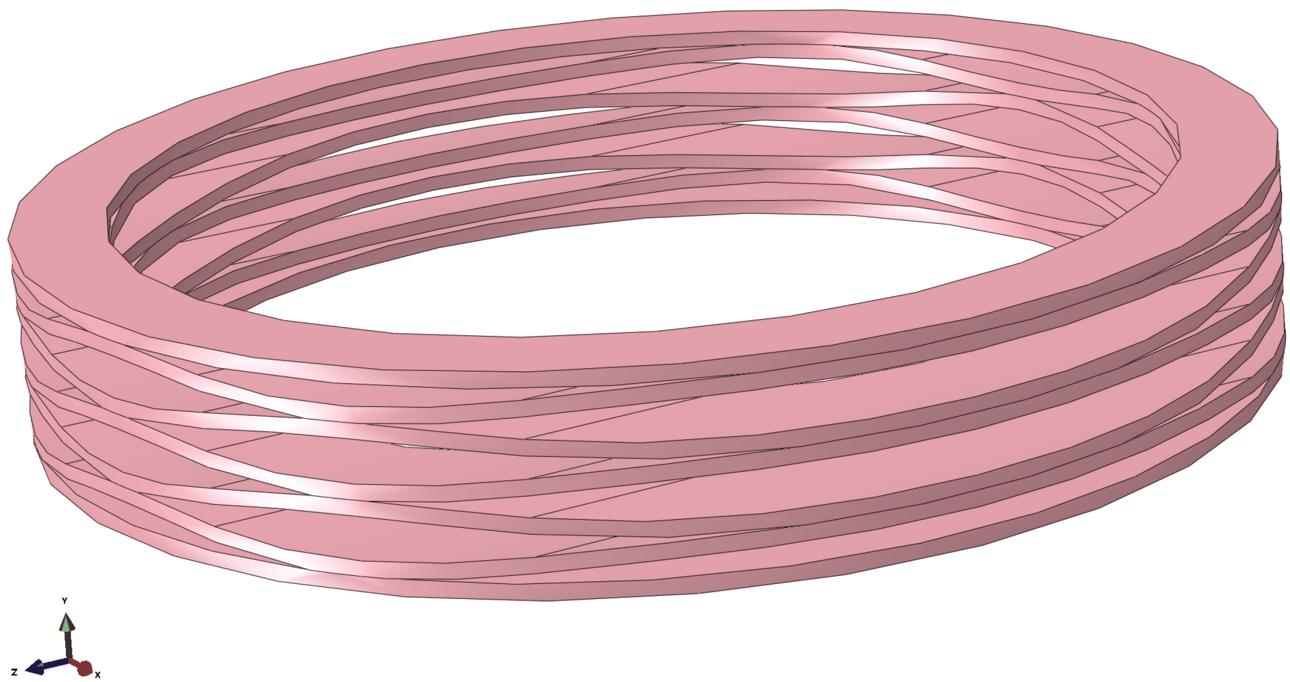

Figure 23. CAD model of capsule 1 spring.

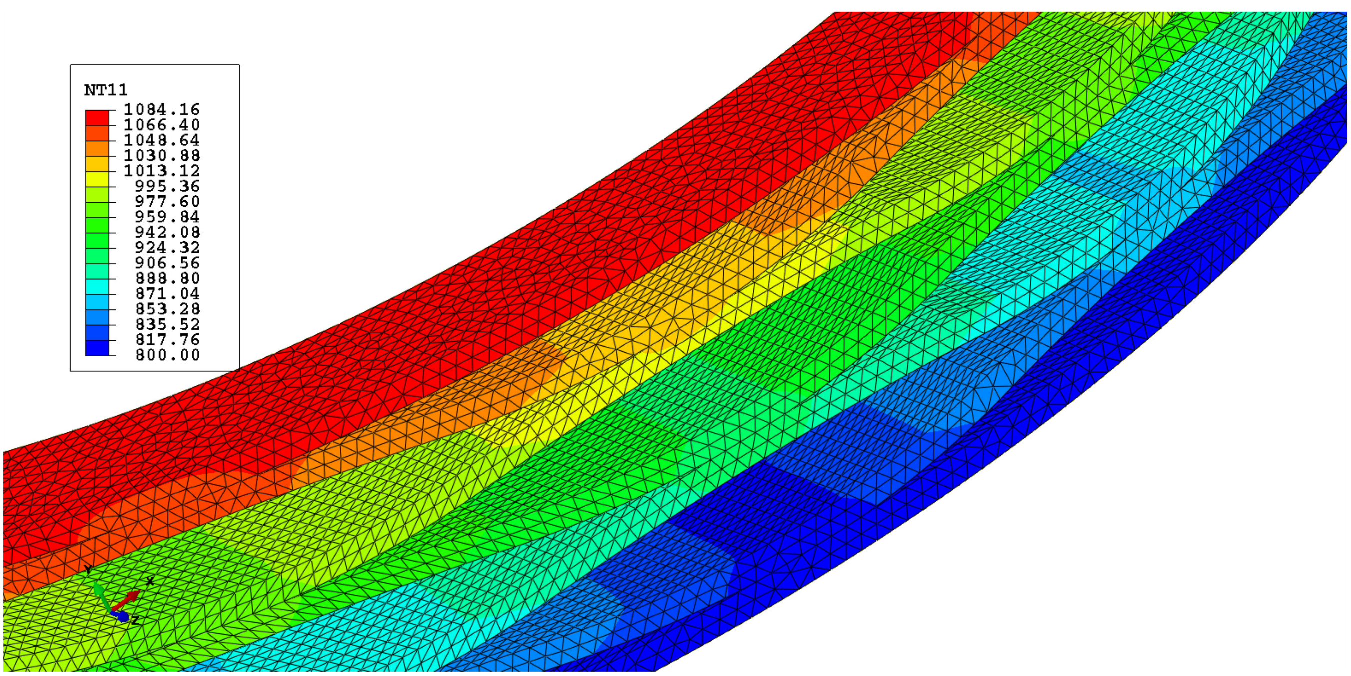

Figure 24. Temperature contour plot of spring, with 800 °F boundary temperature and NeF = 0.75.

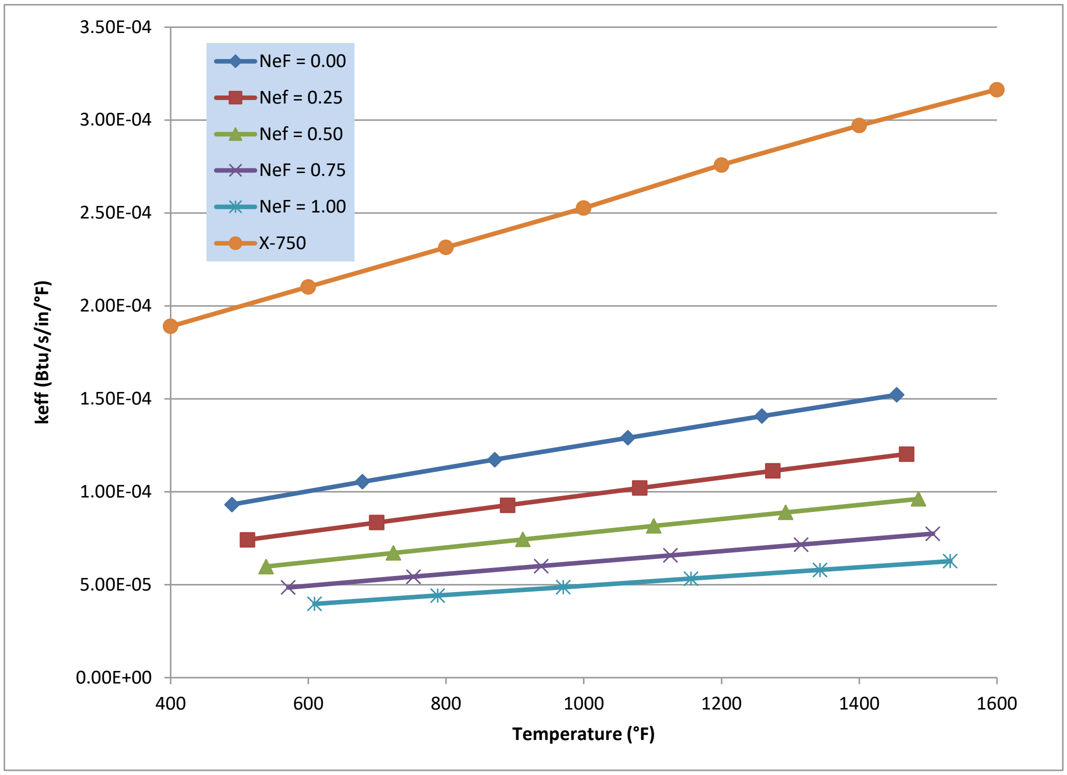

Figure 25. Effective thermal conductivity of spring in capsule 1 varying with NeF and temperature.

NEOLUBE Thickness

The graphite lubricant NEOLUBE® was brushed on the inside of the stainless steel capsule wall to increase the emissivity. The thermal model incorporated this material and reduced the size of the gas gap between the outside of the graphite holder and the capsule wall. Various runs were made after cycle 162B and different thicknesses applied with the goal of reducing the measured minus calculated temperature differences. The following Neolube thicknesses were used in the thermal model for all cycles. Capsules 1 through 4 used 0.0015 in., while capsule 5 used 0.0018 in.

8.0 ANALYSIS RESULTS

The thermal results of the AGR-5/6/7 daily as-run are displayed in the following figures. Figure 26 shows a temperature contour plot cut-away view of the entire model during cycle 162B day 20. This day was chosen since it was when the experiment was at full temperature. The highest temperature of 1446.18 °C is the fuel in capsule 3. The fuel at the top of capsule 1 is also close to the high temperature. The coolest temperature of 50.30 °C occurs at the top outside of the stainless-steel capsule 5. Figure 27 shows a temperature contour plot of all the fuel for all five capsules for the same day. Capsule 3 has the highest temperature as designed. The inner surfaces of the compacts near the top of capsule 1 also have a high temperature. Capsule 5 has the lowest temperature.

Figure 28, Figure 29, Figure 30, Figure 31, and Figure 32 show temperature contour plots with a cut-away view with the finite element mesh of the fuel compacts for capsules 1 through 5 respectively for the same day. The peak fuel temperature in capsules 1 through 5 for this day are 1337 °C, 990 °C, 1446 °C, 940 °C, and 798 °C respectively. In all these plots, the highest temperature is near the inner surface, while the lowest temperature is on the outside top and bottom corners.

A temperature contour plot with a cut-away view of the graphite holders is shown in Figure 33. The peak temperature of 1446 °C occurs in capsule 3. The black lines visible in capsule 3 are the small holes made for the TCs. Black circumferential lines showing the step in the radius on the outside of the graphite holders is also visible. Capsule 3 has two of these, while the other capsules just have one. As designed, there is a large temperature drop across the gas gap between the inner and outer graphite holders on capsule 3.

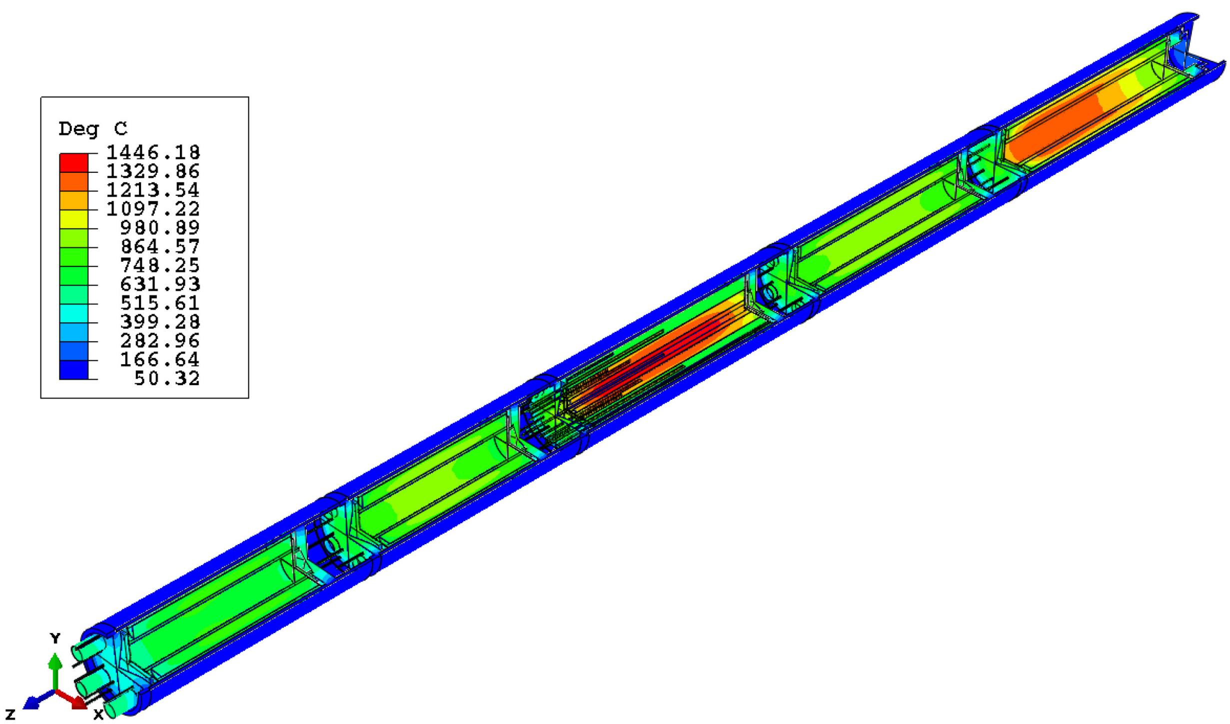

Figure 26. Temperature contour plot (°C) cut-away view of entire experiment during cycle 162B day 20.

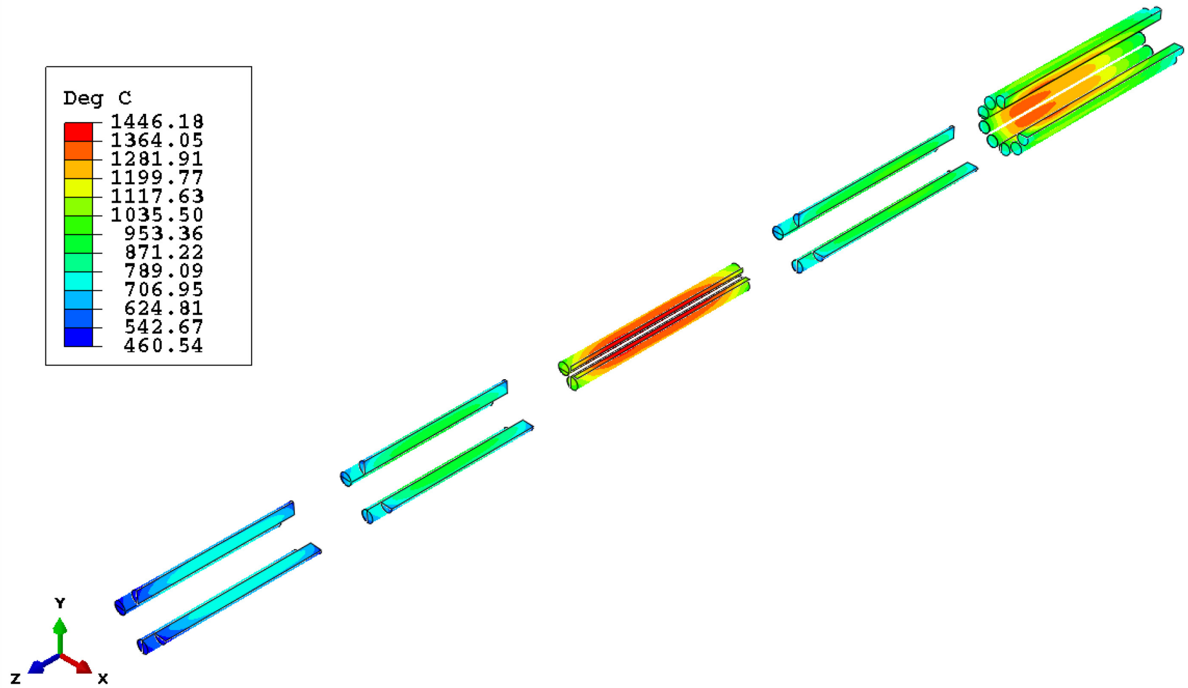

Figure 27. Temperature contour plot (°C) cut-away view of all fuel during cycle 162B day 20.

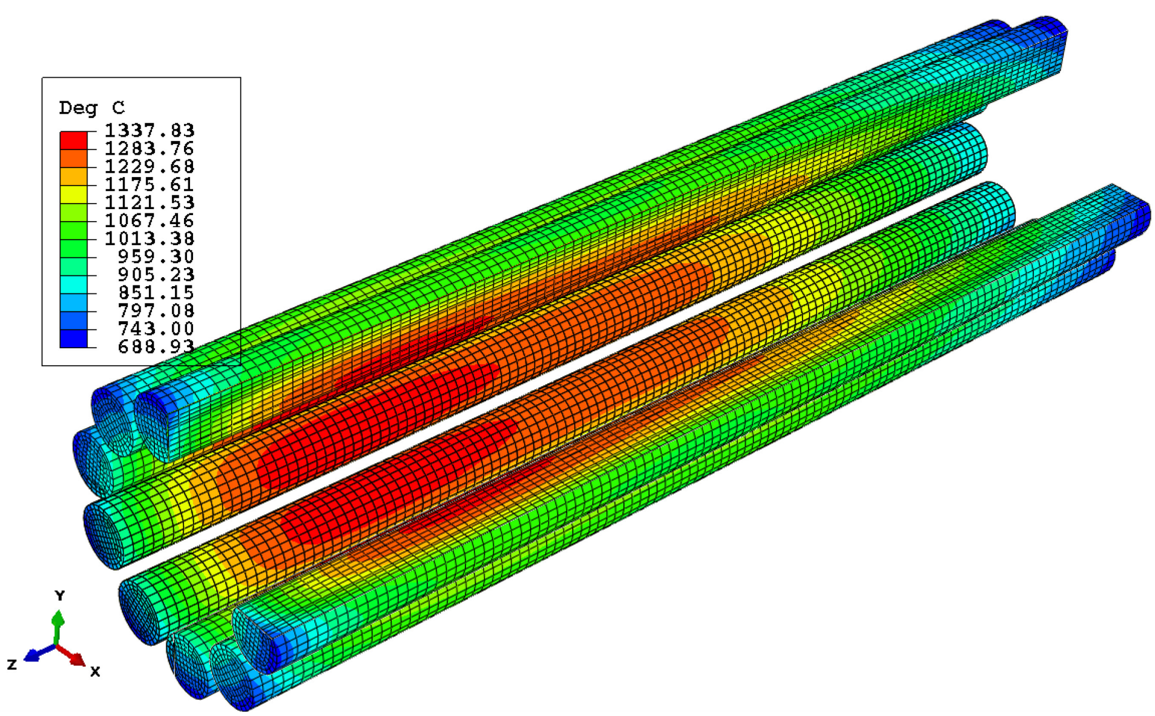

Figure 28. Temperature contour plot (°C) cut-away view of capsule 1 fuel during cycle 162B day 20.

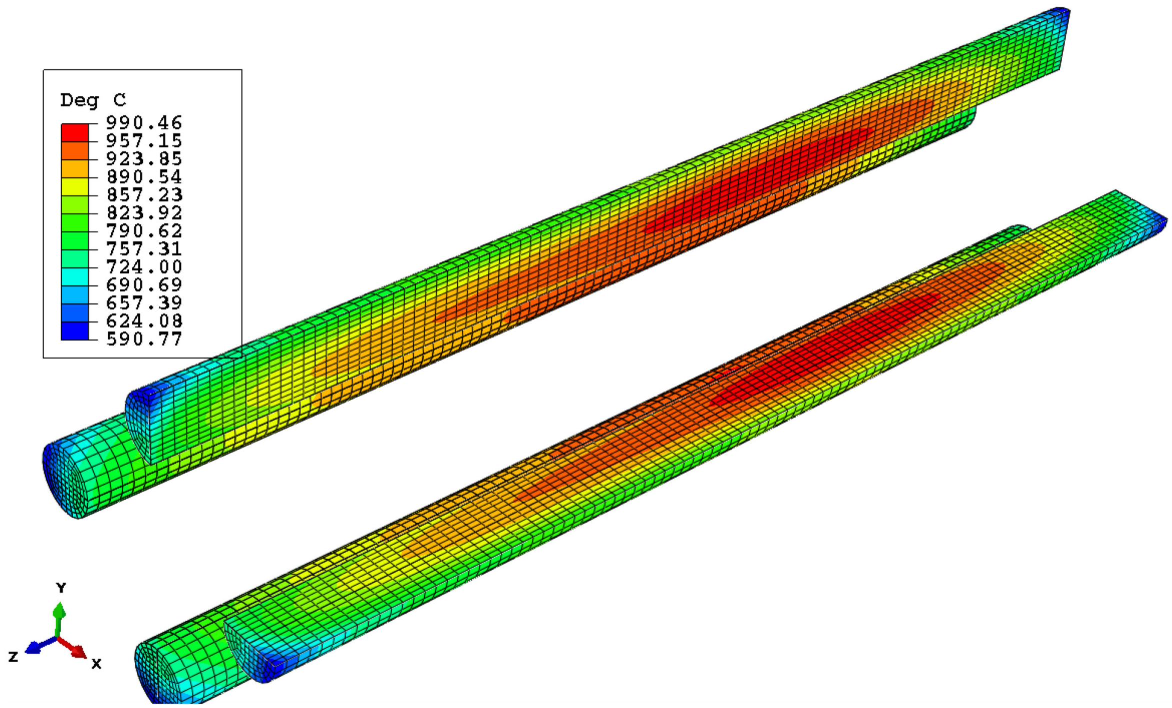

Figure 29. Temperature contour plot (°C) cut-away view of capsule 2 fuel during cycle 162B day 20.

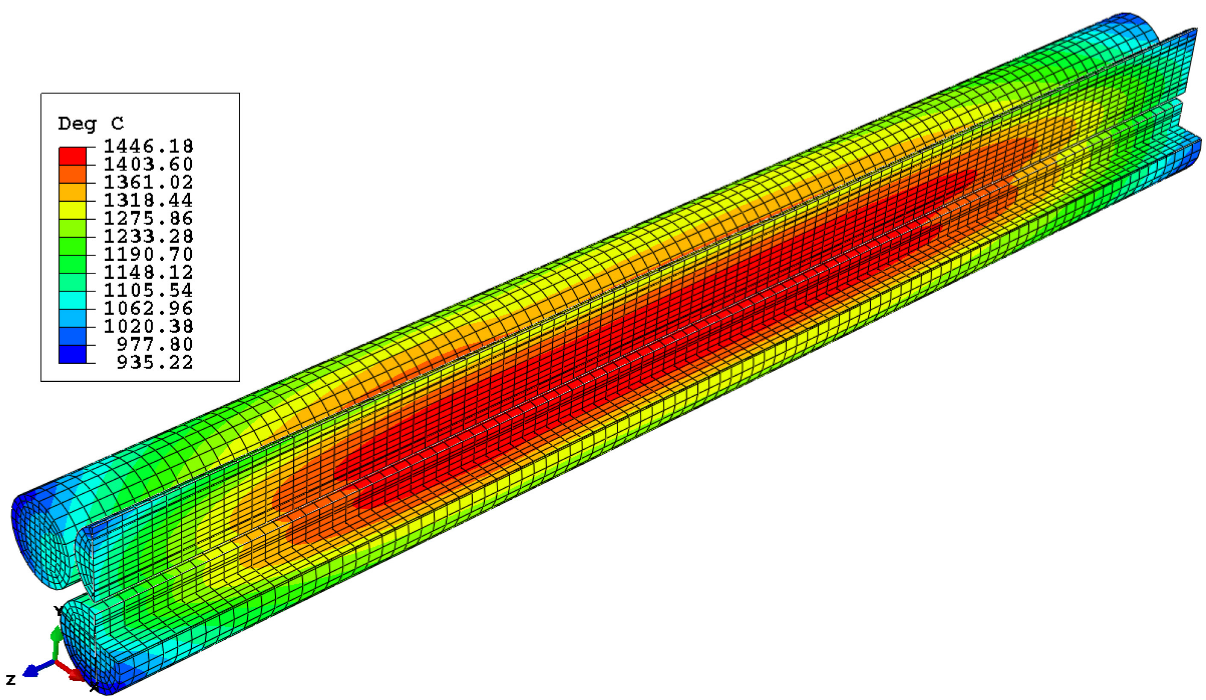

Figure 30. Temperature contour plot (°C) cut-away view of capsule 3 fuel during cycle 162B day 20.

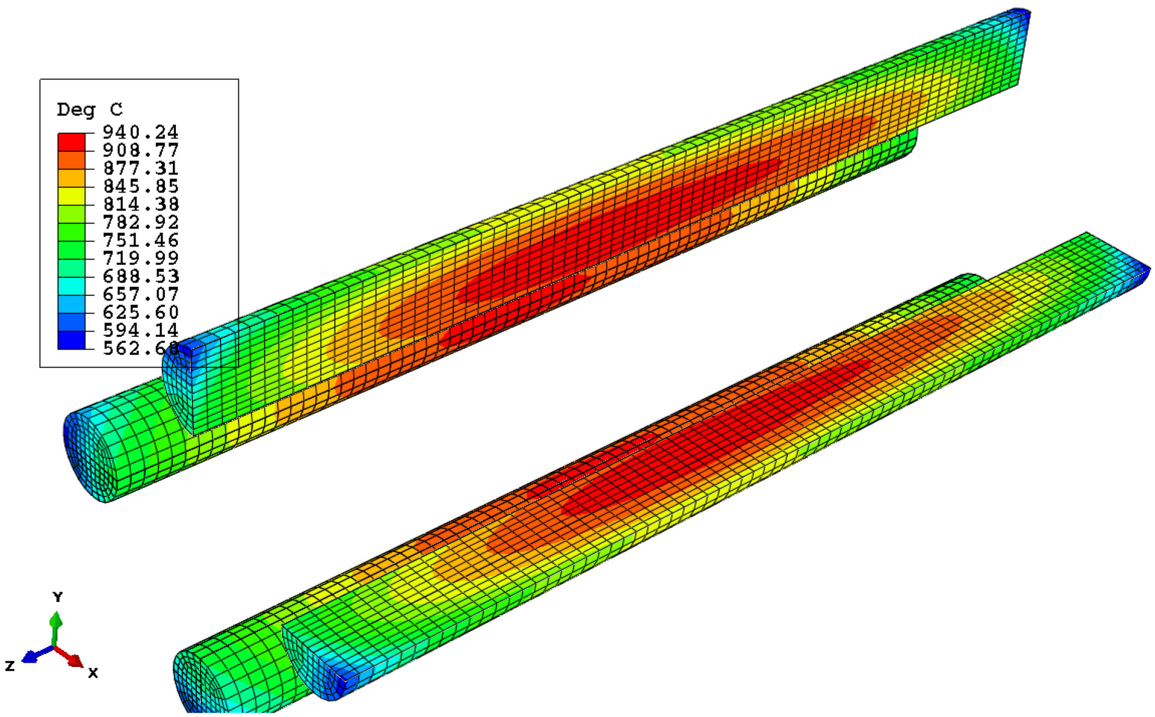

Figure 31. Temperature contour plot (°C) cut-away view of capsule 4 fuel during cycle 162B day 20.

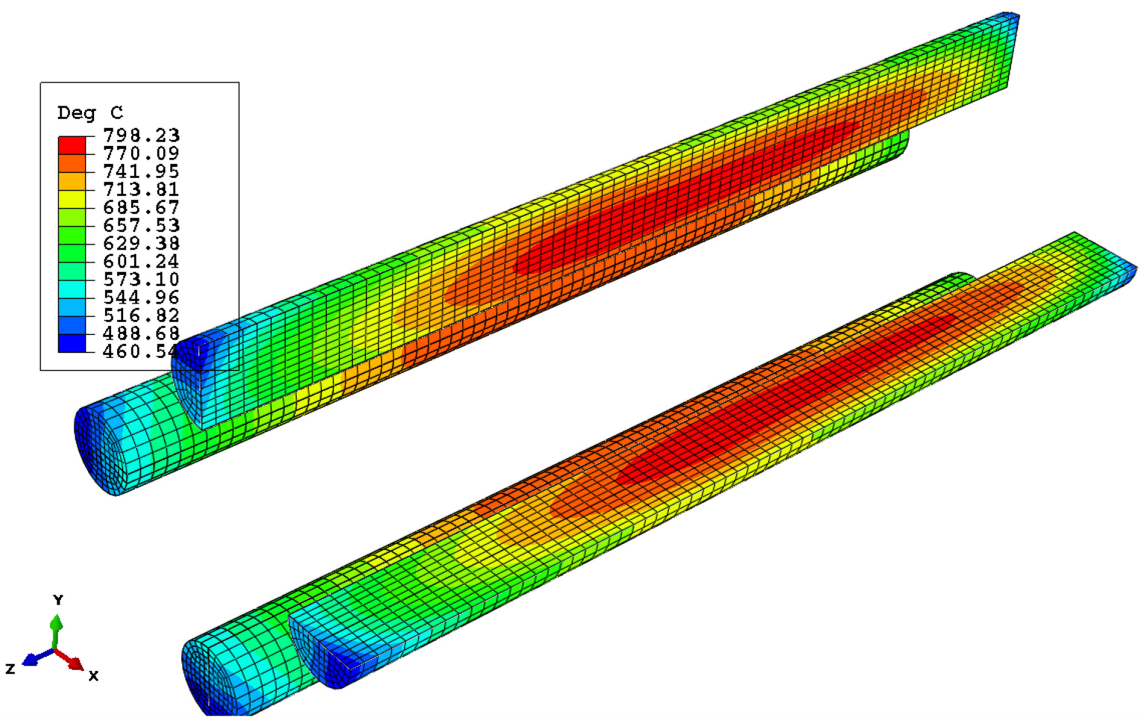

Figure 32. Temperature contour plot (°C) cut-away view of capsule 5 fuel during cycle 162B day 20.

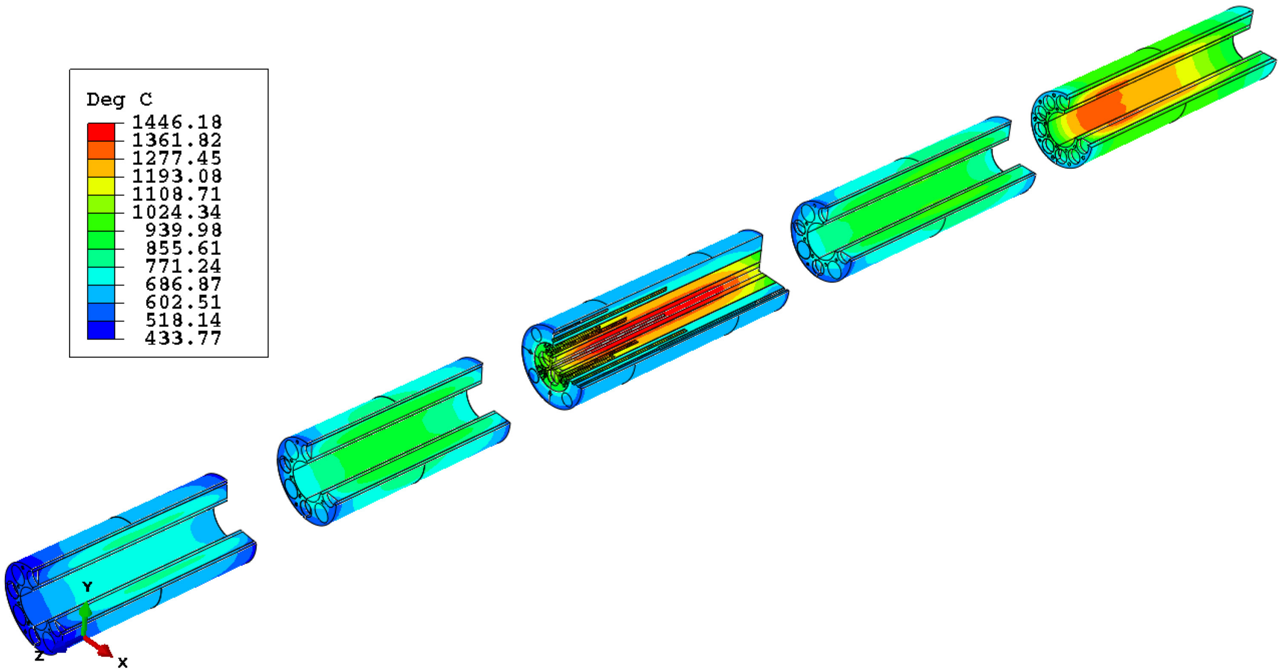

Figure 33. Temperature contour plot (°C) cut-away view of all holders during cycle 162B day 20.

Shown in Figure 34 is a temperature contour plot with a cut-away view of the stainless steel capsules with top and bottom caps for the same day. The tapered top and bottom caps have the highest temperature due to gamma heating, and a small portion of heat from the compacts and holders. The tapering was done to decrease the temperature in the top caps so that the brazing material would not melt. The coolest temperatures are on the outside top that are at the coolant temperature.

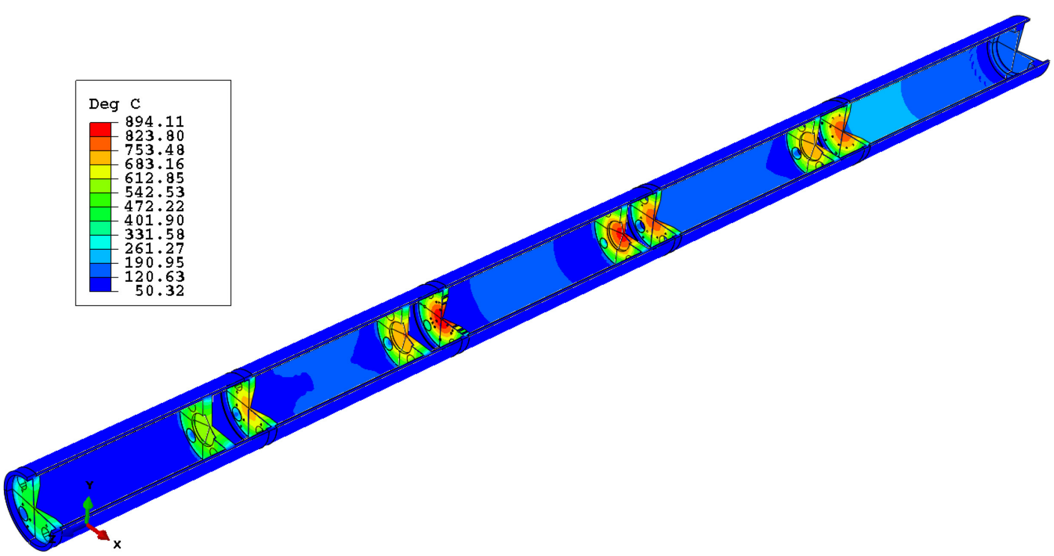

Figure 34. Temperature contour plot (°C) cut-away view of all stainless-steel capsules and bottom and top end-caps during cycle 162B day 20.

Figure 35 shows a temperature contour plot of all the TCs in the model for the same day. The highest temperature of the TCs is in capsule 3 at 1437 °C, while the lowest TC tip temperature is in capsule 5 at 654 °C. The TCs are at various azimuths and depths for all the capsules. The coldest blue portions always occur where the TCs are brazed to the top cap near the outer portion nearest the coolant.

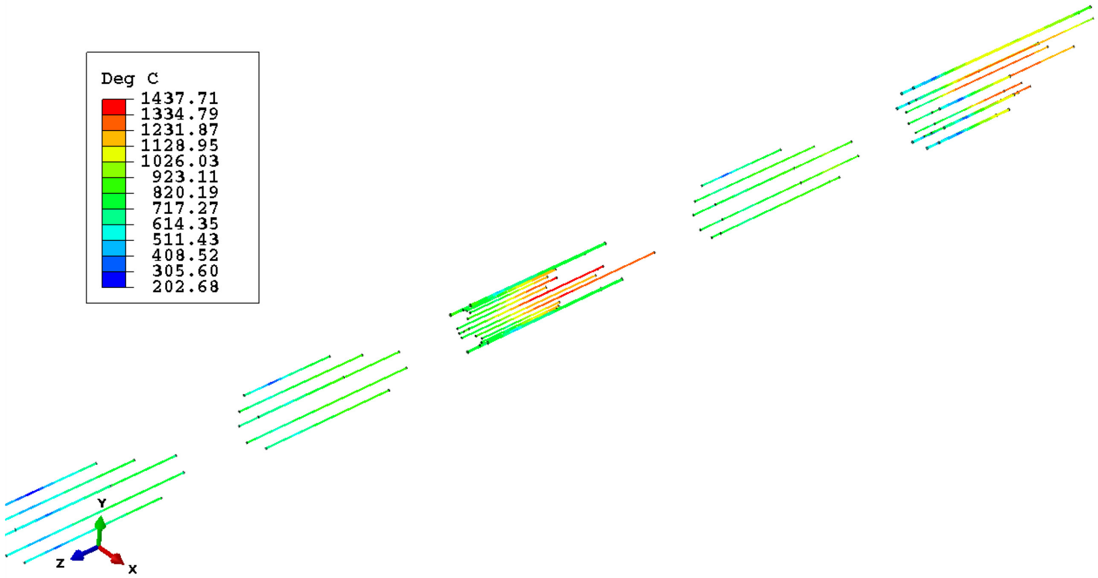

Figure 35. Temperature contour plot (°C) of all TCs during cycle 162B day 20.

Comparison with Measured Temperatures

The model captures a daily temperature for each TC in addition to temperatures for each finite element of all compacts. TC readings during the first cycle (162B) were used for calibration of this thermal model, adjusting input parameters (such as Neolube thickness) within their expected ranges to achieve the best match between measured and calculated TCs. Figure 36 shows a history plot of the TC residual temperatures (measured minus calculated) for all full power days for all cycles. A modest match between calculated and measured TCs during the first cycle was achieved. The continuing good match between measured and calculated TCs for Cycles 163A–168A indicates that the thermal model simulates the thermal conditions well.

Capsule 5 shows excellent agreement between the measured and calculated TC temperatures and capsule 4 shows good agreement, with mostly negative TC residuals indicating the model slightly overpredicts temperature. Capsule 2 TC residuals varied within a wider range (between -60°C and 60°C) and capsule 1 has even larger variation in predictions compared to actual TCs. However, the TC residuals in capsules 1 and 2 lie on both sides of the horizontal line at zero, indicating the current thermal model provides a reasonable fit to data. Capsule 3 had a good agreement during the first four cycles, but TC residuals were much larger during the last three cycles, which might indicate an unexpected change in the capsule 3 gas gap that impacted temperature at TC locations but was not captured by the thermal model. TC drift also could have occurred. The TC residual plots over time ended when TCs failed. A report documenting the uncertainty of the thermal model predictions will be prepared in the future.

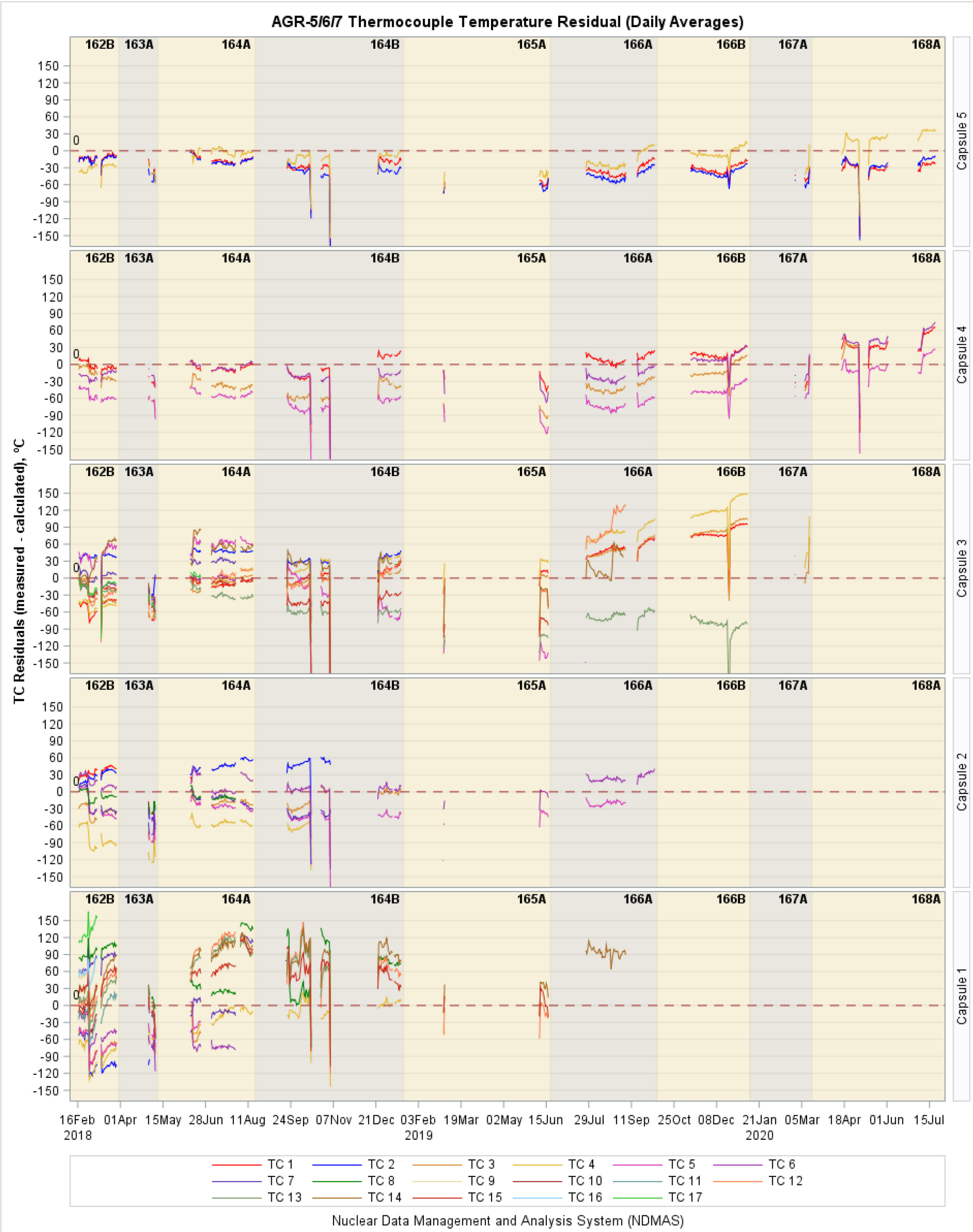

Figure 36. Difference between measured and calculated temperature for TCs in AGR-5/6/7 capsules.

As-Run Daily Fuel Temperatures

The AGR-5/6/7 thermal model provides detailed temperatures calculated for each finite-element volume of the entire test train. The detailed temperatures of 194 fuel compacts are used to calculate daily instantaneous and time-averaged values for minimum, volume-averaged, and maximum (or peak) fuel temperatures per compact and per capsule for each time step (or each day).

Figure 37 shows the calculated daily fuel temperatures (capsule minimum, capsule maximum, and capsule-average) for each of the five capsules of the AGR-5/6/7 test train versus irradiation time in EFPD. Figure 38 shows the corresponding time-average minimum, time-average maximum, and time-average volume-average (TAVA) fuel temperatures versus time for the five capsules. During the last ATR cycle (168A), gas flow for capsule 1 was isolated after purging the capsule with pure neon flow before powering up for this cycle [23]. However, some of gas from the leadout could enter capsule 1 through a break in this capsule gas line, which could increase the capsule 1 neon fraction from zero to the leadout neon fraction. Hence the capsule 1 neon fraction was not known precisely during Cycle 168A. Therefore, capsule 1 temperatures can only be bounded from a minimum value at zero neon fraction (darker-color plots in Figure 37) and maximum value at the leadout neon fraction (light-color plots in Figure 37). The temperature differences between these two cases are approximately 200℃. To be conservative, all temperatures reported in following tables were calculated with capsule 1 temperatures at zero neon fraction.

The instantaneous fuel temperatures remained relatively constant in all capsules for most cycles, except for the two low-power PALM cycles, 163A and 167A. This is because fuel compact heat rates were considerably lower during these PALM cycles [7]. Therefore, the time-average temperature calculations were performed for two scenarios: (1) include all nine cycles and (2) exclude the two low-power PALM cycles (163A and 167A). The daily plots of time-average fuel temperatures are presented in Figure 38 for both scenarios. The time-average values of the volume-average and peak compact temperature at the end of irradiation for both scenarios are presented in Table 2 for each capsule and each experiment. The exclusion of two low-power PALM cycles increases the end-of-irradiation time-average temperatures between 20 to 30 ℃. The instantaneous peak temperature from all volumes and all timesteps for each capsule and experiment are also included in Table 2.

The minimum, volume-averaged and peak values of time-averaged temperatures at the end of irradiation for all 194 compacts are presented in Appendix B for both scenarios (with and without Cycles 163A and 167A).

Table 2. Peak and time-average temperature (°C) per capsule and experiment. The dual values given in the last three columns correspond to values with and without inclusion of data from low-power PALM cycles 163A and 167A.

Capsule and Experiment	Instantaneous Peak Temperature	TA Minimum Temperature	TA Average Temperature	TA Peak Temperature
All Capsule 5 compacts	983	458 / 467	741 / 756	847 / 864
All Capsule 4 compacts	1091	546 / 558	839 / 857	950 / 970
All Capsule 2 compacts	1039	536 / 546	817 / 833	929 / 948
All Capsule 1 compacts (0 Cap 1 Ne)	1386	579 / 588	984 / 1001	1210 / 1231
All AGR-5/6 compacts (0 Cap 1 Ne)	**1386**	**458 / 467**	**898 / 914**	**1210 / 1231**
All AGR-7 Capsule 3 compacts	**1536**	**969 / 989**	**1289 / 1313**	**1405 / 1432**
All Capsule 1 compacts (LO Ne)	*1386*	*614 / 624*	*1022 / 1041*	*1244 / 1267*
All AGR-5/6 compacts (LO Ne)	*1386*	*458 / 467*	*918 / 936*	*1244 / 1267*

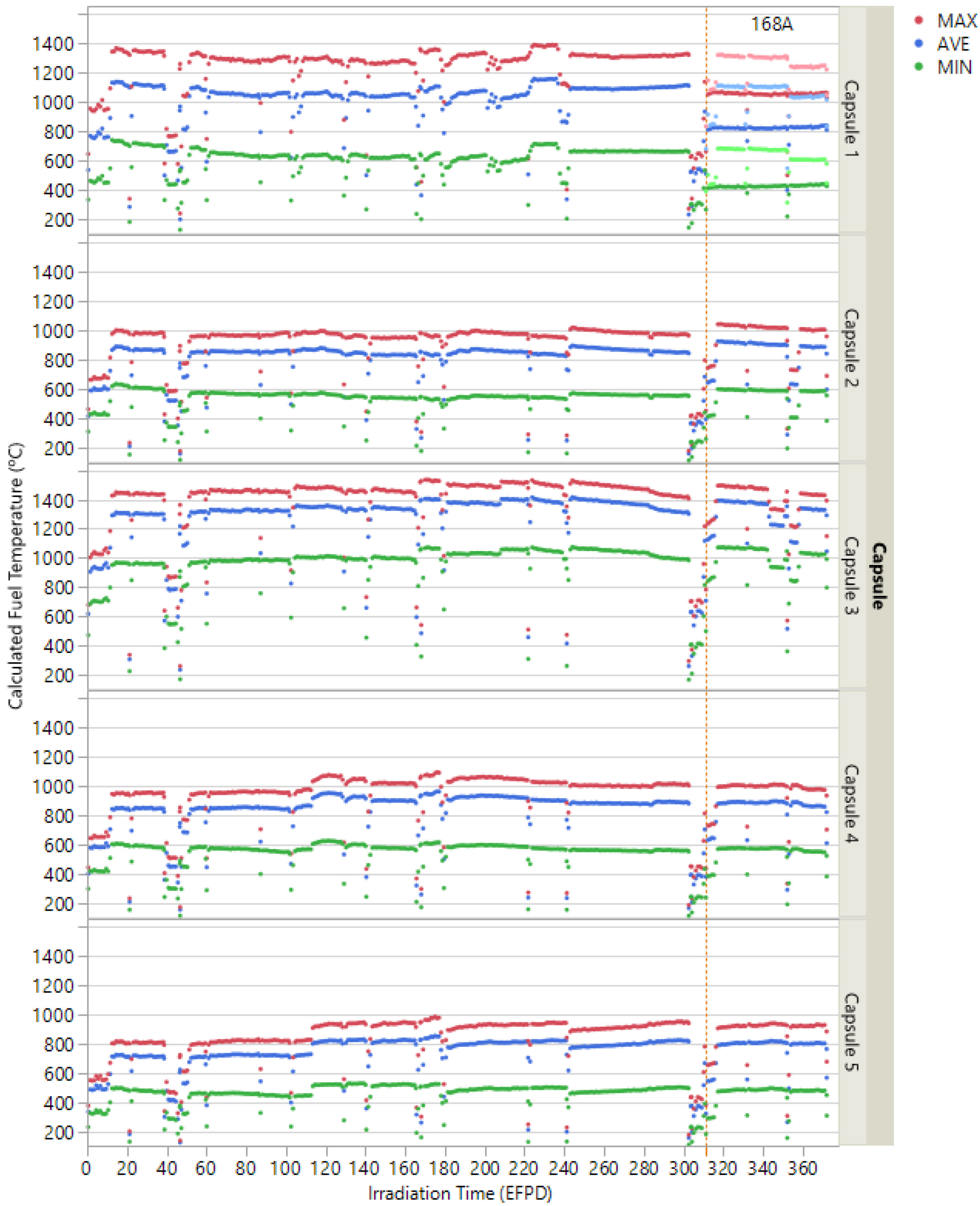

Figure 37. Calculated daily minimum, maximum, and volume-averaged fuel temperatures (light color dots for Capsule 1 are for the assumed leadout neon fraction instead of zero).

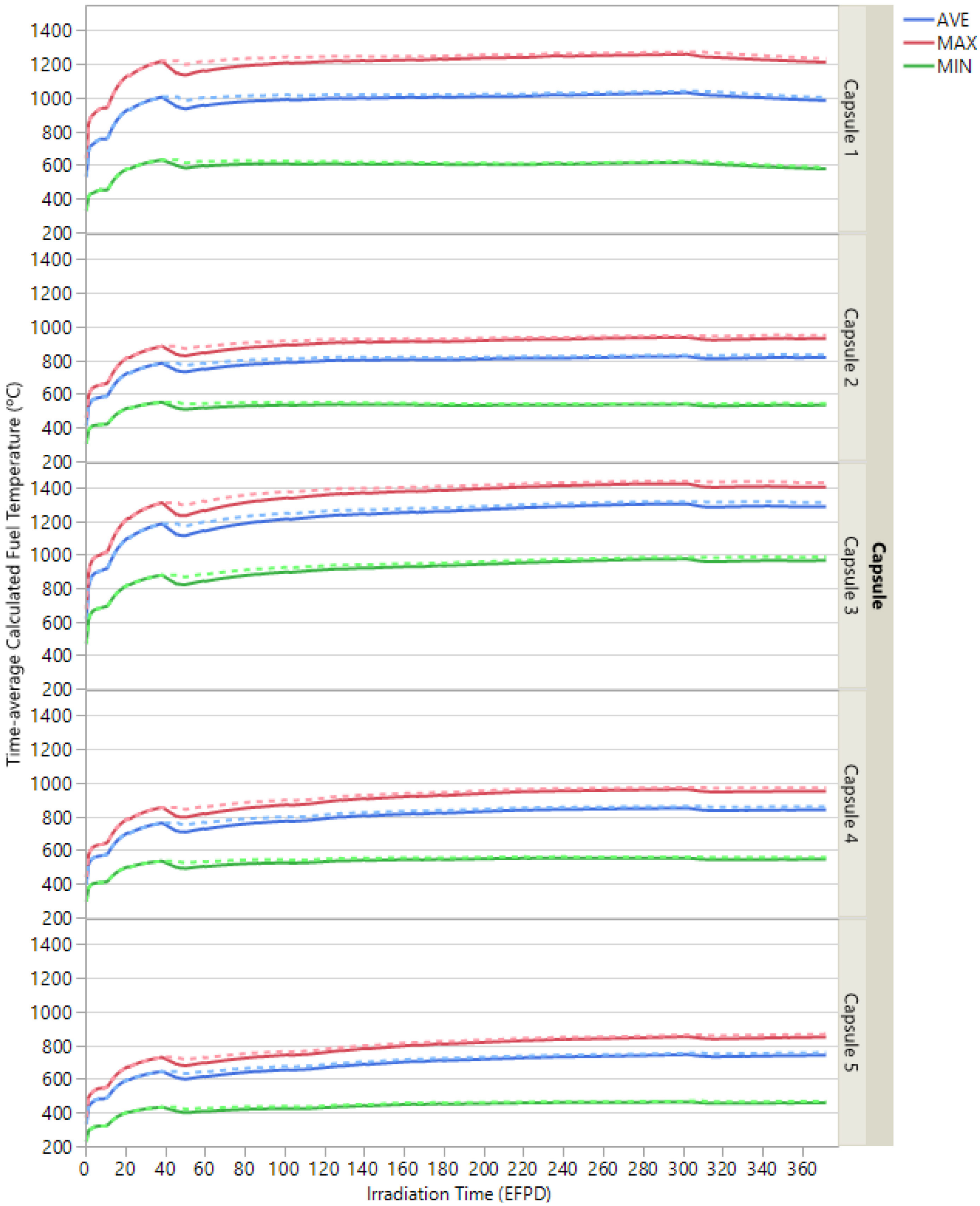

Figure 38. Calculated time-averaged minimum, time-averaged maximum, and time-averaged volume averaged fuel temperatures: solid lines were calculated using all days, and the dashed lines were calculated by excluding the two low-power PALM cycles 163A and 167A. It was assumed that the neon fraction was zero in Capsule 1 during 168A.

Fuel Temperature Distributions

Requirements for the AGR-5/6 fuel temperatures (Capsules 1, 2, 4, and 5) included the time average temperature distribution goals. Thus, the detailed calculated temperatures for all fuel finite-element volumes are used to determine fractions of fuel that were exposed to each temperature range to compare against these requirements.

Instantaneous fuel temperature distributions

Capsule 1 contained the largest number of compacts (90 out of 170 AGR-5/6 compacts) that were exposed to the widest range of temperatures, between 400 ℃ and 1400 ℃. The remaining three AGR-5/6 capsules (2, 4, and 5) contained 80 compacts total and were exposed to lower temperatures, between 400 ℃ and 1050 ℃. Therefore, only capsule 1 contributed to the two highest temperature ranges (T5:1250-1350 ℃ and T4:1050-1250 ℃) and contributed most of the middle range (T3:900-1050 ℃), while the other three capsules only contributed to the three low temperature ranges (T1:<600, T2:600-900 ℃, and T3:900-1050 ℃), as shown in Figure 39. Capsule 1 temperatures were relatively high for most of irradiation, except during the two low-power PALM cycles (163A and 167A) when temperatures in all capsules were significantly lower, and during the last cycle (168A), when it ran on isolated pure neon. During these three cycles, no fuel in capsule 1 contributed to the two highest temperature ranges, T4 and T5, as shown in Figure 39.

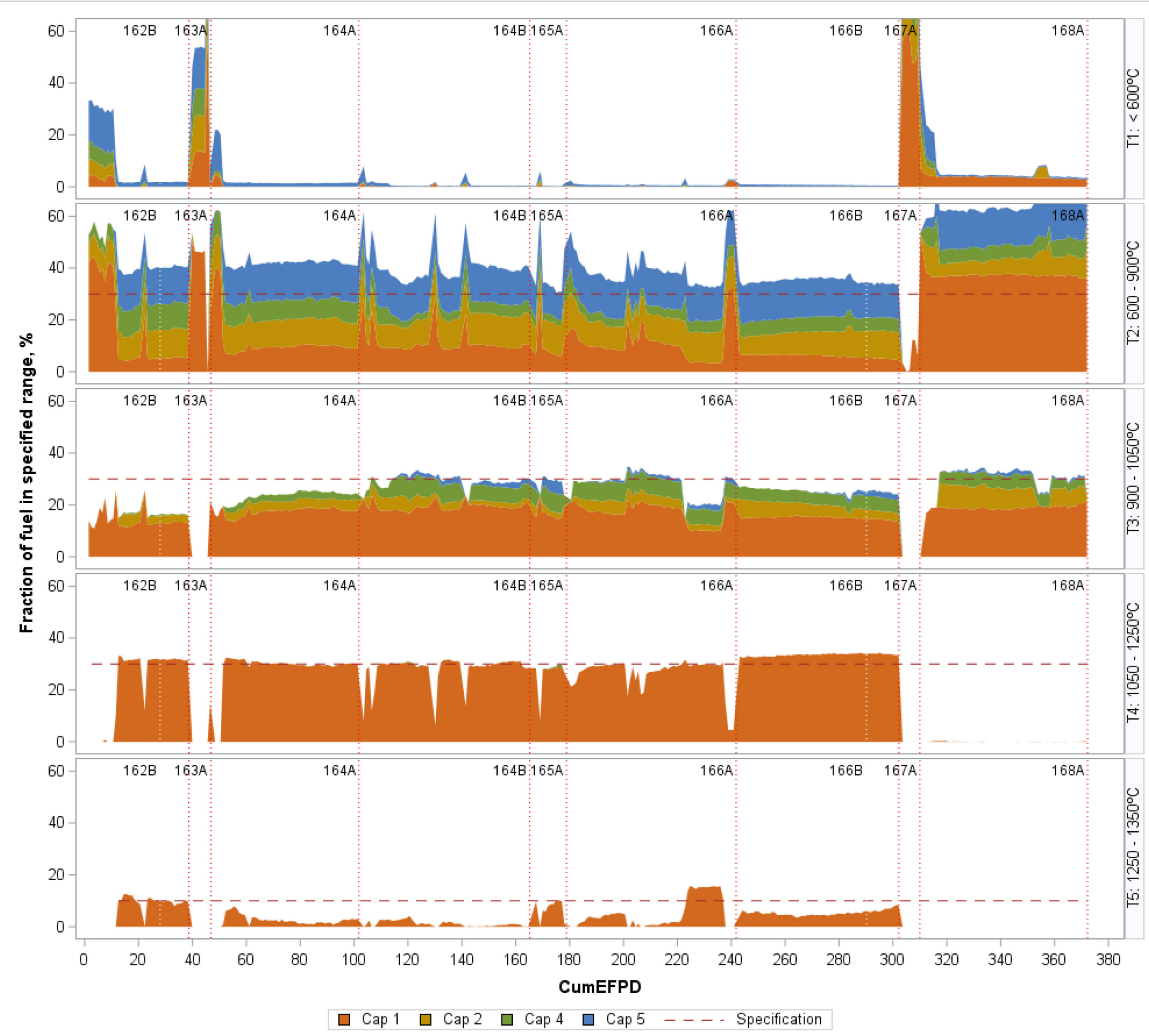

Figure 39. AGR-5/6 daily fuel fraction by instantaneous temperature range and capsule.

Requirements for AGR-7 Capsule 3 temperatures were only associated with peak temperatures. However, fuel proportion by temperature range plot was also calculated for capsule 3 shown in Figure 40. During the two low-power PALM cycles, 163A and 167A, capsule 3 temperatures were mostly lower than 900 ℃, whereas in other cycles capsule 3 fuel temperatures peaked as high as approximately 1550 ℃.

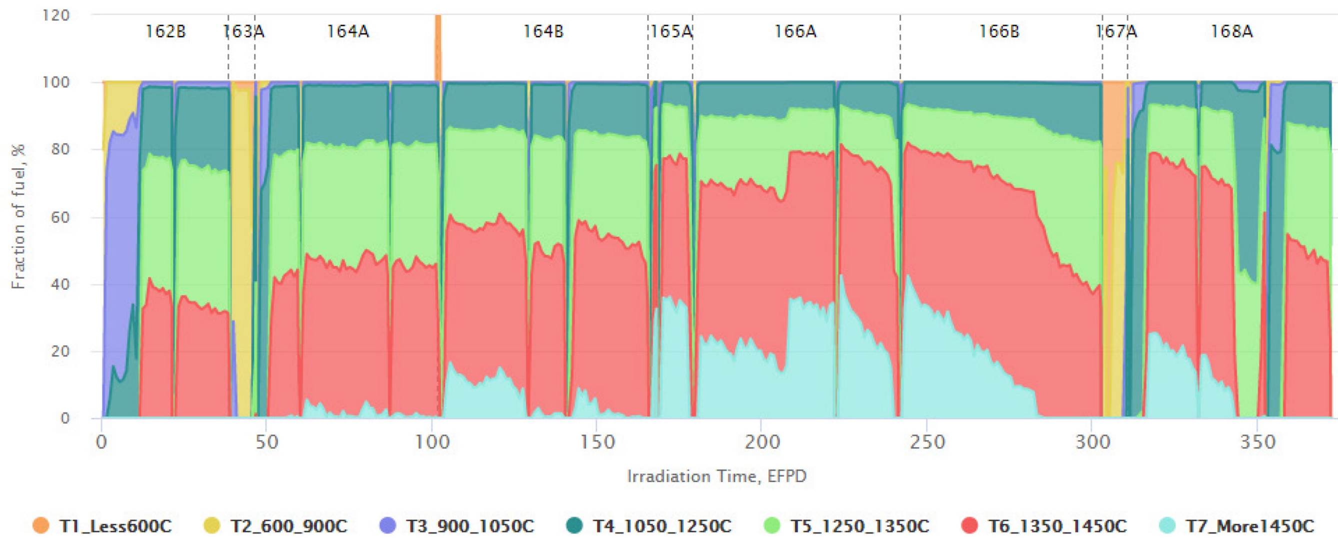

Figure 40. AGR-7 Fuel fraction by instantaneous temperature range as function of irradiation time.

Time-average fuel temperature distributions

For time-average fuel temperature distribution, the time-average temperatures of each finite volume over the entire irradiation were calculated first. Then, the fuel volumes were binned into the specified temperature ranges for each day.

The data during the two low-power PALM cycles, 163A and 167A, were excluded from the time averaging calculation of fuel distribution due to negligible fuel burnup during these cycles. AGR-5/6 fuel fractions by time-average temperature range and capsule are presented in Figure 41 and AGR-7 Capsule 3 fuel fractions are presented in Figure 42. Exclusion of the two low-power PALM cycles increased temperatures, resulting in better compliance with the goals for time-average temperature distribution, as shown in Table 3. Time-averaged temperatures at the end of irradiation (excluded Cycles 163A and 167A; and used zero neon fraction for capsule 1 during Cycle 168A).(percent numbers in parenthesis were time averaged from all nine cycles).

Table 3. Time-averaged temperatures at the end of irradiation (excluded Cycles 163A and 167A; and used zero neon fraction for capsule 1 during Cycle 168A). Percentages represent the percent of particles in the various temperature ranges.

Temperature range	Contributing capsule(s)	Actual data	Specification
AGR-5/6 Experiment – Capsules 1, 2, 4, and 5			
< 600 °C	1, 2, 4, 5	1.0% (1.3%)	-
≥ 600 °C and < 900 °C	1, 2, 4, 5	47.5% (51.5%)	30%
≥ 900 °C and < 1050 °C	1, 2, 4	27.3% (25.9%)	30%
≥ 1050 °C and < 1250 °C	1	24.2% (21.3%)	30%
≥ 1250 °C and < 1400 °C	1	0.0% (0.0%)	10%

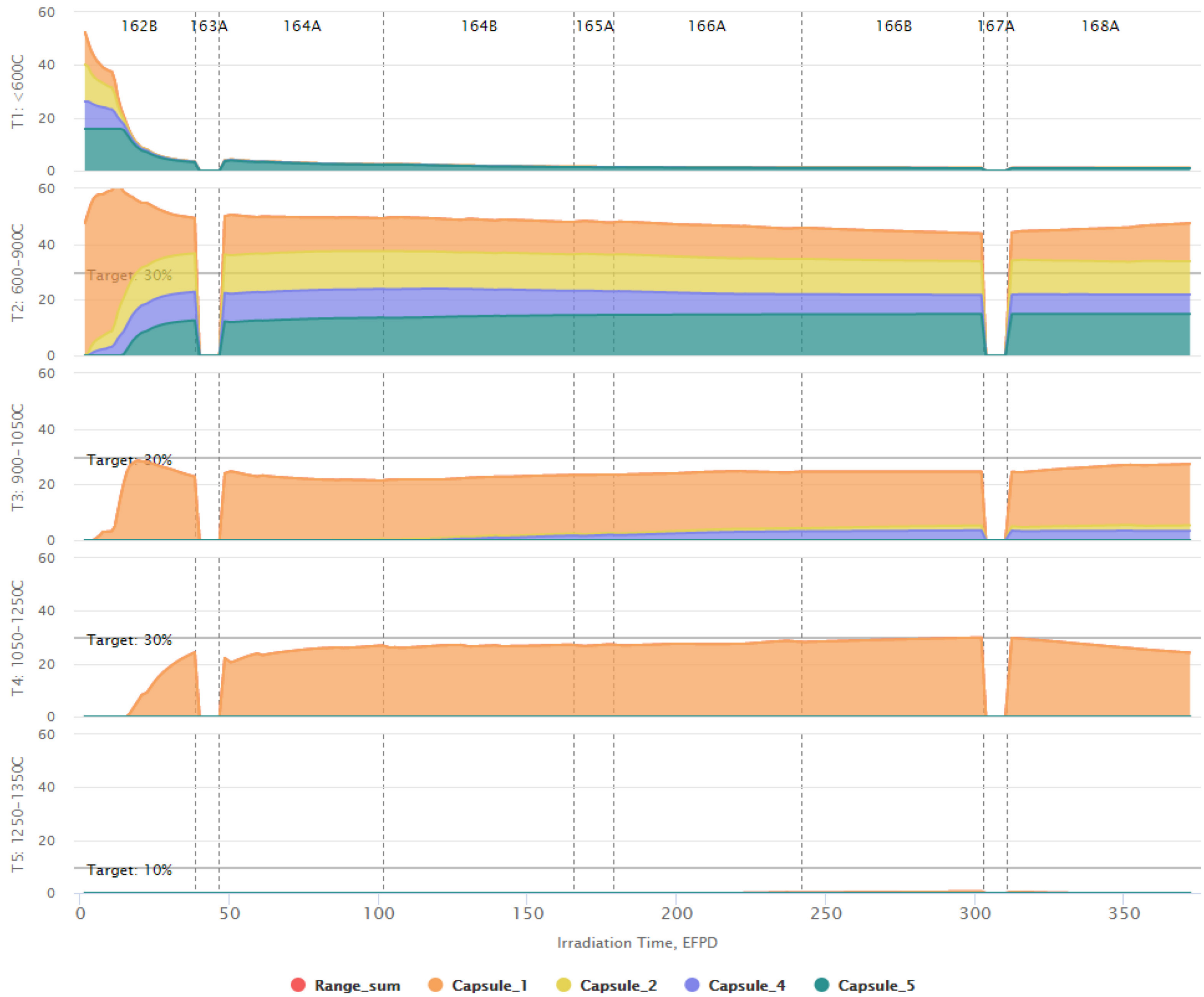

Figure 41. AGR-5/6 fuel fractions by time-average temperature range and capsule (excluded Cycles 163A and 167A).

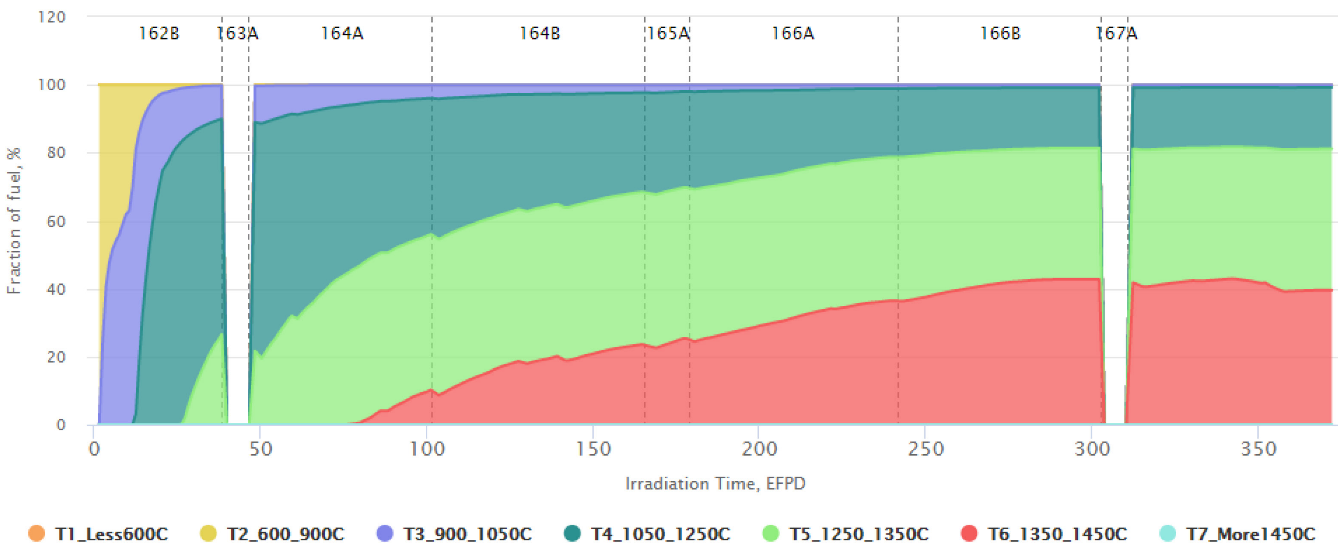

Figure 42. AGR-7 fuel fractions by time-average temperature range (excluded Cycles 163A and 167A).

Waterfall Plots

A waterfall plot showing the proportion greater than specified temperature bands for AGR-5/6 including capsules 1,2,4, and 5 is displayed in Figure 43. The neon fraction was assumed to be zero for capsule 1 during the last cycle (168A). Figure 44 shows a waterfall plot for AGR-5/6 without capsule 1.

Figure 45 shows the waterfall plot for AGR-7 for capsule 3. The temperature bands in this plot range from 1000 °C to 1500 °C. Approximately 20% of the fuel was above 1450 °C for 80 days.

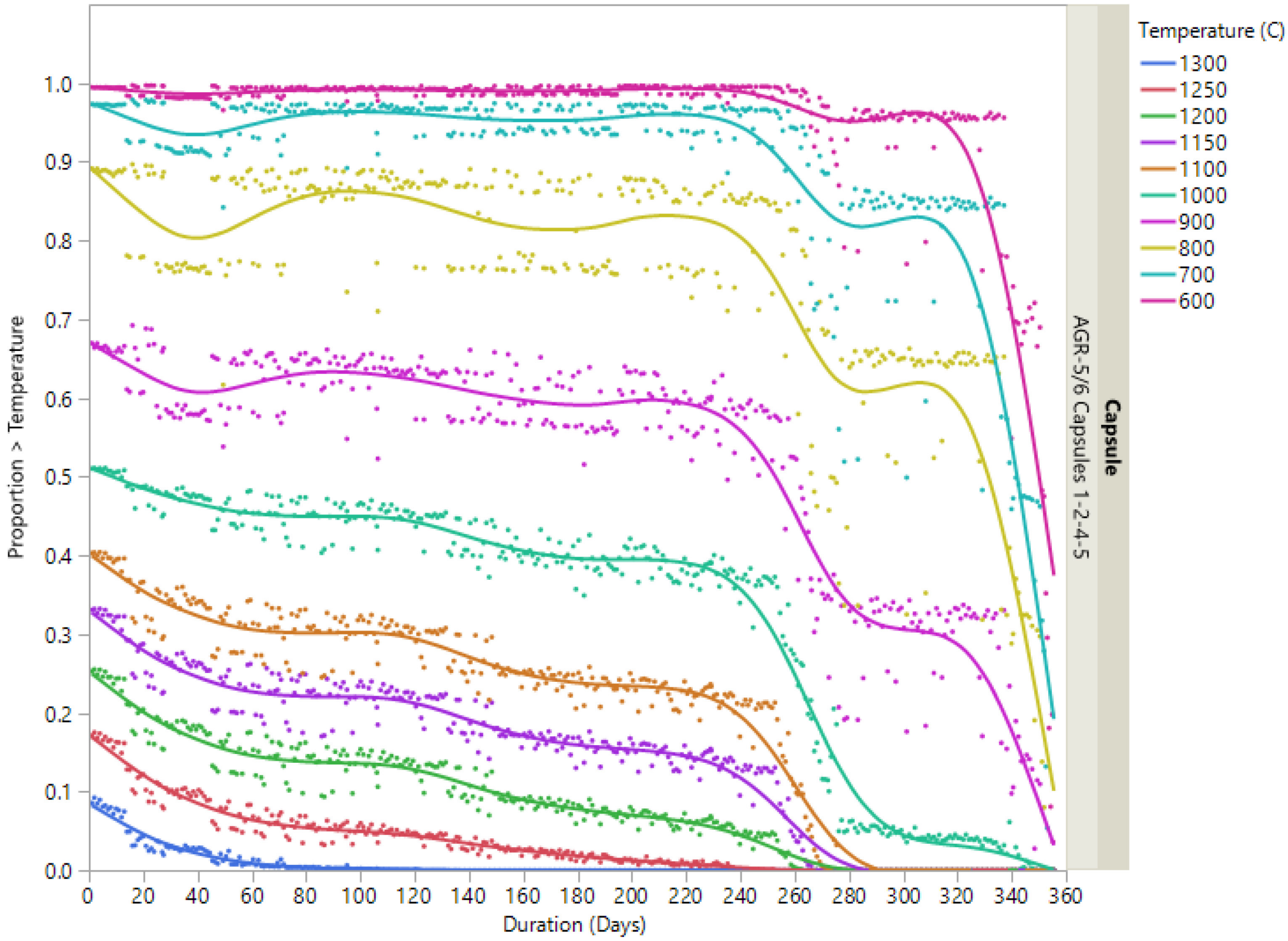

Figure 43. Waterfall plot showing proportion greater than specified temperature bands versus duration (days) for AGR-5/6 with capsules 1,2,4,5 included.

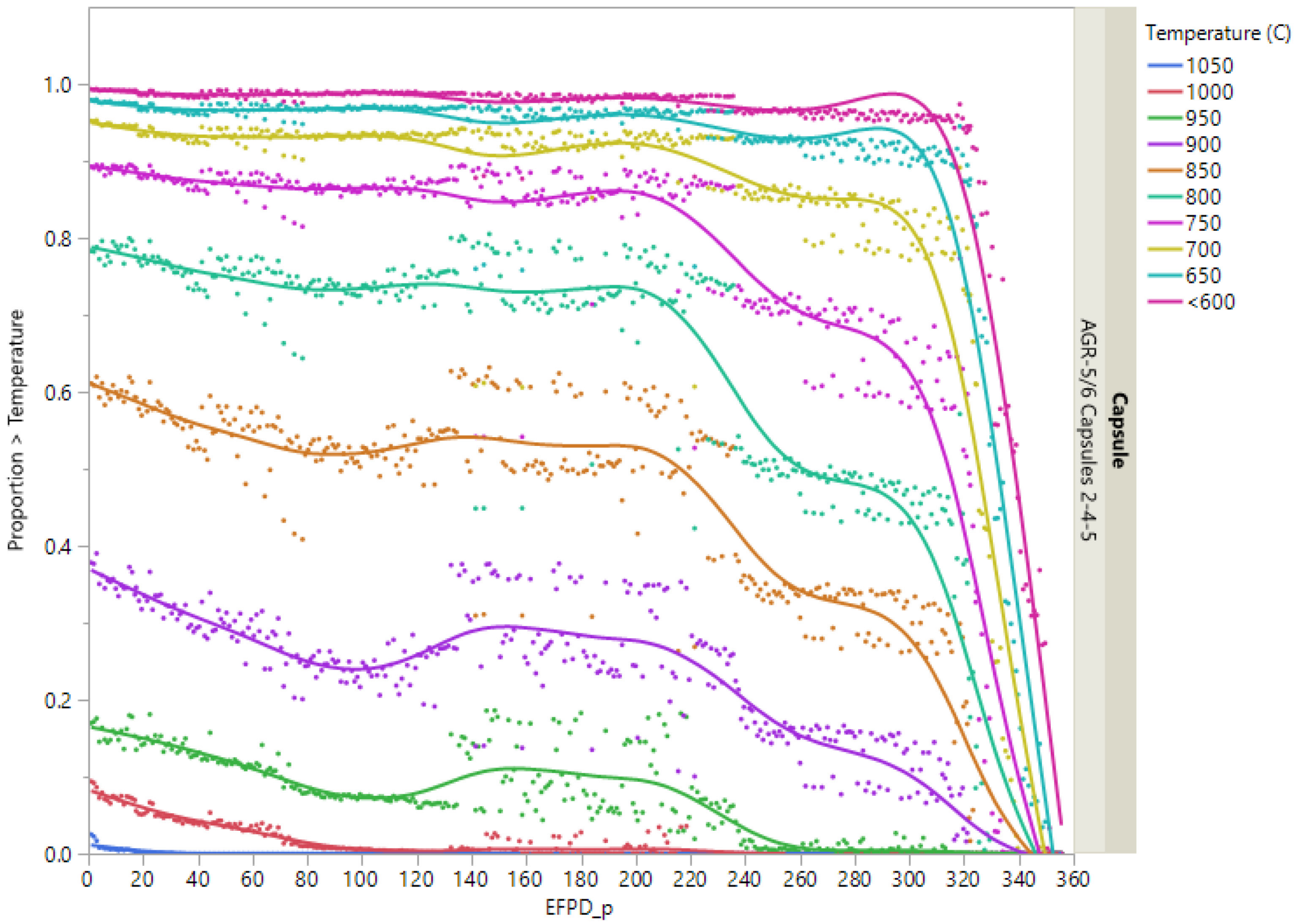

Figure 44. Waterfall plot showing proportion greater than specified temperature bands versus duration (days) for AGR 5/6 with capsules 2,4,5 included.

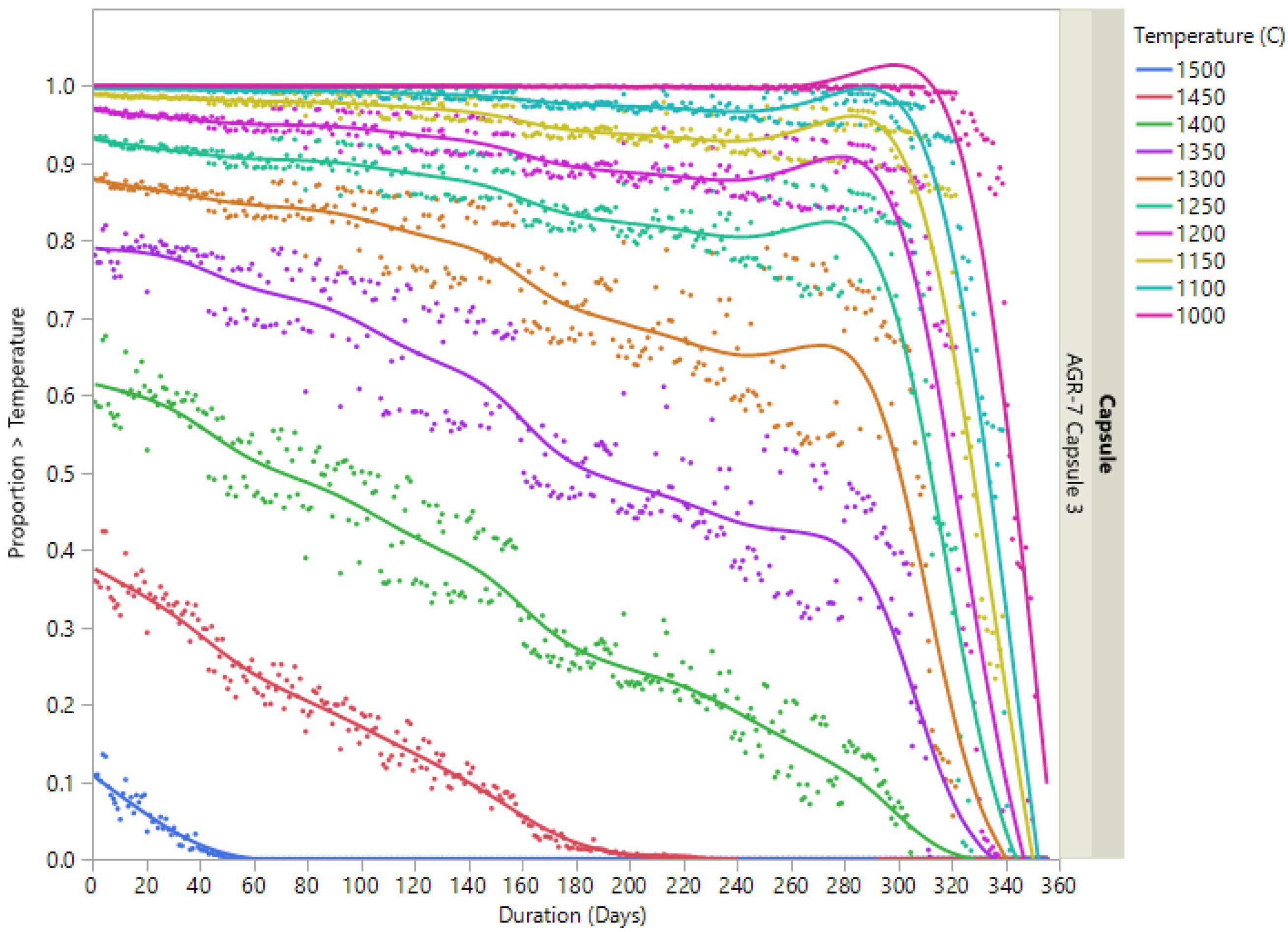

Figure 45. Waterfall plot showing proportion greater than specified temperature bands versus duration (days) for AGR 7 capsule 3.

As-Run Temperatures Versus Requirements

A range of irradiation fuel temperatures were specified for each AGR-5/6 capsule to achieve the desired fuel-compact temperature distribution in the test train per [24]. This goal led to time-averaged target irradiation temperatures from less than 900 °C to over 1250 °C, which conservatively spans the range expected in a prismatic reactor. The primary goal of AGR-7 was to demonstrate the available performance margin with respect to temperature for UCO fuel; thus, its fuel was to be tested at a higher time averaged peak temperature target of 1500 °C.

The requirements for fuel compact irradiation temperatures as enumerated in the AGR-5/6/7 Irradiation Test Specification SPC-1352 [24], are listed below with comments on the performance of the experiment with respect to each:

AGR 5/6 Requirements

• *The instantaneous peak temperature for each capsule shall be ≤ 1800 °C* – met requirement. The instantaneous peak temperature reached the highest temperature of 1386 °C for fuel compacts in capsule 1 (Table 2) during Cycle 166A.

• *The time average, peak temperature goal should be 1350 ± 50 °C* – lower than requirement. Time-average peak temperature was 1231 °C (in capsule 1), when the two low-power PALM cycles, 163A and 167A were excluded and zero neon fraction was used for capsule 1 during Cycle 168A.

• *The time average, minimum temperature goal should be ≤700 °C* – met requirement. Time average, minimum temperature is 467 °C (in capsule 5), when the two low-power PALM cycles, 163A and 167A were excluded.

• *The time average temperature distribution goals* – the portion of fuel in the lowest temperature range was higher than anticipated, and no fuel reached the highest temperature range:

- *≥600 °C and <900 °C for about 30% of the fuel – 47.5% actual,*
- *≥900 °C and <1050 °C for about 30% of the fuel – 27.3% actual,*
- *≥1050 °C and <1250 °C for about 30% of the fuel – 24.2% actual, and*
- *≥1250 °C and <1400 °C for about 10% of the fuel – 0.0% actual.*

AGR 7 Requirements

• *The instantaneous peak temperature for each capsule shall be ≤1800 °C* – met requirement. The instantaneous peak temperature reached the highest temperature of 1536 °C for fuel compacts in Capsule 3 (Table 2) during the high-power PALM cycle 165A.

• *The time average, peak temperature goal should be 1500 ± 50 °C for at least one capsule* – slightly lower than the requirement. The time-average peak temperature was 1432 °C when the two low-power PALM cycles, 163A and 167A were excluded (Table 2).

Offset Holder Results for Cycle 162B

Figure 46 shows temperature contour plots at day 41 of 42 of cycle 162B with a cross section view of capsule 1 at a location 1.5 in. below the top of the graphite holder. The base case that has the graphite holder perfectly centered is in the center of the figure. The gas gap for this centered case as this elevation is 0.006 in. The temperatures are slightly hotter on the southwest side since it is closest to the ATR core center as shown in Figure 1 and receives a slightly higher dose of neutrons. The top figure (north) has had the gap increased by 0.001 in. on the north side and shows hotter temperatures since the gas gap is larger and harder to conduct through. All calculations were performed with a 0.001 in. offset. Rotating around the figure shows temperatures hottest on the outside where the gas gap is larger.

Figure 47 shows the TRMS value of the temperature measured minus temperature calculated for all of Cycle 162B varying with gap orientation in 45-degree increments. The TRMS values of the graphite holder being centered are on the left side of the plot for all capsules combined and each individual capsule. Moving from left to right shows the TRMS value starting with north and rotating around in a clockwise fashion to northwest. The gold/beige line shows the combination of all capsules. This is heavily weighted toward capsules 1 and 3 since they each have 17 thermocouples. Capsule 2 has eight thermocouples and capsules 4 and 5 have six thermocouples each. The gold/beige line representing all capsules has its lowest value of 39°C TRMS at northwest. The orange line depicts capsule 1 and it is also lowest at northwest. Capsule 2 is represented by the purple line and has its lowest value of 35°C at the north. Capsule 3 is shown in gold and has its lowest value of 27°C on the east. Capsule 4 is shown in blue and has its lowest value of 18°C on the east, while Capsule 5 is shown in green and has its lowest value of 15°C in the northeast. Capsule 5 shows the smallest difference between measured minus calculated temperatures.

These calculations for the offset show that each capsule could be moved in a direction and magnitude that would help decrease the measured minus calculated temperatures. All the results presented above in this report were performed with the holder being perfectly centered with the capsule. Future reports will explore the option of optimizing magnitude and direction offset for each capsule for each cycle.

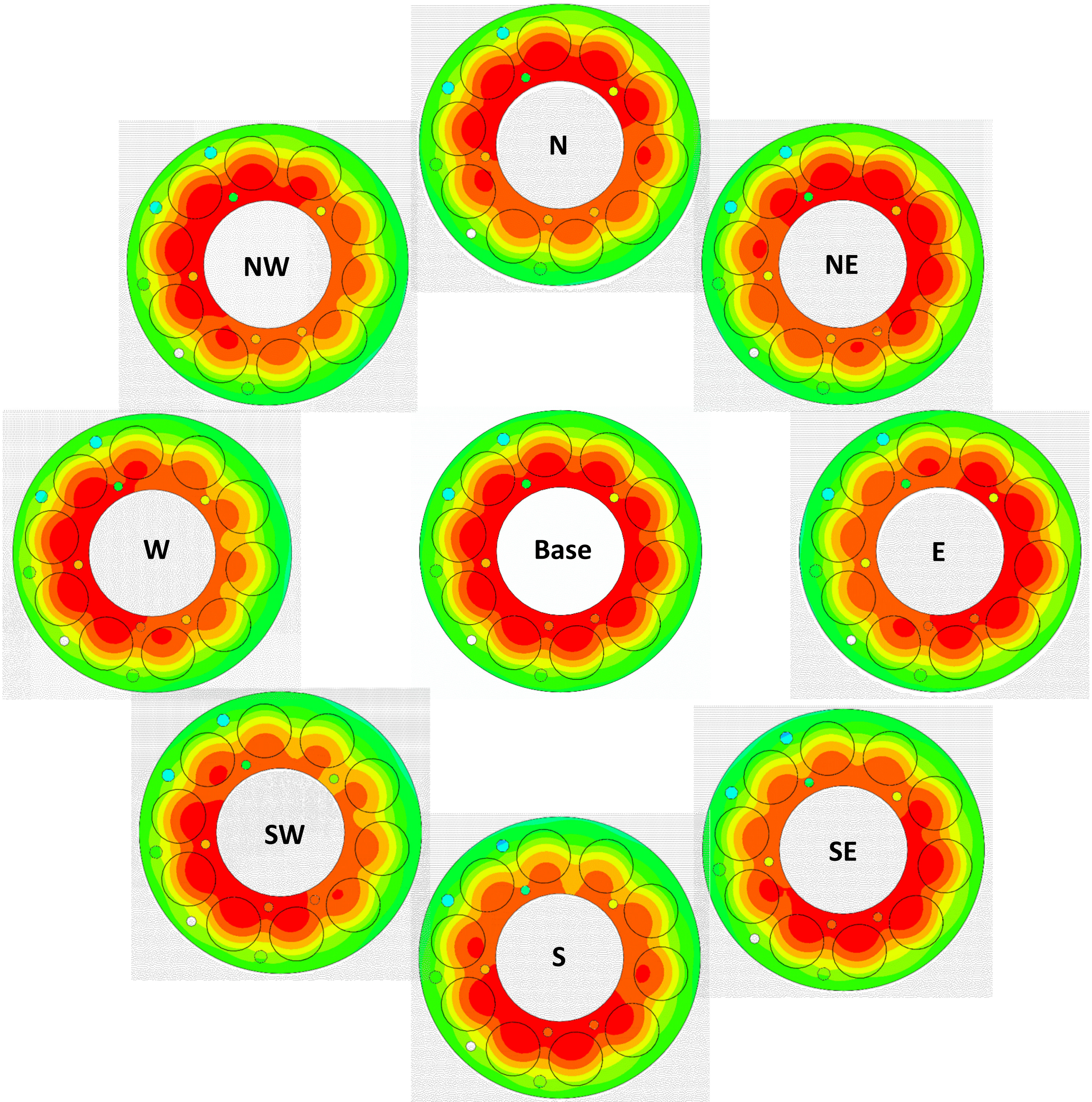

Figure 46. Temperature contour plot showing cut section in capsule 1 at 1.5 inches from top of graphite holder varying by holder offset in eight directions taken on the second-to-last day of irradiation of the first ATR cycle 162B.

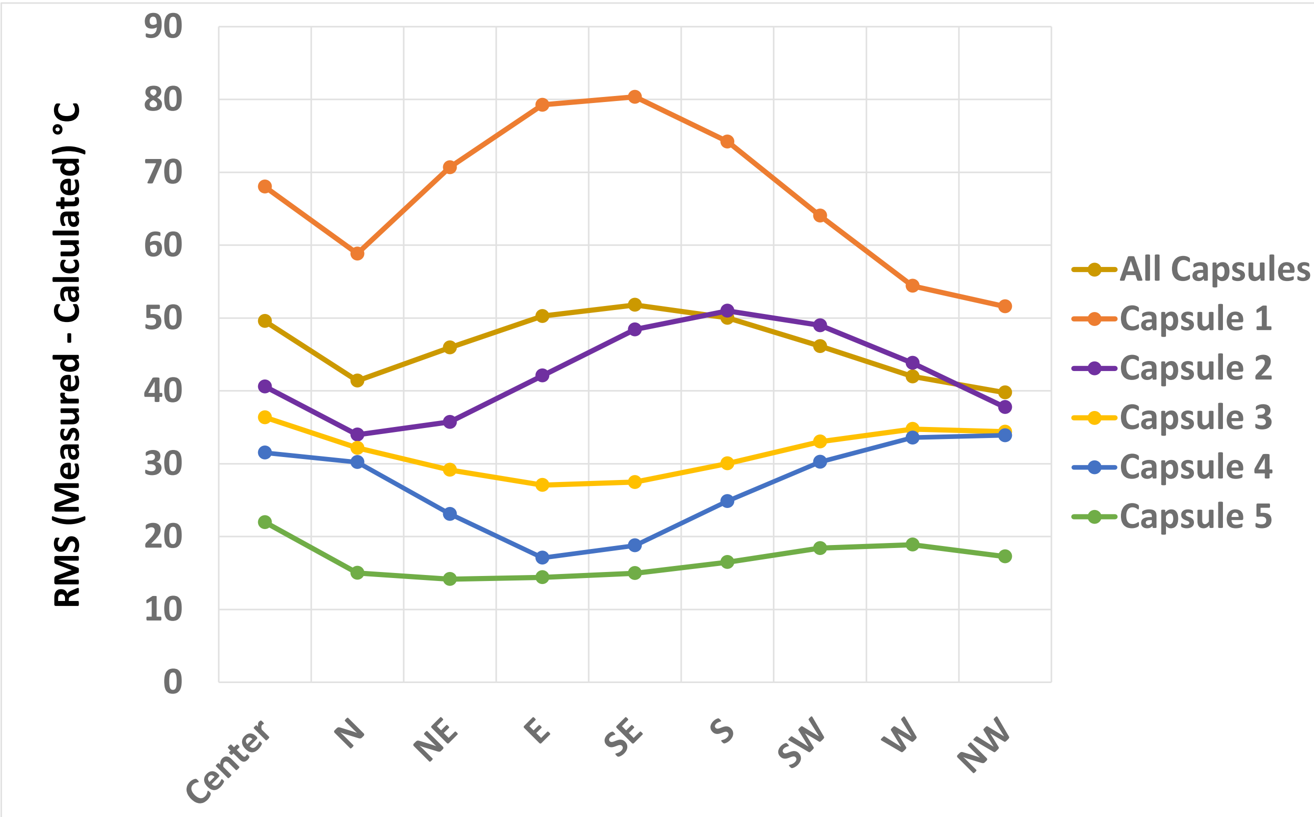

Figure 47. TRMS (measured – calculated) °C for first irradiation cycle varying by gap orientation at center and 45 degree increments.

9.0 DATA FILES

The files used for the thermal analysis of the AGR-5/6/7 daily as-run are contained in the `/projects/agr/agr567/` directory on HPC. Here is a listing of that directory:

```
haw@r7i5n8:/projects/agr/agr567=> ll
total 384
drwxrws--- 12 agr  227 Jul 29 10:14 ./
drwxrws---  6 agr  114 Sep  4  2019 ../
drwxrwsr-x  2 agr  437 May 19  2020 162B/
drwxrwsr-x  2 agr  388 Dec 11  2018 163A/
drwxrwsr-x  2 agr  388 Feb 26  2019 164A/
drwxrwsr-x  2 agr  436 Jul 22 09:36 164B/
drwsrws---  2 agr  436 Oct 29  2019 165A/
drwxrwsrwx  2 agr  436 Nov 12  2019 166A/
drwxrwsr-x  2 agr  513 Feb 24  2020 166B/
drwxrwsrwx  2 agr  436 Jul 27 17:44 167A/
drwxrwsrwx  2 agr  716 Oct 27  2020 168A/
drwx--S---  2 agr 2503 Aug 10 11:01 ABAQUSfiles/
```

A sample listing of the `162B` directory in Table 4 shows the input and output files used for the daily as-run thermal analysis for cycle 162B. Table 5 shows a listing and description of the ABAQUS files. A Fortran program was written for each cycle to create the daily input including gas mixtures, heat rates, and fast neutron fluence. These files are listed in the ABAQUS directory.

Table 4. Input and output files in `/projects/agr/agr567/162B` directory on HPC.

File Name in 162B	Description 162B
`agr567_base_case_162B.all_fuel_degC`	Output file containing each finite element volume for the first day and each finite element temperature (°C) for each day. Created from `agr567_all_compacts.py` in ABAQUSfiles directory.
`agr567_base_case_162B.TCs_degC`	Output file containing each TC temperature for each day. Created from `agr567_TCs_Temp.py*` in ABAQUSfiles directory.
`combo.agr567.162B.GRANT.output`	Fast neutron fluence of each ¼ axial segment of each compact for each day
`combog.agr567.162B.GRANT.output`	Fast neutron fluence of each 1.0 in. segment of each graphite holder for each day
`fima5.inq.162B.agr567.output.compact`	FIMA results of compacts (output from neutronics not needed for thermal analysis, but reported in main body of report)
`gr_heat.agr567.162B`	Graphite holder heat generation rate for each 1.0 in of each holder for each day

File Name in 162B	Description 162B
heatcompacts.agr567.162B.GRANT.output	Compact heat generation rate for each ¼ axial segment of each compact for each day
heatcomponents.agr567.162B.GRANT.output	All other material components heat generation rate for each day
neonfraction.162B	Neon fraction for each capsule for each day
neonfraction_bias.162B	Neon fraction bias for each capsule for each day

Table 5. Input and output files in /projects/agr/agr567/ABAQUSfiles directory.

File Name ABAQUSfiles	Description ABAQUSfiles
agr567_all_compacts.py	Python script that reads the .odb file and creates the *.all_fuel_DegC file that contains each finite element volume for the first day and each finite element temperature for each day
agr567_base_case_162B.f	Fortran file used by ABAQUS for cycle 162B
agr567_base_case_162B.inp	ABAQUS input file for cycle 162B
agr567_base_case_162B.odb	ABAQUS output database file for cycle 162B
agr567_base_case_162B.sh	PBS script to launch cycle 162B ABAQUS run with qsub command
agr567_base_case_163A.f	Same as above
agr567_base_case_163A.inp	Same as above
agr567_base_case_163A.odb	Same as above
agr567_base_case_163A.sh	Same as above
agr567_base_case_164A.f	Same as above
agr567_base_case_164A.inp	Same as above
agr567_base_case_164A.odb	Same as above
agr567_base_case_164A.sh	Same as above
agr567_base_case_164B.f	Same as above
agr567_base_case_164B.inp	Same as above
agr567_base_case_164B.odb	Same as above
agr567_base_case_164B.sh	Same as above
agr567_base_case_165A.f	Same as above
agr567_base_case_165A.inp	Same as above
agr567_base_case_165A.odb	Same as above
agr567_base_case_165A.sh	Same as above
agr567_base_case_166A.f	Same as above
agr567_base_case_166A.inp	Same as above
agr567_base_case_166A.odb	Same as above

File Name ABAQUSfiles	Description ABAQUSfiles
agr567_base_case_166A.sh	Same as above
agr567_base_case_166B.f	Same as above
agr567_base_case_166B.inp	Same as above
agr567_base_case_166B.odb	Same as above
agr567_base_case_166B.sh	Same as above
agr567_base_case_167A.f	Same as above
agr567_base_case_167A.inp	Same as above
agr567_base_case_167A.odb	Same as above
agr567_base_case_167A.sh	Same as above
agr567_base_case_168A_cap1_0.f	Cycle 168A ABAQUS fortran file for zero neon fraction in capsule 1
agr567_base_case_168A_cap1_0.inp	Cycle 168A ABAQUS input file for zero neon fraction in capsule 1
agr567_base_case_168A_cap1_0.odb	Cycle 168A ABAQUS output database file for zero neon fraction in capsule 1
agr567_base_case_168A_cap1_0.sh	Cycle 168A PBS script to launch ABAQUS for zero neon fraction in capsule 1
agr567_base_case_168A_cap1_leadout.f	Cycle 168A ABAQUS fortran file for neon fraction equal to leadout in capsule 1
agr567_base_case_168A_cap1_leadout.inp	Cycle 168A ABAQUS input file for neon fraction equal to leadout in capsule 1
agr567_base_case_168A_cap1_leadout.odb	Cycle 168A ABAQUS output database file for neon fraction equal to leadout in capsule 1
agr567_base_case_168A_cap1_leadout.sh	Cycle 168A PBS script to launch ABAQUS for neon fraction equal to leadout in capsule 1
agr567.cae	ABAQUS computer aided engineering file that was used to create finite element model
AGR-567 Calculations.xlsx	Excel spreadsheet with 15 tabs that contain all of the input parameter calculations
agr567_TCs_Temp.py*	Python script that reads the output database file and creates the *.TCs_degC file for each cycle
look.f	Fortran file for cycle 162B day 20 to plot heat generation rates
look.inp	ABAQUS input file for cycle 162B day 20 to plot heat generation rates
look.odb	ABAQUS output database file for cycle 162B day 20 to plot heat generation rates
look.sh	PBS script to launch ABAQUS for look.inp file
spring.degF	Average surface temperature on top of spring. Output from spring.py python file.
spring.inp	ABAQUS input file for spring model.
spring.odb	ABAQUS output database for spring model
spring.py*	Python script to calculate average temperature on top of spring

File Name ABAQUSfiles	Description ABAQUSfiles
spring.sh	PBS script to launch ABAQUS for spring model
step_writer_agr567_162B.f	Fortran file to write daily inputs for ABAQUS input file for cycle 162B
step_writer_agr567_162B.mak*	Make file to create executable from fortran file for cycle 162B
step_writer_agr567_163A.f	Same as above
step_writer_agr567_163A.mak*	Same as above
step_writer_agr567_164A.f	Same as above
step_writer_agr567_164A.mak*	Same as above
step_writer_agr567_164B.f	Same as above
step_writer_agr567_164B.mak*	Same as above
step_writer_agr567_165A.f	Same as above
step_writer_agr567_165A.mak*	Same as above
step_writer_agr567_166A.f	Same as above
step_writer_agr567_166A.mak*	Same as above
step_writer_agr567_166B.f	Same as above
step_writer_agr567_166B.mak*	Same as above
step_writer_agr567_167A.f	Same as above
step_writer_agr567_167A.mak*	Same as above
step_writer_agr567_168A_cap1_0.f	Same as above
step_writer_agr567_168A_cap1_0.mak*	Same as above
step_writer_agr567_168A_cap1_leadout.f	Same as above
step_writer_agr567_168A_cap1_leadout.mak*	Same as above

10.0 DRAWINGS

The ABAQUS model of the AGR-5/6/7 experiment was created according the following list of drawings

Drawing Number	Rev.	Drawing Title
120390	18	ATR Inner Flux Trap Baffle Assembly and Details (sheet 6)
604661	5	ATR Advanced Gas Reactor (AGR-5/6/7) Capsule 1 – Assembly and Details
604662	7	ATR Advanced Gas Reactor (AGR-5/6/7) Capsule 2 – Assembly and Details
604663	6	ATR Advanced Gas Reactor (AGR-5/6/7) Capsule 3 – Assembly and Details
604664	4	ATR Advanced Gas Reactor (AGR-5/6/7) Capsule 4 – Assembly and Details
604665	4	ATR Advanced Gas Reactor (AGR-5/6/7) Capsule 5 – Assembly and Details
604680	2	ATR ADVANCED GAS REACTOR (AGR-5/6/7) THERMOCOUPLE STD-N, SPINEL-N, AND CAMB-N ASSEMBLIES AND DETAILS
605060	-	ATR Advanced Gas Reactor (AGR-5/6/7) In-Core Intermediate Neutron Filter Final Machining Detail

11.0 CONCLUSIONS

This report documents the results of thermal analyses to predict the daily as-run temperatures for the AGR-5/6/7 experiment. A finite element model was created for the entire test train with all five capsules. The fuel compacts, graphite holders, stainless-steel capsule walls and all other major components were individually modeled along with each thermocouple. Gas gaps were modeled to change with fast neutron fluence and thermal expansion. Daily heat rates for each compact and component in the model were input from daily as-run physics analyses. Daily gas compositions for each capsule were input. The thermal conductivity of the compacts and graphite holders varied with fast neutron fluence.

Gas mixture thermal conductivity was implemented using experimentally attained values from literature. Fluence and temperature-dependent thermal conductivity was used for the graphite components and the fuel compacts. Radiation heat transfer was implemented. The model was tuned to try and match the thermocouple readings during the first cycle by adjusting the Neolube (graphite lubricant used to increase emissivity on stainless steel capsule) thickness. The gas mixture for capsule 1 during the final cycle was undetermined. A run was made for a lower limit and upper limit for the neon gas fraction for this cycle.

Capsule 5 thermal model predictions agreed the best with measured thermocouples at about -30 °C for the entire irradiation based on inspection from figures. Capsule 1 and capsule 3 had the largest variation in difference between measured and calculated thermocouple temperatures. This difference was about ±120 °C for capsule 1 for the first cycle and about ±75 °C for capsule 3 for the first cycle. Capsule 2 averaged a temperature difference (measured minus calculated) of about ±50 °C while capsule 4 averaged about -40 °C.

Thermocouple failure is lightly discussed in this report. The thermocouples failed the earliest and most often in capsule 1 (most failures) while capsule 5 had the fewest failures.

Time-average, volume-average (TAVA) temperature values were calculated and discussed. These TAVA temperatures showed that the fuel temperatures were controlled very evenly throughout irradiation. Target temperature bins for AGR-5/6 were mostly met except for the highest temperature. Target temperature bins for AGR-7 (1500 ±50 °C) were not quite achieved.

Waterfall plots showing the fraction of fuel below a specified temperature band for each day were displayed and discussed. Calculations were performed for offsetting the holder in various directions by 0.001 in. for the first cycle when compared with the measured thermocouple values. Future uncertainty and sensitivity reports will investigate this further.

12.0 REFERENCES

[1] G. L. Hawkes, J. W. Sterbentz, J. T. Maki, B. T. Pham, "Thermal Predictions of the AGR-3/4 Experiment with Post Irradiation Examination Measured Time-Varying Gas Gaps," ASME J of Nuclear Rad Sci 3(4), 041007 (Jul 31, 2017), Paper No: NERS-17-1008; doi: 10.1115/1.4037095

[2] G. L. Hawkes, J. W. Sterbentz, B. T. Pham, "Thermal Predictions of the AGR-2 Experiment with Variable Gas Gaps," Nuclear Technology / Volume 190 / Number 3 / June 2015 / Pages 245-253, Technical Paper / Thermal Hydraulics / dx.doi.org/10.13182/NT14-73

[3] G. L. Hawkes, J.W. Sterbentz, J. Maki, B. Pham, "Daily Thermal Predictions of the AGR-1 Experiment with Gas Gaps Varying with Time," paper # 12111, International Congress on the Advances in Nuclear Power Plants (ICAPP 2012), Chicago, IL, Jun 24-28, 2012.

[4] B. T. Pham, et. al., "AGR 5/6/7 Irradiation Test Final As-Run Report," INL/EXT-21-64221, Sep 2021.

[5] The MCNP Code Development Team, MCNP Code Manual, https://mcnp.lanl.gov/references.shtml, Los Alamos National Laboratory, accessed Dec 2017.

[6] P. E. Murray, "Thermal Analysis of the AGR-5-6-7 Experiment," ECAR-2966 Rev5, Oct 23, 2018.

[7] J. W. Sterbentz, "JMOCUP Physics Depletion Calculations for the As-Run AGR-5/6/7 TRISO Particle Experiment in ATR Northeast Flux Trap," ECAR-5321 Rev0, Dec 8, 2020.

[8] J. Kestin, K. Knierim, E. A. Mason, B. Najafi, S. T. Ro, M. Waldman, "Equilibrium and Transport Properties of the Noble Gases and Their Mixtures at Low Density," J. Phys. Chem, Vol. 13, No. 1, pp 229-303, 1984.

[9] Dassault Systèmes, ABAQUS version 6.14-2, www.simulia.com or www.abaqus.com, Providence, Rhode Island, 2014.

[10] R. Gontard, H. Nabielek, "Performance Evaluation of Modern HTR TRISO Fuels," Forschungszentrum Jülich GmbH, HTA-IB-05/90, July 31, 1990.

[11] R. J. M. Konings, Editor in Chief, "Comprehensive Nuclear Materials, Volume 4, Radiation Effects in Structural and Functional Materials for Fission and Fusion Reactors," Section 4.11.5.7 Table 9, ISBN: 978-0-08-056033-5, 2012 Copyright Elsevier.

[12] Gonzo, E. E., 2002, "Estimating Correlations for the Effective Thermal Conductivity of Granular Materials," Chem. Eng. J., 90(3), pp. 299–302.

[13] \\fserob1\Projects\Orbit\R&D\Fuels\AGR\AGR-5&6 Data\Capsules\Compact IDs Cans & Drums_16Jan2018_Rev6.xlsx

[14] INL Work Request 16-261, https://inl-my.sharepoint.com/:b:/r/personal/joe_palmer_inl_gov/Documents/Wordy/AGR-5_6_7/Fabrication/WR%2016-261/WP%2016-261%20complete%20WO.pdf?csf=1&web=1&e=Xsj1GM, accessed Aug 2021.

[15] W. Windes, D. Swank, D. Rohrbaugh, and J. Lord. "AGC-2 Graphite Preirradiation Data Analysis Report," United States: N. p., 2013. Web. doi:10.2172/1097190.

[16] ASTM, 2014. Standard practice for testing graphite and boronated graphite materials for high-temperature gas-cooled nuclear reactor components. Designation C781-08, ASTM International, West Conshohocken, Pennsylvania.

[17] D. T. Rohrbaugh, “AGC 2 Irradiated Material Properties Analysis. United States: N. p., 2017. Web. doi:10.2172/1369362.

[18] D. Swank, Joseph Lord, David Rohrbaugh, and William Windes. AGC-2 Graphite Pre-irradiation Data Package. United States: N. p., 2010. Web. doi:10.2172/991897.

[19] Taiju Shibata, Motokuni Eto, Eiji Kunimoto, Shusaku Shiozawa, Kazuhiro Sawa, Tatsuo Oku and Tadashi Maruyama, “Draft of Standard for Graphite Core Components in High Temperature Gas-cooled Reactors,” Japan Atomic Energy Agency Research 2009-042, Jan 2010.

[20] James Sterbentz, “Fast Fluence to DPA Conversion Factors for the AGR Experiments in ATR,” Personal Email, Oct 19, 2019.

[21] William Windes. Data Report on Post-Irradiation Dimensional Change of AGC-1 Samples. United States: N. p., 2012., Appendix A, Web. doi:10.2172/1056006.

[22] NDMAS, Nuclear Data Management and Analysis System, https://ndmashome.inl.gov/htr/agrSite/agrIrrSite/AGR567IrrSite/SitePages/Home.aspx, AGR5_DailyIrrad.xlsx, accessed Aug 2021.

[23] B. T. Pham, “AGR-5/6/7 Data Qualification Report for ATR Cycles 162B through 168A,” INL/EXT-21-62180, Rev. 0, April 2021.

[24] D.W. Marshall, “AGR-5/6/7 Fuel Specification,” SPC-1352, Rev. 8, March 9, 2017.

Appendix A

ABAQUS Version 6.14-2 Validation Report on Falcon

```
Thu Apr  2 08:11:22 MDT 2020
ABQ EXE: abq6142
COMPUTER: r2i2n0
OS: Linux
OS TYPE: 4.12.14-95.16-default
t1
================================================
ODB: Test-1
dictTest[Test-1].Keys:  ['Grp1']
          NT11-n325
Max error: 1.20%      <----------
    Max1:  37.3320     Min1:  10.5200 Range:
26.8120
Abq Max2:  37.7813 Abq Min2:  10.6362 Range:
27.1451
          NT11-n281
Max error: 1.48%      <----------
    Max1:  55.1070     Min1:  13.9970 Range:
41.1100
Abq Max2:  54.7760 Abq Min2:  14.2043 Range:
40.5717
================================================

t2
================================================
ODB: Test-2
dictTest[Test-2].Keys:  ['Grp2', 'Grp1']
          NT15-n61
Max error: 1.34%      <----------
    Max1:  37.3320     Min1:  10.5200 Range:
26.8120
Abq Max2:  37.7366 Abq Min2:  10.6609 Range:
27.0756
          NT11-n61
Max error: 1.54%      <----------
    Max1:  55.1070     Min1:  13.9970 Range:
41.1100
Abq Max2:  54.7444 Abq Min2:  14.2131 Range:
40.5313
================================================

t3
================================================
ODB: Test-3
dictTest[Test-3].Keys:  ['Grp1']
          NT11-n130
Max error: 1.65%      <----------
    Max1:  44.5920     Min1:  12.5210 Range:
32.0710
Abq Max2:  44.7825 Abq Min2:  12.7270 Range:
32.0555
          NT11-n59
Max error: 1.85%      <----------
    Max1:  55.3390     Min1:  14.7770 Range:
40.5620
Abq Max2:  55.0396 Abq Min2:  15.0511 Range:
39.9885
================================================

t4
================================================
ODB: Test-4
dictTest[Test-4].Keys:  ['Grp1']
          NT11-n281
Error: 0.00%   <----------
Ans:       13.7600    Abq:       13.7600
          NT11-n303
Error: 0.00%   <----------
Ans:       11.3200    Abq:       11.3200
          NT11-n325
Error: 0.00%   <----------
Ans:        4.0000    Abq:        4.0000
          NT11-n314
Error: 0.00%   <----------
Ans:        8.2700    Abq:        8.2700
          NT11-n292
Error: 0.00%   <----------
Ans:       13.1500    Abq:       13.1500
================================================

t5
================================================
ODB: Test-5
dictTest[Test-5].Keys:  ['Grp3', 'Grp2', 'Grp1',
'Grp5', 'Grp4']
          NT13-n62
Error: 0.00%   <----------
Ans:       11.3200    Abq:       11.3200
          NT12-n62
Error: 0.00%   <----------
Ans:       13.1500    Abq:       13.1500
          NT11-n62
Error: 0.00%   <----------
Ans:       13.7600    Abq:       13.7600
          NT15-n62
Error: 0.00%   <----------
Ans:        4.0000    Abq:        4.0000
          NT14-n62
Error: 0.00%   <----------
Ans:        8.2700    Abq:        8.2700
================================================

t6
================================================
ODB: Test-6
dictTest[Test-6].Keys:  ['Grp1']
          NT11-n533
Max error: 0.39%      <----------
    Max1:  80.7640     Min1:  61.8970 Range:
18.8670
```

```
Abq Max2:  80.4914 Abq Min2:  61.7364 Range:
18.7551
         NT11-n803
Max error: 0.38%      <----------
    Max1:  94.5930     Min1:  71.5310 Range:
23.0620
Abq Max2:  94.3007 Abq Min2:  71.2781 Range:
23.0226
================================================

t7
================================================
ODB: Test-7
dictTest[Test-7].Keys:  ['Grp1']
         HFL-e56
Error: 0.19%   <----------
Ans:       -0.1700    Abq:       -0.1697
================================================

t8
================================================
ODB: Test-8
dictTest[Test-8].Keys:  ['Grp1']
         HFL-e1121
Error: 1.74%   <----------
Ans:        0.1710    Abq:        0.1740
         HFL-e3678
Error: 2.25%   <----------
Ans:       -0.1620    Abq:       -0.1656
================================================

t9
================================================
ODB: Test-9
dictTest[Test-9].Keys:  ['Grp1']
         NT11-n13
Error: 0.01%   <----------
Ans:       50.0010    Abq:       50.0036
         NT11-n17
Error: 0.00%   <----------
Ans:       55.5500    Abq:       55.5500
         NT11-n328
Error: 0.20%   <----------
Ans:       51.6040    Abq:       51.7074
         NT11-n38
Error: 0.05%   <----------
Ans:       50.0890    Abq:       50.1148
         NT11-n28
Error: 0.11%   <----------
Ans:       50.7010    Abq:       50.7550
         NT11-n218
Error: 0.01%   <----------
Ans:       50.0110    Abq:       50.0176
         NT11-n32
Error: 0.10%   <----------
Ans:       50.3060    Abq:       50.3555


         NT11-n324
Error: 0.20%   <----------
Ans:       52.4260    Abq:       52.5321
         NT11-n4
Error: 0.08%   <----------
Ans:       51.0600    Abq:       51.1006
         NT11-n320
Error: 0.16%   <----------
Ans:       53.6690    Abq:       53.7552
================================================

t10
================================================
ODB: Test-10
dictTest[Test-10].Keys:  ['Grp1']
         NT11-n325
Error: 0.15%   <----------
Ans:      215.7130    Abq:      216.0345
================================================

t11
================================================
ODB: Test-11
dictTest[Test-11].Keys:  ['Grp1']
         HFL-e55
Error: 0.02%   <----------
Ans:       -5.5000    Abq:       -5.4989
================================================

t12
================================================
ODB: Test-12
dictTest[Test-12].Keys:  ['Grp1']
         NT11-n336
Error: 0.00%   <----------
Ans:      406.6667    Abq:      406.6667
```

Appendix B

Compact Time-averaged Temperature, Burnup, and Fast neutron Fluence at the End of Irradiation (168A)

The low fission powers during the two low-power PALM cycles (163A and 167A) led to significantly lower fuel temperatures in all capsules. Therefore, the time-average temperature calculations were performed for two scenarios: the first one included all days of irradiation and the second one excluded two low-power PALM cycles. The time-average fuel temperatures in Table B1 for both scenarios and Capsule 1 neon fractions during Cycle 168A were zero. The compact notation is capsule-level-stack.

Table B1. Compact time-averaged temperature, burnup, and fast neutron fluence at the end of irradiation.

Capsule	Compact	Time-averaged Minimum Temperature (°C)	Time-Averaged Volume-averaged Temperature (°C)	Time-Averaged Peak Temperature (°C)	Burnup (% FIMA)	Fast neutron Fluence (10^{25} n/m^2, E >0.18MeV)
Capsule 5	5-1-1	489 / 499	696 / 711	805 / 822	9.16	3.27
Capsule 5	5-1-2	489 / 499	695 / 710	804 / 821	9.17	3.25
Capsule 5	5-1-3	495 / 505	706 / 721	818 / 835	9.38	3.39
Capsule 5	5-1-4	496 / 506	706 / 721	817 / 834	9.40	3.4
Capsule 5	5-2-1	686 / 700	774 / 790	829 / 846	8.84	3.01
Capsule 5	5-2-2	685 / 699	774 / 789	828 / 845	8.82	2.99
Capsule 5	5-2-3	696 / 710	786 / 802	842 / 859	8.98	3.12
Capsule 5	5-2-4	695 / 709	785 / 801	842 / 859	8.99	3.13
Capsule 5	5-3-1	707 / 721	785 / 800	832 / 849	8.43	2.71
Capsule 5	5-3-2	706 / 720	784 / 800	832 / 849	8.43	2.7
Capsule 5	5-3-3	716 / 730	796 / 812	846 / 863	8.59	2.81
Capsule 5	5-3-4	716 / 730	796 / 812	846 / 863	8.60	2.82
Capsule 5	5-4-1	724 / 738	791 / 807	834 / 850	7.98	2.4
Capsule 5	5-4-2	723 / 738	791 / 807	834 / 851	7.96	2.39
Capsule 5	5-4-3	734 / 748	803 / 819	847 / 864	8.16	2.48
Capsule 5	5-4-4	734 / 748	803 / 819	847 / 864	8.17	2.49
Capsule 5	5-5-1	663 / 677	747 / 762	813 / 830	7.43	2.06
Capsule 5	5-5-2	662 / 676	747 / 762	813 / 830	7.44	2.05
Capsule 5	5-5-3	672 / 685	757 / 773	826 / 842	7.64	2.13
Capsule 5	5-5-4	672 / 686	758 / 774	826 / 843	7.67	2.14
Capsule 5	5-6-1	459 / 468	622 / 635	727 / 742	6.75	1.68
Capsule 5	5-6-2	458 / 467	621 / 634	726 / 741	6.75	1.67
Capsule 5	5-6-3	464 / 473	630 / 643	737 / 752	7.03	1.74

Capsule	Compact	Time-averaged Minimum Temperature (°C)	Time-Averaged Volume-averaged Temperature (°C)	Time-Averaged Peak Temperature (°C)	Burnup (% FIMA)	Fast neutron Fluence (10^{25} n/m^2, E >0.18MeV)
Capsule 5	5-6-4	464 / 473	631 / 644	738 / 753	7.05	1.74
Capsule 5 compacts		**458 / 467**	**741 / 756**	**847 / 864**	**8.20**	**2.57**
Capsule 4	4-1-1	547 / 559	758 / 775	868 / 887	13.77	4.8
Capsule 4	4-1-2	546 / 558	757 / 774	867 / 886	13.72	4.78
Capsule 4	4-1-3	553 / 565	769 / 786	882 / 902	14.06	5.01
Capsule 4	4-1-4	553 / 565	769 / 786	882 / 901	14.09	5.03
Capsule 4	4-2-1	750 / 766	850 / 868	913 / 933	13.72	4.7
Capsule 4	4-2-2	750 / 765	849 / 867	912 / 932	13.70	4.68
Capsule 4	4-2-3	761 / 777	863 / 882	928 / 948	14.02	4.9
Capsule 4	4-2-4	761 / 777	863 / 881	928 / 947	14.07	4.93
Capsule 4	4-3-1	785 / 801	875 / 893	930 / 950	13.55	4.57
Capsule 4	4-3-2	784 / 800	875 / 893	930 / 950	13.53	4.55
Capsule 4	4-3-3	796 / 812	889 / 907	945 / 965	13.83	4.77
Capsule 4	4-3-4	796 / 812	888 / 907	945 / 965	13.87	4.79
Capsule 4	4-4-1	806 / 822	888 / 907	935 / 955	13.24	4.42
Capsule 4	4-4-2	805 / 822	888 / 906	935 / 954	13.21	4.4
Capsule 4	4-4-3	816 / 833	901 / 919	948 / 968	13.52	4.61
Capsule 4	4-4-4	817 / 833	902 / 920	950 / 970	13.56	4.62
Capsule 4	4-5-1	771 / 787	865 / 884	927 / 947	12.84	4.24
Capsule 4	4-5-2	770 / 786	864 / 882	927 / 946	12.83	4.23
Capsule 4	4-5-3	780 / 796	876 / 894	940 / 960	13.11	4.42
Capsule 4	4-5-4	781 / 797	877 / 896	942 / 962	13.15	4.44
Capsule 4	4-6-1	566 / 578	765 / 782	872 / 891	12.37	4.01
Capsule 4	4-6-2	565 / 577	763 / 779	870 / 889	12.35	4
Capsule 4	4-6-3	571 / 583	773 / 790	883 / 902	12.62	4.18
Capsule 4	4-6-4	572 / 584	774 / 791	884 / 903	12.65	4.2
Capsule 4 compacts		**546 / 558**	**839 / 857**	**950 / 970**	**13.39**	**4.55**
Capsule 2	2-1-1	536 / 546	736 / 752	844 / 861	13.51	4.56
Capsule 2	2-1-2	536 / 546	736 / 752	844 / 861	13.52	4.56
Capsule 2	2-1-3	542 / 552	748 / 763	858 / 875	13.82	4.77
Capsule 2	2-1-4	541 / 552	746 / 761	855 / 873	13.81	4.77
Capsule 2	2-2-1	728 / 743	828 / 845	896 / 914	14.03	4.72
Capsule 2	2-2-2	728 / 743	828 / 845	896 / 914	14.02	4.72
Capsule 2	2-2-3	739 / 753	842 / 859	911 / 929	14.33	4.94
Capsule 2	2-2-4	737 / 752	840 / 856	909 / 927	14.33	4.94
Capsule 2	2-3-1	768 / 782	857 / 874	912 / 931	14.38	4.85

Capsule	Compact	Time-averaged Minimum Temperature (°C)	Time-Averaged Volume-averaged Temperature (°C)	Time-Averaged Peak Temperature (°C)	Burnup (% FIMA)	Fast neutron Fluence (10^{25} n/m^2, E >0.18MeV)
Capsule 2	2-3-2	768 / 782	857 / 874	913 / 931	14.36	4.85
Capsule 2	2-3-3	779 / 794	872 / 889	929 / 947	14.67	5.07
Capsule 2	2-3-4	778 / 792	870 / 886	926 / 945	14.69	5.07
Capsule 2	2-4-1	763 / 777	858 / 875	913 / 931	14.60	4.96
Capsule 2	2-4-2	763 / 777	859 / 875	913 / 931	14.61	4.95
Capsule 2	2-4-3	775 / 789	874 / 890	929 / 948	14.91	5.18
Capsule 2	2-4-4	773 / 788	871 / 888	927 / 945	14.92	5.19
Capsule 2	2-5-1	733 / 747	835 / 851	900 / 917	14.78	5.05
Capsule 2	2-5-2	734 / 747	836 / 852	901 / 918	14.78	5.04
Capsule 2	2-5-3	745 / 759	850 / 867	917 / 935	15.09	5.28
Capsule 2	2-5-4	744 / 757	848 / 864	914 / 933	15.09	5.29
Capsule 2	2-6-1	726 / 739	821 / 838	880 / 898	14.89	5.13
Capsule 2	2-6-2	726 / 739	822 / 838	881 / 899	14.88	5.12
Capsule 2	2-6-3	736 / 750	835 / 852	897 / 915	15.21	5.36
Capsule 2	2-6-4	735 / 749	834 / 850	895 / 913	15.21	5.36
Capsule 2	2-7-1	706 / 720	808 / 824	871 / 889	14.92	5.18
Capsule 2	2-7-2	705 / 719	808 / 824	872 / 889	14.92	5.17
Capsule 2	2-7-3	716 / 729	820 / 836	886 / 903	15.25	5.42
Capsule 2	2-7-4	715 / 729	819 / 836	885 / 903	15.26	5.42
Capsule 2	2-8-1	544 / 554	743 / 758	844 / 861	14.93	5.21
Capsule 2	2-8-2	542 / 553	742 / 757	843 / 861	14.93	5.2
Capsule 2	2-8-3	549 / 560	753 / 769	857 / 874	15.25	5.44
Capsule 2	2-8-4	549 / 560	753 / 768	856 / 874	15.26	5.44
Capsule 2 compacts		**536 / 546**	**817 / 833**	**929 / 948**	**14.66**	**5.07**
Capsule 1	1-1-1	614 / 625	786 / 801	904 / 921	5.78	1.62
Capsule 1	1-1-2	614 / 624	786 / 800	903 / 920	5.66	1.62
Capsule 1	1-1-3	618 / 629	789 / 803	907 / 924	5.86	1.64
Capsule 1	1-1-4	620 / 630	796 / 810	915 / 932	6.13	1.69
Capsule 1	1-1-5	628 / 638	803 / 818	924 / 941	6.47	1.73
Capsule 1	1-1-6	629 / 640	809 / 824	932 / 949	6.63	1.75
Capsule 1	1-1-7	630 / 641	810 / 825	933 / 950	6.67	1.75
Capsule 1	1-1-8	629 / 640	805 / 820	927 / 944	6.42	1.73
Capsule 1	1-1-9	621 / 632	798 / 813	920 / 937	6.16	1.69
Capsule 1	1-1-10	619 / 630	791 / 806	911 / 928	5.89	1.65
Capsule 1	1-2-1	766 / 779	909 / 925	1015 / 1033	7.34	2.07
Capsule 1	1-2-2	765 / 779	908 / 924	1013 / 1032	7.35	2.07

Capsule	Compact	Time-averaged Minimum Temperature (°C)	Time-Averaged Volume-averaged Temperature (°C)	Time-Averaged Peak Temperature (°C)	Burnup (% FIMA)	Fast neutron Fluence (10^{25} n/m^2, E >0.18MeV)
Capsule 1	1-2-3	768 / 781	912 / 928	1018 / 1036	7.42	2.11
Capsule 1	1-2-4	774 / 787	919 / 936	1026 / 1045	7.56	2.16
Capsule 1	1-2-5	781 / 795	928 / 945	1036 / 1055	7.71	2.21
Capsule 1	1-2-6	786 / 800	936 / 952	1044 / 1063	7.84	2.23
Capsule 1	1-2-7	787 / 801	937 / 953	1046 / 1064	7.85	2.23
Capsule 1	1-2-8	783 / 797	932 / 948	1040 / 1059	7.73	2.2
Capsule 1	1-2-9	777 / 790	925 / 941	1033 / 1052	7.58	2.16
Capsule 1	1-2-10	770 / 783	916 / 932	1023 / 1041	7.42	2.11
Capsule 1	1-3-1	842 / 856	993 / 1010	1097 / 1117	8.11	2.48
Capsule 1	1-3-2	841 / 855	991 / 1009	1095 / 1115	8.11	2.48
Capsule 1	1-3-3	844 / 858	995 / 1012	1099 / 1119	8.15	2.52
Capsule 1	1-3-4	850 / 864	1003 / 1020	1107 / 1127	8.26	2.58
Capsule 1	1-3-5	858 / 872	1012 / 1030	1117 / 1138	8.40	2.63
Capsule 1	1-3-6	863 / 877	1020 / 1038	1126 / 1147	8.50	2.65
Capsule 1	1-3-7	864 / 878	1022 / 1040	1129 / 1149	8.50	2.66
Capsule 1	1-3-8	861 / 875	1017 / 1035	1124 / 1144	8.40	2.63
Capsule 1	1-3-9	854 / 868	1010 / 1027	1116 / 1136	8.29	2.58
Capsule 1	1-3-10	847 / 861	1000 / 1017	1105 / 1125	8.17	2.52
Capsule 1	1-4-1	896 / 911	1052 / 1071	1151 / 1172	8.68	2.85
Capsule 1	1-4-2	895 / 910	1051 / 1069	1149 / 1170	8.69	2.84
Capsule 1	1-4-3	897 / 912	1054 / 1072	1152 / 1173	8.73	2.89
Capsule 1	1-4-4	903 / 918	1061 / 1080	1160 / 1181	8.80	2.96
Capsule 1	1-4-5	911 / 926	1070 / 1089	1169 / 1190	8.95	3.02
Capsule 1	1-4-6	917 / 932	1079 / 1098	1178 / 1199	9.05	3.04
Capsule 1	1-4-7	918 / 933	1082 / 1101	1181 / 1203	9.03	3.04
Capsule 1	1-4-8	915 / 930	1077 / 1096	1177 / 1198	8.95	3.02
Capsule 1	1-4-9	908 / 923	1069 / 1088	1169 / 1190	8.82	2.96
Capsule 1	1-4-10	900 / 915	1059 / 1078	1159 / 1180	8.74	2.89
Capsule 1	1-5-1	909 / 924	1076 / 1095	1169 / 1190	9.17	3.19
Capsule 1	1-5-2	908 / 923	1075 / 1094	1167 / 1188	9.19	3.18
Capsule 1	1-5-3	911 / 925	1078 / 1097	1170 / 1191	9.21	3.23
Capsule 1	1-5-4	915 / 930	1084 / 1103	1178 / 1199	9.27	3.3
Capsule 1	1-5-5	922 / 937	1093 / 1112	1187 / 1209	9.36	3.37
Capsule 1	1-5-6	927 / 942	1101 / 1120	1195 / 1216	9.46	3.39
Capsule 1	1-5-7	929 / 943	1104 / 1123	1197 / 1218	9.46	3.39
Capsule 1	1-5-8	926 / 941	1100 / 1120	1194 / 1215	9.38	3.36

Capsule	Compact	Time-averaged Minimum Temperature (°C)	Time-Averaged Volume-averaged Temperature (°C)	Time-Averaged Peak Temperature (°C)	Burnup (% FIMA)	Fast neutron Fluence (10^{25} n/m^2, E >0.18MeV)
Capsule 1	1-5-9	920 / 935	1093 / 1112	1186 / 1208	9.29	3.3
Capsule 1	1-5-10	914 / 928	1084 / 1103	1177 / 1198	9.23	3.24
Capsule 1	1-6-1	909 / 924	1087 / 1106	1195 / 1216	9.61	3.49
Capsule 1	1-6-2	908 / 923	1085 / 1104	1193 / 1215	9.61	3.49
Capsule 1	1-6-3	910 / 925	1088 / 1107	1196 / 1218	9.63	3.54
Capsule 1	1-6-4	915 / 930	1095 / 1114	1204 / 1225	9.68	3.62
Capsule 1	1-6-5	922 / 937	1104 / 1123	1214 / 1236	9.79	3.68
Capsule 1	1-6-6	927 / 942	1111 / 1130	1219 / 1241	9.88	3.7
Capsule 1	1-6-7	928 / 943	1112 / 1131	1220 / 1243	9.86	3.7
Capsule 1	1-6-8	925 / 940	1109 / 1129	1218 / 1240	9.78	3.68
Capsule 1	1-6-9	920 / 935	1103 / 1122	1211 / 1233	9.70	3.62
Capsule 1	1-6-10	913 / 928	1094 / 1113	1202 / 1224	9.64	3.55
Capsule 1	1-7-1	922 / 937	1111 / 1131	1219 / 1242	10.00	3.76
Capsule 1	1-7-2	922 / 937	1110 / 1130	1220 / 1242	10.01	3.76
Capsule 1	1-7-3	924 / 939	1113 / 1133	1224 / 1246	10.02	3.82
Capsule 1	1-7-4	929 / 944	1120 / 1140	1230 / 1253	10.12	3.9
Capsule 1	1-7-5	935 / 950	1129 / 1149	1238 / 1261	10.19	3.97
Capsule 1	1-7-6	940 / 956	1134 / 1154	1243 / 1266	10.36	3.99
Capsule 1	1-7-7	941 / 957	1135 / 1155	1243 / 1266	10.34	3.99
Capsule 1	1-7-8	938 / 953	1132 / 1152	1241 / 1263	10.22	3.97
Capsule 1	1-7-9	933 / 948	1126 / 1146	1234 / 1257	10.13	3.9
Capsule 1	1-7-10	926 / 942	1117 / 1137	1225 / 1248	10.04	3.82
Capsule 1	1-8-1	912 / 928	1112 / 1132	1220 / 1243	10.43	4
Capsule 1	1-8-2	913 / 929	1114 / 1134	1222 / 1244	10.44	4
Capsule 1	1-8-3	915 / 931	1117 / 1138	1226 / 1249	10.49	4.06
Capsule 1	1-8-4	920 / 936	1123 / 1144	1232 / 1255	10.59	4.14
Capsule 1	1-8-5	925 / 941	1130 / 1150	1240 / 1263	10.75	4.21
Capsule 1	1-8-6	929 / 945	1133 / 1154	1244 / 1267	10.89	4.23
Capsule 1	1-8-7	929 / 945	1134 / 1154	1244 / 1267	10.91	4.23
Capsule 1	1-8-8	926 / 942	1131 / 1152	1241 / 1264	10.76	4.21
Capsule 1	1-8-9	920 / 937	1124 / 1145	1235 / 1258	10.62	4.14
Capsule 1	1-8-10	915 / 931	1116 / 1137	1226 / 1249	10.49	4.06
Capsule 1	1-9-1	632 / 643	967 / 986	1174 / 1197	11.09	4.17
Capsule 1	1-9-2	632 / 644	969 / 987	1176 / 1199	11.12	4.16
Capsule 1	1-9-3	634 / 645	972 / 991	1180 / 1203	11.22	4.22
Capsule 1	1-9-4	638 / 649	977 / 995	1186 / 1209	11.33	4.31

Capsule	Compact	Time-averaged Minimum Temperature (°C)	Time-Averaged Volume-averaged Temperature (°C)	Time-Averaged Peak Temperature (°C)	Burnup (% FIMA)	Fast neutron Fluence (10^{25} n/m^2, E >0.18MeV)
Capsule 1	1-9-5	639 / 650	982 / 1001	1192 / 1215	11.53	4.38
Capsule 1	1-9-6	643 / 655	985 / 1004	1195 / 1218	11.68	4.4
Capsule 1	1-9-7	642 / 653	985 / 1004	1196 / 1219	11.67	4.4
Capsule 1	1-9-8	640 / 652	982 / 1001	1193 / 1216	11.57	4.38
Capsule 1	1-9-9	637 / 649	977 / 996	1187 / 1210	11.40	4.31
Capsule 1	1-9-10	634 / 646	970 / 989	1178 / 1201	11.24	4.22
Capsule 1 compacts		**614 / 624**	**1022 / 1041**	**1244 / 1267**	**9.12**	**3.18**
All AGR-5/6 compacts		**458 / 467**	**918 / 936**	**1244 / 1267**	**10.64**	**3.64**
Capsule 3	3-1-1	970 / 990	1167 / 1191	1301 / 1328	13.58	5.37
Capsule 3	3-1-2	969 / 990	1169 / 1193	1302 / 1329	13.76	5.48
Capsule 3	3-1-3	970 / 991	1169 / 1193	1303 / 1329	13.77	5.49
Capsule 3	3-2-1	1177 / 1200	1293 / 1318	1374 / 1400	14.43	5.42
Capsule 3	3-2-2	1180 / 1203	1295 / 1320	1375 / 1401	14.61	5.54
Capsule 3	3-2-3	1180 / 1203	1295 / 1320	1374 / 1401	14.62	5.54
Capsule 3	3-3-1	1235 / 1258	1329 / 1354	1391 / 1417	14.67	5.42
Capsule 3	3-3-2	1238 / 1261	1330 / 1355	1392 / 1418	14.84	5.55
Capsule 3	3-3-3	1238 / 1262	1330 / 1355	1391 / 1418	14.88	5.55
Capsule 3	3-4-1	1246 / 1268	1335 / 1359	1393 / 1419	14.73	5.41
Capsule 3	3-4-2	1249 / 1271	1336 / 1361	1394 / 1420	14.91	5.54
Capsule 3	3-4-3	1249 / 1272	1336 / 1361	1394 / 1420	14.95	5.54
Capsule 3	3-5-1	1241 / 1264	1332 / 1356	1392 / 1418	14.69	5.39
Capsule 3	3-5-2	1245 / 1267	1334 / 1358	1394 / 1420	14.86	5.51
Capsule 3	3-5-3	1245 / 1268	1334 / 1358	1394 / 1420	14.89	5.52
Capsule 3	3-6-1	1236 / 1259	1336 / 1361	1404 / 1430	14.56	5.34
Capsule 3	3-6-2	1239 / 1262	1338 / 1363	1405 / 1431	14.72	5.46
Capsule 3	3-6-3	1241 / 1264	1338 / 1363	1405 / 1432	14.77	5.47
Capsule 3	3-7-1	1190 / 1213	1318 / 1343	1401 / 1428	14.27	5.28
Capsule 3	3-7-2	1191 / 1214	1319 / 1344	1402 / 1429	14.46	5.4
Capsule 3	3-7-3	1193 / 1216	1320 / 1345	1402 / 1429	14.49	5.41
Capsule 3	3-8-1	969 / 989	1192 / 1217	1339 / 1366	13.62	5.18
Capsule 3	3-8-2	971 / 991	1193 / 1217	1340 / 1366	13.80	5.29
Capsule 3	3-8-3	971 / 991	1193 / 1218	1340 / 1367	13.81	5.3
All AGR-7 compacts		**969 / 989**	**1289 / 1313**	**1405 / 1432**	**14.45**	**5.43**